August 2014

Kinetics of Aluminization and Homogenization in Wrought H-X750 Nickel-Base Superalloy

Sean Reilly
University of Massachusetts Amherst

Recommended Citation

KINETICS OF ALUMINIZATION AND HOMOGENIZATION IN WROUGHT H-X750 NICKEL-BASE SUPERALLOY

A Thesis Presented

by

SEAN H. REILLY

Submitted to the Graduate School of the

University of Massachusetts Amherst in partial fulfillment

of the requirements for the degree of

MASTER OF SCIENCE IN MECHANICAL ENGINEERING

May 2014

MECHANICAL AND INDUSTRIAL ENGINEERING

KINETICS OF ALUMINIZATION AND HOMOGENIZATION IN WROUGHT H-X750 NICKEL-BASE SUPERALLOY

A Thesis Presented

by

SEAN H. REILLY

Approved as to style and content by:

_____

Robert W. Hyers, Chair

_____

Jonghyun Lee, Member

_____

David U. Furrer, Member

_____

Donald L. Fisher, Department Head

Mechanical and Industrial Engineering

DEDICATION

To my parents. Without them, none of this would have been possible for me.

ACKNOWLEDGMENTS

ABSTRACT

KINETICS OF ALUMINIZATION AND HOMOGENIZATION IN WROUGHT H-X750 NICKEL-BASE SUPERALLOY

MAY 2014

SEAN REILLY, B.S. ENGINEERING, COLORADO SCHOOL OF MINES

M.S.M.E., UNIVERSITY OF MASSACHUSETTS AMHERST

M.B.A., UNIVERSITY OF MASSACHUSETTS AMHERST

Directed by: Dr. Robert W. Hyers

In sub-millimeter sheets of wrought H-X750 Nickel-base superalloy, aluminum-rich coatings are bonded to matrix with a vapor phase aluminization process. If an appropriate amount of aluminum is bonded to matrix with homogenization treatment, the resulting diffusion couple will diffuse into coherent (γ/γ') heterogeneous phases creating matrix that is both precipitation and solid solution strengthened.

The diffusional mechanisms for solid solution mass transport involved with the growth and dispersion of bonded aluminum-rich coatings in the aluminization process only differ from the no external mass flow homogenization process with annealing treatment in that the boundary conditions are different. In each case these forces that activate diffusion at the macroscopic level are connected to the activation energies of random walks of atoms on a wide scale at the angstrom level.

An overview of wrought Nickel-base superalloy is presented. Starting with thin sheets the alloy will be aluminized and homogenized. The research from this study will determine the parameters for the movement of the phase boundaries, mass transport, and the time variant

concentration fields for both the aluminization and homogenization processes. This is predictable for both single dimension fluxes assuming the interdiffusivities and fluxes at the phase boundaries are known. Because mass-transport is related to the movement of the phase boundaries through density, an investigation into the less dense aluminum-rich coatings and resultant matrix is also included.

TABLE OF CONTENTS

Page

LIST OF TABLES

LIST OF FIGURES

LIST OF ACRONYMS

BCC, Body Centered Cubic

BSE, Back-Scatter Electrons

CVD, Chemical Vapor Deposition

EDS, Energy-dispersive X-Ray Spectroscopy

EPMA, Electron Probe Micro-Analyzer

FCC, Face Centered Cubic

ISS, Initial Substrate Surface

RFIN, Reaction Front of Inward Grown NiAl Layer

RFON, Reaction Front of Outward Grown NiAl Layer

SE, Secondary Electrons

SEM, Scanning Electron Microscopy

SOR, Successive Over Relaxation

PREFACE

The literature survey, and aluminization and homogenization experiment from my Master's Thesis is based off the experiment from the dissertation by Sara Jane Perez-Bergaquist at the University of Michigan. [1]

Copyright Permission to use Figure 1 [69] was granted by the Minerals, Metals, and Materials Society Publications Manager

CHAPTER 1

AN OVERVIEW OF WROUGHT NICKEL SUPERALLOY

1.1 Introduction

Aircraft engines are more efficient when the engine is hotter. Running the engine at higher temperatures provide an advantage in that it creates better energy efficiency, more power, and thrust, but higher temperatures also make the engine environment more stressful and corrosive. Nickel superalloys are unique in that they can handle a corrosive environment and stress for long periods of time at high temperature. Presently, no other material is like it in terms of strength, resistance to creep, and oxidation at high temperature.

It is well-known that what gives Nickel-base superalloy its strength and resistance to creep at high temperature is the volume fraction of (γ') which is an ordered $L1_2$ phase of Ni_3Al, Ni_3Nb, Ni_3Ta, and Ni_3Ti. The aluminization process can create aluminum rich bonded coatings at the surface of Nickel and Nickel-base superalloy. The volume fraction of (γ') can be maximized producing coherent (γ/γ') throughout the alloy with a long diffuse if an optimal amount of aluminum is added with an aluminization process.

Using H-X750 Nickel-base superalloy, a high activity vapor phase aluminization experiment can create bonded aluminum rich coatings on the surface of the substrate.

With a long heat treatment, the bonded aluminum rich coatings diffuse into the superalloy creating a single coherent (γ/γ') throughout the alloy.

The objective of this research is to investigate the parameters relating to the diffusion of mass in H-X750 Nickel-base superalloy in the aluminization and homogenization process with a flat panel. These processes are permitted by macroscopic fluxes driven by atom jumping at the angstrom level on a wide scale. Further, this research will observe how mass diffusion compares with volumetric diffusion.

1.2 Manufacturing

Nickel-base superalloys come in four categories: wrought, conventionally cast, directionally solidified, and single crystal. Differences between the four categories largely depend on grain orientation and the volume fraction of (γ'). [2]

Wrought alloys are typically made of ingots from a Vacuum Induction Furnace.   These ingots are melted by subsequent Vacuum Arc Remelt (VAR) or Electro Slag Remelt (ESR). The difference between VAR and ESR is that ESR uses slag as a heating element and refining agent while VAR uses an electric arc to continually melt electrodes. The electrodes are made with varying amounts of transition metal or refractory elements. The temperature of the melt is controlled in the crucible by flowing water to control solidification rate.   Carbides are added to the melt in order to control grain size. As the melt solidifies, the grain size is controlled and its orientation is equiaxed. Wrought alloys often contain lesser amounts of the elements Aluminum, Niobium, Tantalum, or

Titanium due to macrosegregation during solidifiication. Higher concentrations of these elements increase the volume fraction of (γ') which reduces ductility. Additionally the (γ') solvus temperature increases.   [80]

The melt is then poured as a slab (12'') and then hot rolled to a smaller thickness (2-3''). The alloy is then cold rolled with an intermediate annealing process, which is repeated until the nickel alloy is rolled to its final gage (0.02''). By some variation of this proprietary manufacturing process, wrought X-750 alloy is made.
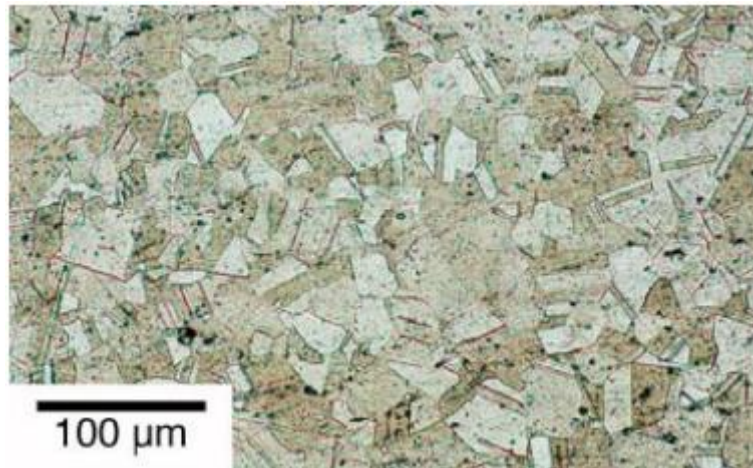
Figure 1: Grain structure of Wrought X-750 Sheet [69]

Table 1: Composition of H-X750 Alloy									
Ni	Cr	Fe	Ti	Nb	Al	Co	Mn	Si	C
70	16	8	2.5	1	0.8	1	0.35	0.35	0.08

1.3 H-X750 Surface Observation

The surface of two H-X750 samples were observed under a Scanning Electron

Microscope (SEM) with secondary electrons (SE) using a Zeiss EVO 50. The first sample

was electroremoved in a nickel sulfamate solution at 37.8 deg C for eight hours at 5V,

1.0 Amps. The second sample was the alloy unpolished, received from the

manufacturer.

The grains from figure 1 measured about 25 microns on average which was equivalent

in size to the grains in figure 2.

In the unpolished alloy, some minor scratches measuring tens of micrometers in length

can be seen in the 200x image.   Parallel tiny hills and valleys can be observed in the

2000x image. Tiny hills and valleys measured tens of micrometers in length. The hills

and valleys were measured to be hundreds of nanometers deep in the 10000x image.

Small spherical subgrains were present in the tiny valleys of the observed sample.
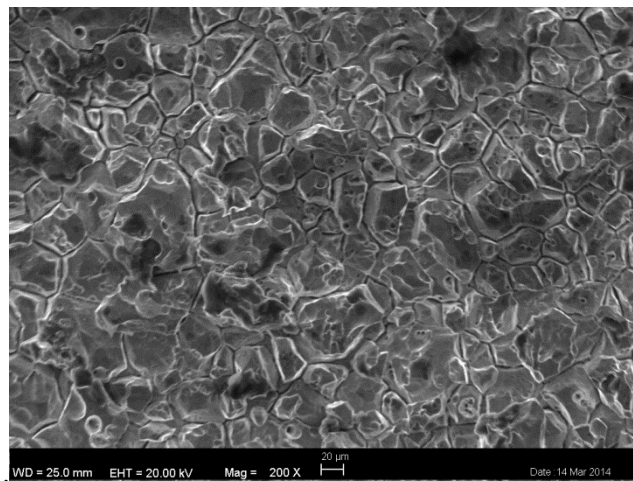
Figure 2: SE Photograph of electroremoved H-X750 at 200x
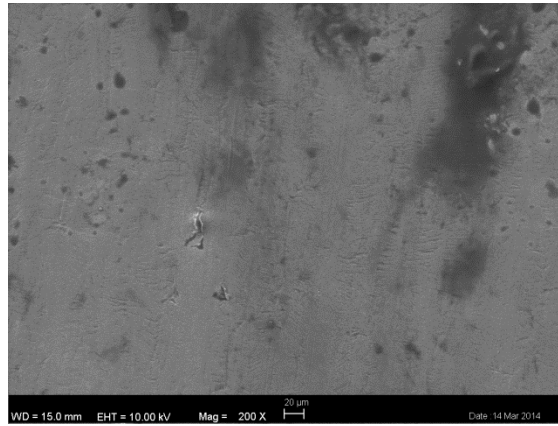
Figure 3: SE Photograph of pure H-X750 at 200x
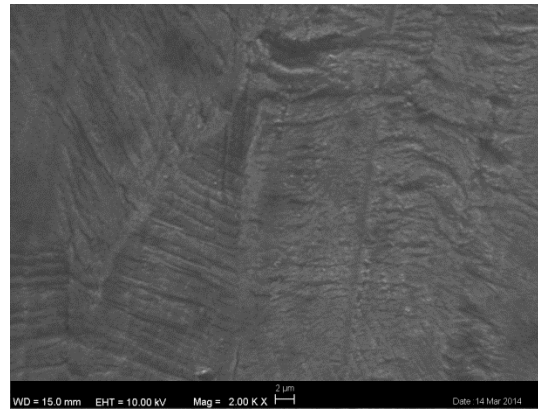
Figure 4: SE Photograph of pure H-X750 at 2000x
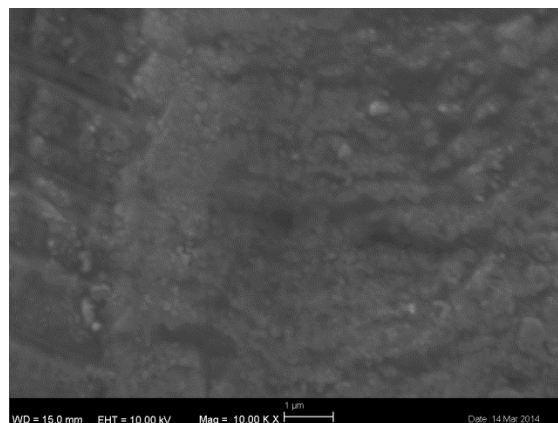
Figure 5: SE Photograph of pure H-X750 at 10000x

CHAPTER 2

ALUMINIZATION BY PACK CEMENTATION

2.1 Aluminization by Pack Cementation

Pack cementation is inexpensive and satisfies 80-90% of the world market for diffusion coatings on gas turbine components. [13] The purpose of pack cementation is to produce bonded aluminum-rich coatings on the surface of the substrate.

The pack cementation coating process is an in situ chemical vapor deposition process (CVD). In CVD, a substrate is exposed to a volatile gas where the gas reacts with the substrate and deposits a film onto the substrate surface.

In pack cementation, a substrate is buried in pack mixture containing donor element, halide activator, and an inert filler. This mixture is heated to high temperature in an inert atmosphere to prevent oxidation.   The donor element chemically reacts with the activator producing a partial pressure of volatile gas away from the substrate surface. The volatile gas reacts with the substrate depositing a bonded coating at the surface by vapor phase diffusion. Finally, the bonded coating at the surface is carried through matrix by solid state diffusion. The mass transport for the donor element starts in pack mixture and finishes with the donor element rich coating bonded to the material.

Aluminum depleted zones in the pack mixture surround the specimen. The width of these aluminum depleted zones increase as Aluminum is deposited from the pack to the

bonded coating. These depleted zones are indicative of donor element transport to the

base alloy and a decline in the aluminum deposition capability of the bulk pack. [14]

2.1.1 Aluminization Chemistry

The decomposition of the activator produces byproducts that react with the donor

aluminum to produce aluminum-halides. The aluminum-halides react with the surface

of the substrate to produce an aluminum-rich alloy on the surface of the substrate.

Understanding these processes will yield an equation for mass deposition.

While some activators are salts or reactive gases, ammonia-halides are often used.

Ammonia-halides are solid at room temperature, do not spontaneously decompose, and

vaporize under high temperature.

(1)
$$NH_4X \;=\; NH_3 \;+\; HX$$

(2)
$$2NH_3 \;=\; N_2 \;+\; 3H_2$$

The decomposition products of an ammonia-halide produce ammonia and a reactive gas

(HX). Ammonia decomposes to stable elements at high temperature. The reactive gas

bonds to the donor aluminum or aluminum alloy to produce volatile vapor phases of

aluminum (AlX_3, AlX_2, AlX).

7

(3) $Al~(l)~+~3HX~(g)~=~3/2~H_2(g)~+~AlX_3~(g)$

(4) $Al~(l)~+~2HX~(g)~=~H_2(g)~+~AlX_2(g)$

(5) $Al~(l)~+~HX~(g)~=~\frac{1}{2}~H2(g)~+~AlX(g)$
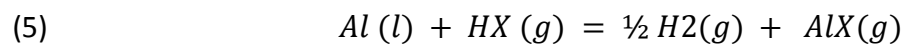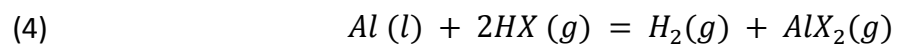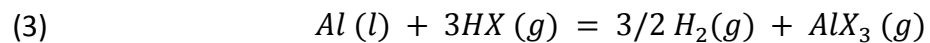
The equilibrium constants for the reactions that produce the volatile vapor phases of

aluminum are determined by the difference in Gibbs free energies of formation

between the products and reactants. This difference must be negative for the reaction

to be spontaneous.

(6) $\Delta G~=~-RT~ln(K_{eq})$

Table 2: Gibbs Energies for Reactive Gas and Aluminum Deposition Agents [71]

Species	Phase (Matter)	Chemical Formula	ΔG_f° (kJ/mol) at 1100K
Aluminum Monochloride	Gas	AlCl	-141.042
Aluminum Dichloride	Gas	$AlCl_2$	-315.317
Aluminum Chloride	Liquid	$AlCl_3$	-443.094
Hydrogen Chloride	Gas	HCl	-101.430

Activity (a) is a measurement of the effective concentration of a species in a mixture. It is related to the difference in chemical potential (μ) for an ideal solution. For ideal solutions, the properties of mixtures can be expressed simply by Raoult's law using the rule of mixtures. The activity coefficient accommodates for deviations from the ideal solution to the actual solution.

(7)
$$\mu = \mu^\circ + RT \ln a$$

The relation between activity and surface concentration is given below for 1000 deg C.
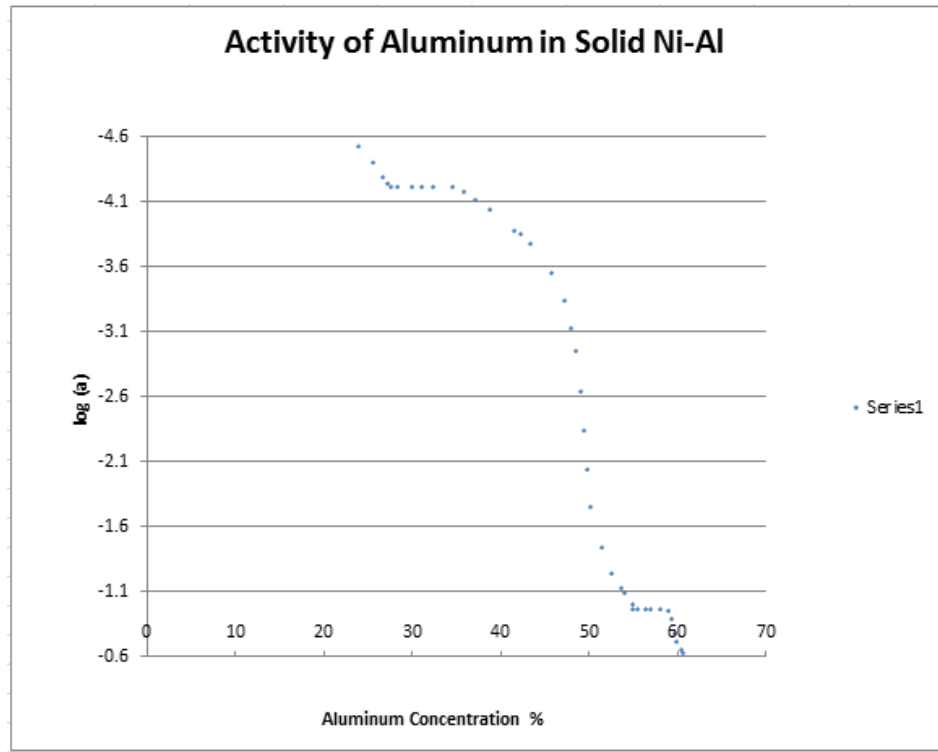
Figure 6: Activity of Aluminum in solid Ni-Al at 1000 deg C extracted from data by Steiner and Komarek [70]

(8)
$$K_1 = \frac{P_x a}{P_{AlX}} = \frac{P_4 a}{P_1}$$

(9)
$$K_2 = \frac{P_x^2 a}{P_{AlX_2}} = \frac{P_4^2 a}{P_2}$$

(10)
$$K_3 = \frac{P_x^3 a}{P_{AlX_3}} = \frac{P_4^3 a}{P_3}$$

(11)
$$0 = D_1(P_1 - P_1') + 2D_2(P_2 - P_2') + 3D_3(P_3 - P_3') + D_4(P_4 - P_4')$$

In pack mixture, far from the surface of the material to be coated, the volatile gases are at an equilibrium partial pressure. The sum of the partial pressures of the volatile gases in pack mixture is 1 atm, which assumes that the system is an open system. The equilibrium constants for these volatile gases are dependent on the activity and the ratio of partial pressures of the products and reactants of molecular compounds as determined by the forward and reverse behavior of chemical equilibrium. At the surface, the partial pressures of the volatile gases are less than the equilibrium.

The surface partial pressures of each species can be solved with equation 8 to equation 10 and the halogen balance at the surface with equation 11 because the partial pressure p_4 is known. These four equations will have four unknowns so that the equilibrium partial pressures of the ith phase and the surface partial pressures of the ith phase can both be solved for. [3] From this solution, the rate constant (k_g) for the vapor phase can be determined. The mass added per unit area is a parabolic function with respect to time and (k_g).

(12)
$$w_g{}^2 = k_g t = \frac{2\rho \epsilon M t}{lRT} \sum_{i=1}^{n} D_i (p_i - p_i')$$

$$\rho - donor\ element\ pack\ density,\ \ M - Molar\ Mass,$$

$$\epsilon/_l - correlation\ factor = \frac{0.79}{4}, D - gas\ diffusivity$$

2.1.1.1 Discussion

The rate constant is calculated in Appendix B from data in Appendix A using an activity

of 0.01 for partial pressures at the surface. This was the same assumption Levine and

Caves [3] made in their work. An activity of 1 represents the partial pressures in the

pack mixture. The donor element pack density from Appendix A was changed from 0.04

g/cm^3 [72] to 0.015 g/cm^3. 0.015 g/cm^3 was the donor element pack density in the pack

mixture from the Aluminization experiment from section 2.1.3.

All other data in Appendix B was taken from Appendix A for a temperature T = 800 deg

C. A mass rate constant (k_g) is determined using equation 12 to be 1.058 x 10^{-7}g^2/cm^4-s.

The kinetic constant for determining boundary layer movement is the square root of the

mass rate constant multiplied by the specific volume of (δ) Ni$_2$Al$_3$, which is 7.711 x 10^{-7}

m/s$^{.5}$. In section 4.1.3, an empirical method exists for determining boundary layer

movement using diffusivity constants, phase concentrations, and concentration

discontinuities. The kinetic constant determined by this method is shown in Appendix C

as 4.753 x 10^{-7} m/s$^{.5}$. The closeness of these two results suggests that there is a

relationship between boundary layer movement, mass diffusion and density.

2.1.2 Surface Composition

Surface composition has no time dependence, but is not fixed. It varies with the

aluminum content in the pack and activator type. For low activity packs, the surface

concentration is constant throughout the aluminization process, where the gas and

metal phase chemical reactions occur rapidly enough to maintain equilibrium at the

surface. In this case, the rate controlling behavior of mass deposition is dominated by solid state diffusion.

In high activity packs, the pack is incapable of delivering Aluminum rapidly enough to the surface. The interdiffusivity of the outer most aluminum-rich phase is more diffusive and equilibrium surface composition does not exist at the interface. The pack is incapable of delivering Aluminum rapidly enough to the surface to maintain this equilibrium; therefore, the surface concentration will change over the course of aluminization. [14] In this case, the rate controlling behavior of mass deposition can be dominated by both vapor phase and solid state diffusion. [43]

2.1.3 Aluminization Experiment

The pack mixture used in this experiment consisted of 15%-2%-83% wt. mixture, similar to the pack mixture used in the experiment by Das, Singh, and Joshi. [12]. 15 % aluminum was the donor element; 2 % ammonia chloride was the halide activator; and 83 % aluminum oxide was the inert filler.

Aluminum was sourced by cutting aluminum foil into smaller pieces which ranged from hundreds of micrometers to a few millimeters. Powdered aluminum is typically used in these experiments [1] [12][14]; however, powdered aluminum is flammable. Since the operating temperature is above the melting temperature of aluminum (~660 deg C), the dispersion of aluminum throughout the crucible will be assisted by the molten aluminum.

The pack mixture is mixed and filled into a 5mL ceramic crucible; an H-X750 sample is buried completely in the pack mixture and then semi-sealed over the crucible with a ceramic lid. The crucible is lowered into a 26mm inner diameter quartz test tube and held in a vertical tube furnace where a two-step high activity heat treatment is applied for one hour (details of this heat treatment are provided in the following section). During heat treatment, Argon flows through the test tube to provide an inert atmosphere.   Argon flows through a Pyrex glass valve mounted on top of the test tube to supply argon to the reaction chamber and release exhaust gases. An inert atmosphere is important because oxidation poses a safety and fire hazard by combustion of aluminum. Since the quartz test tube and valve are an open system some of the Aluminum halide gas is lost to the atmosphere as well as other gaseous byproducts. Once the experiment is complete, the test tube and crucible are cooled to room temperature, and samples are removed from the mixture.

This experiment was completed for five H-X750 samples of varying thicknesses: a 100 micron sample (sample 5), a 100 micron sample with short heat treatment (sample 4), a 250 micron sample (sample 3), a 400 micron sample (sample 2), and a 600 micron sample (sample 1). The sample area, initial sample mass, final sample mass, and amount of retort used for the aluminization experiment is provided below in Table 3. The scale used to measure the samples was accurate to +/- 0.001 gram.
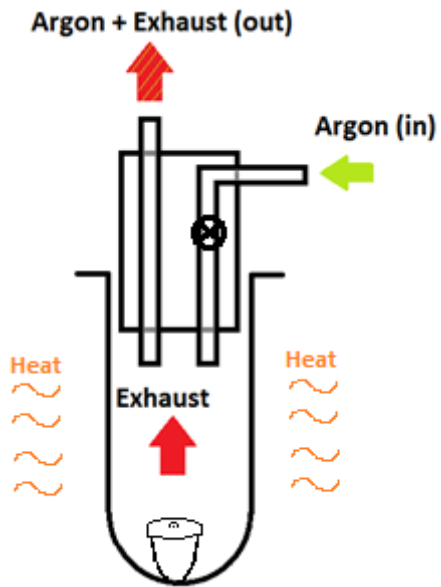
Figure 7: Flow schematic of test tube and valve

Table 3: H-X750 sample mass, and area properties

	Sample				
	5	4	3	2	1
	100 µm	100 µm (Interrupted)	250 µm	400 µm	600 µm
Area (mm^2)	16.31	20.95	8.491	9.150	27.72
Before Mass (g)	0.013	0.019	0.012	0.024	0.152
After Mass (g)	0.031	0.021	0.024	0.039	0.191
Retort (g)	4.666	4.778	3.350	4.022	4.021
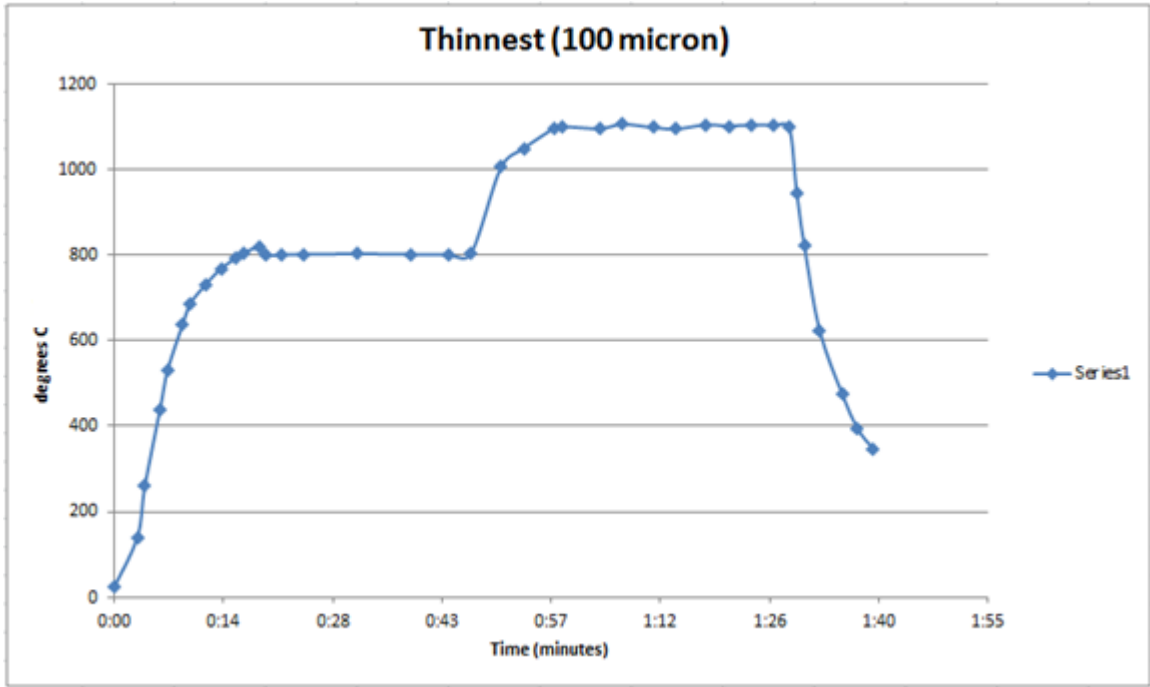
Figure 8: Heat treatment profile sample 5
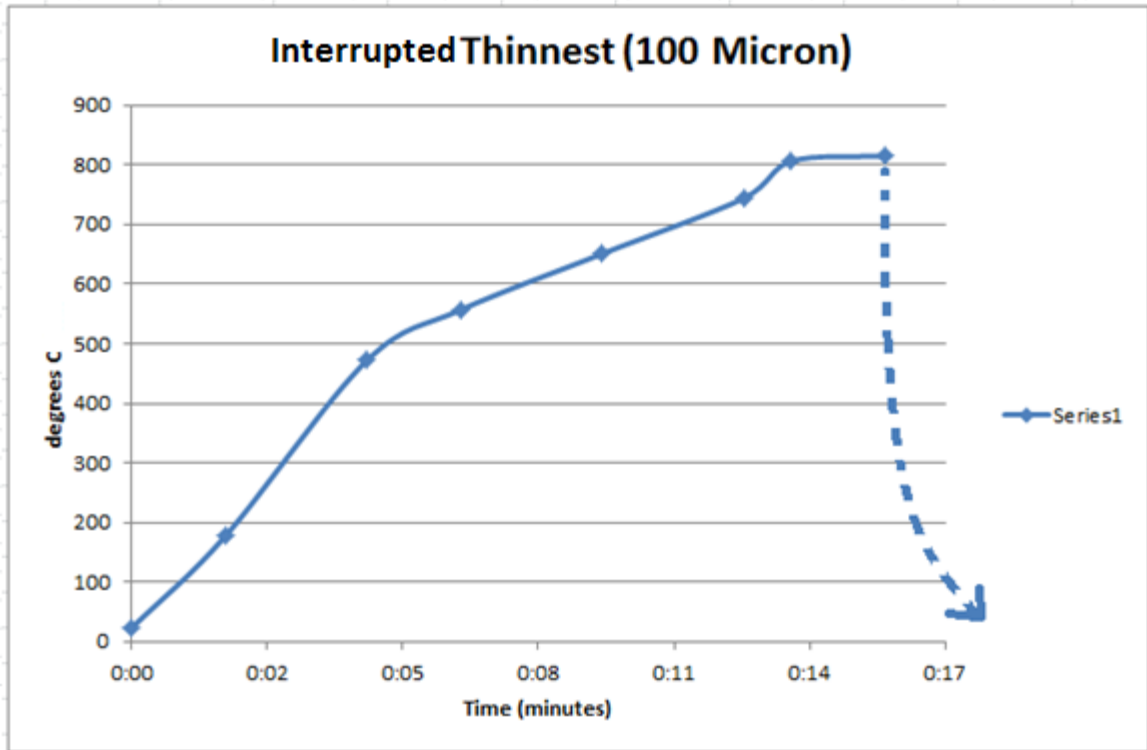
Figure 9: Heat treatment profile for sample 4, cooling curve estimated
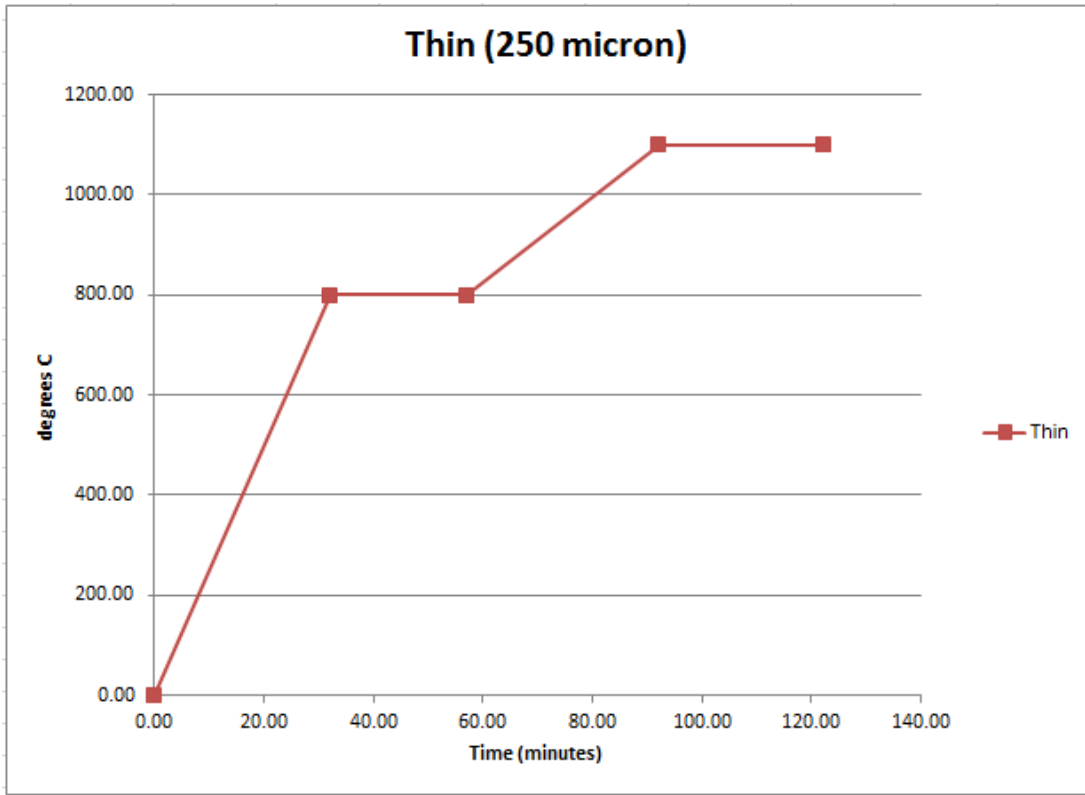
Figure 10: Heat treatment profile for sample 3
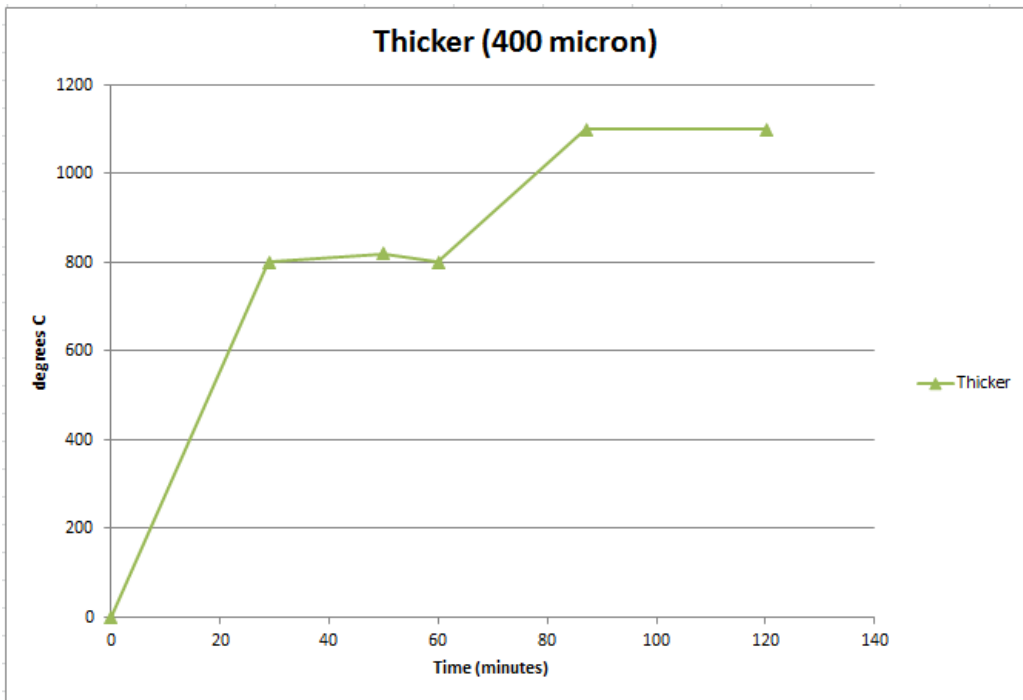
Figure 11: Heat treatment profile for sample 2
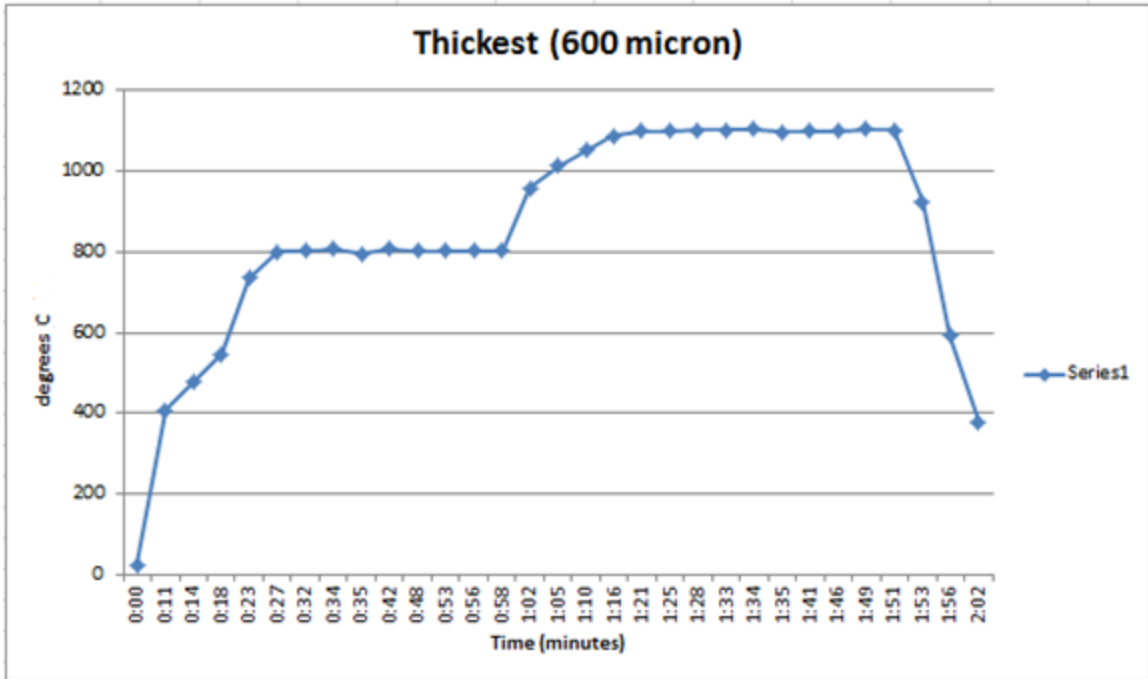
Figure 12: Heat treatment profile for sample 1

2.1.4 Low Activity and High Activity Vapor Phase Aluminization

Low activity donor element mixtures were investigated, but not performed. For mixtures to be low activity, the aluminum content in pack must be less than 60% Al at. 60 percent is significant corresponding to the Ni-Al phase diagram that partitions (δ) Ni_2Al_3 and a two-phase mixture of (δ) Ni_2Al_3 and hyperstoichiometric (β) NiAl. A low activity process results in only an outward diffusion of nickel. Hypostoichiometric (β) Ni-Al will form at the substrate surface while no (δ) Ni_2Al_3 will form. Low activity processes are normally done with a single step high temperature treatment (1000-1200 deg C). [16]
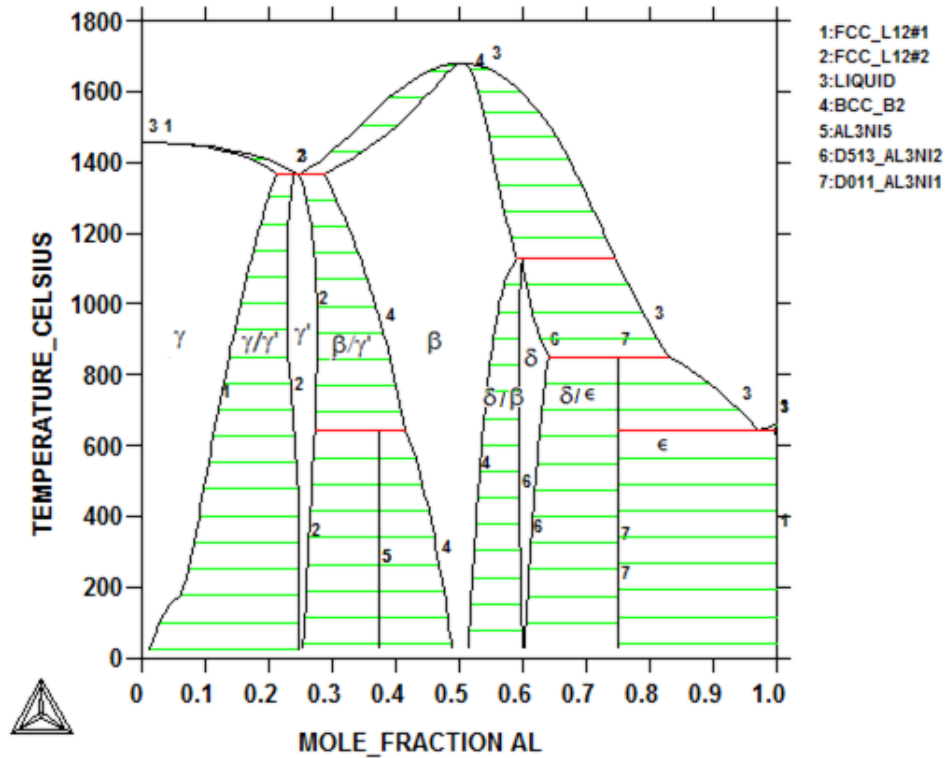
Figure 13: Ni-Al Phase Diagram

For high activity pack mixtures, the aluminum content must be greater than 60% Al at.

This results in an inward diffusion of aluminum followed by an outward diffusion of

nickel. The process is conducted as a two-step process; however, it can be conducted as

a single step process as suggested by Das et al. [12]   The two-step process is conducted

at a low temperature (~800 deg C) for 30 minutes followed by a high temperature heat

treatment (~1100 deg C) for 30 minutes to convert the microstructure to a state suitable

for coating. The high temperature treatment is to thicken the layer of (β)–NiAl and

decompose (δ)-Ni_2Al_3 into a phase field containing (δ)-Ni_2Al_3 and (β)–NiAl.

For a single step process, the treatment is done as a single heat treatment above 1000 deg C. Both single step and two step high activity aluminization processes form similar coating structures, but coating thicknesses are larger for the two step process. [12]

2.1.5 Boundary Layer Movement for Different Aluminization Heat Treatment Processes

The boundary layer movement is different for a two-step high activity process, a single step high activity process, and a single step low activity process.

The low temperature heat treatment is characterized by a predominant inward flux of Aluminum which penetrates the surface creating a phase field of (δ & β) into the alloy. Outward movement of the initial substrate surface (ISS) is smaller than the penetration of the reaction front of the outward grown (β) NiAl layer (RFON) and the reaction front of the inward grown (β) NiAl layer (RFIN). The RFIN moves slightly faster than the RFON making the thickness of (β) thinner than the outermost (δ & β) coating. During this heat treatment, less than or equal to 67 percent of the aluminum pickup for the entire aluminization process is achieved. [12]   A finite difference solution for this process can be viewed in figure 40 (a, b, c, & d).

The high temperature heat treatment is characterized by less mass pickup and a simultaneous inward flux of Aluminum and outward flux of Nickel, similar to partial homogenization. The base nickel reacts with the outer aluminum rich coating similar to a high temperature low activity process.   The RFON moves toward the surface while the RFIN is slow in comparison. The effect thickens the intermediate layer of (β).

Because of the high diffusivity of (δ) and less mass pickup, the gradient in the outer-most layer disappears. The finite difference solution for this process can be viewed in Figure 42 (b & c).

For a single step high activity aluminization process, the treatment produces the same diffusion coatings as a two-step high activity process by an inward flux of Aluminum following an outward flux of Nickel. The layer sequence is the same; however, the thicknesses of (δ & β) and (β) are smaller for a single step process.   For one half-hour of heat treatment, the mass pickup from a single step process is approximately equal to 67 percent of the total mass pickup. [12]

2.1.6 Substrate Carbides, Kirkendall Porosities, and Impurities

In either a single step or two-step high activity process, substrate carbides may remain in (δ & β) indicative of the initial inward diffusion of aluminum, but do not dissolve. These carbides do not exist in the (β) phase because this layer precludes any possibility of the presence of these carbides. [12]

For high activity processes, impurities and cement particles do not penetrate the substrate surface. Particles adhering to the surface remain there before and after aluminization because the formation of new phase takes place between nickel and the already formed compound; therefore, there is no Kirkendall effect which brings impurities into the substrate in high activity processes. [26]

For a low activity process, the aluminization treatment is conducted as a single high temperature heat treatment. The process is achieved exclusively by an outward flux of Nickel growing a layer of (β) outwardly at the surface. This is slightly different for nickel and nickel-base superalloy due to Kirkendall porosities formed behind the ISS in pure nickel. [26] Often, nickel-base superalloy contain significant amounts of Aluminum (3 to 6%) compared to the case of pure nickel. For nickel-base superalloy, an outward zone of (β) is grown by the outward flux of nickel the same way in pure nickel; but, a more aluminum rich internal zone of is also formed by the outward flux of nickel. This internal zone is rich in elements that constitute the alloy. Kirkendall porosities are generally absent in nickel-base superalloy because there is less nickel transported in nickel-base superalloy than in pure nickel.

For a low activity process using both pure nickel and nickel-base superalloy, impurities and cement particles become embedded in coating. Because nickel exclusively diffuses outward in (β), particles and other impurities already in contact with the surface become entrapped to the bonded surface. Small amounts of cement particles eventually dissolve following a long homogenization slightly changing the composition of the alloy. Embedded impurities are dangerous because they favor spalling of protective coatings during thermal cycling. For low activity processes, cleaning the surface prior to aluminization is critical to having alloy components of good quality. [26]

2.2 H-X750 Phase Diagram

The H-X750 binary phase diagram reveals what phases will be present when the alloy and its aluminum coating transition to the steady state. While aluminization treatment adds mass and cultivates aluminum rich coatings on the alloy surface, the homogenization treatment transitions the diffusion couple from (γ) + the aluminum rich coating to a homogenous binary or tertiary alloy by adding no external mass. The nature of the aluminization and homogenization diffusion processes are primarily contributed by activities and diffusion coefficients of aluminum and nickel. Other major alloying elements like Fe, Cr, and C are involved secondarily to the diffusion process [5]

By knowing the mass added to the sample, the steady state profile can be determined. For H-X750 alloy, this transition from (γ) to (γ/γ') occurs at 3 percent wt. Aluminum for 1000 deg. C (figure 14). [1] The phase change to ($\gamma/\beta/\gamma'$) occurs at 10 percent for 1000 deg. C (figure 16). Further adding aluminum to 20 percent will change the alloy composition to mostly (β) for 1000 deg. C (figure 17). It is important not to add too much aluminum because formation of (β) is incoherent with (γ/γ') and will create brittleness in the alloy. Table 4 predicts the steady state for the samples in this experiment assuming no physical change is made to the aluminized alloy.

Table 4: Predicted sample steady state

	Sample				
	100 μm	100 μm (Interrupted)	250 μm	400 μm	600 μm
Before Mass (g)	0.013	0.019	0.012	0.024	0.152
After Mass (g)	0.031	0.021	0.024	0.039	0.191
Change	>35%	10%	>35%	>35%	22%
As is steady state	(δ/β)	(γ/γ′)	(δ/β)	(δ/β)	(β)

Phase diagram. Al concentration VS Temperature
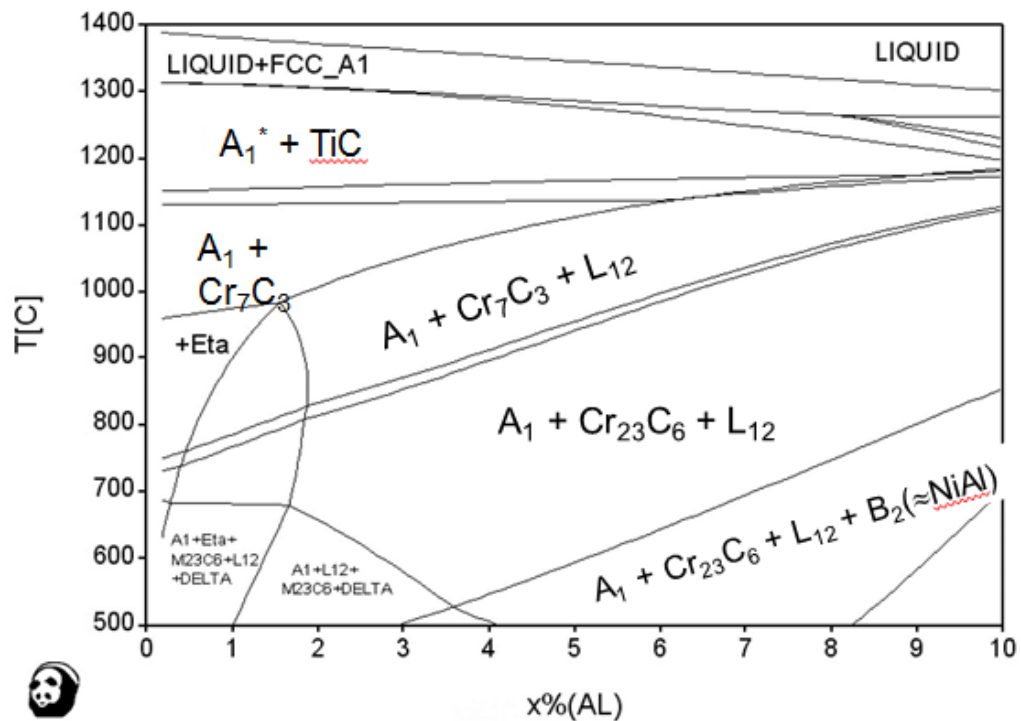
* A_1 – disordered Ni-based FCC solid solution
  L_{12}/B_2 – ordered FCC/BCC phase ($\approx$ Ni3Al / NiAl)

Figure 14: Pandat binary phase diagram for X-750

Phase diagram. Nominal composition.

Al	Ti	Fe	Nb	Cr	Co	Mn	Si	C	Ni
0.08	2.50	8.00	1.00	16.00	1.64	0.35	0.35	0.08	70.00
0.17	2.96	8.13	0.61	17.46	1.58	0.36	0.71	0.38	67.64
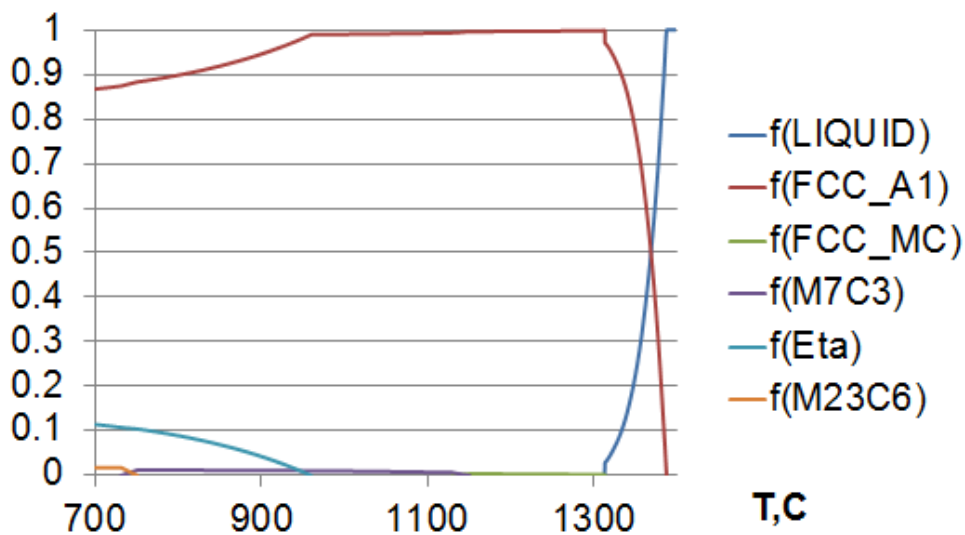
Figure 15: Temperature - Composition diagram for γ-X750

Phase diagram. 5 wt. % Al

Al	Ti	Fe	Nb	Cr	Co	Mn	Si	C	Ni
5.00	2.40	7.60	0.95	15.20	1.56	0.33	0.33	0.08	66.55
9.97	2.70	7.32	0.55	15.73	1.42	0.32	0.63	0.34	61.02
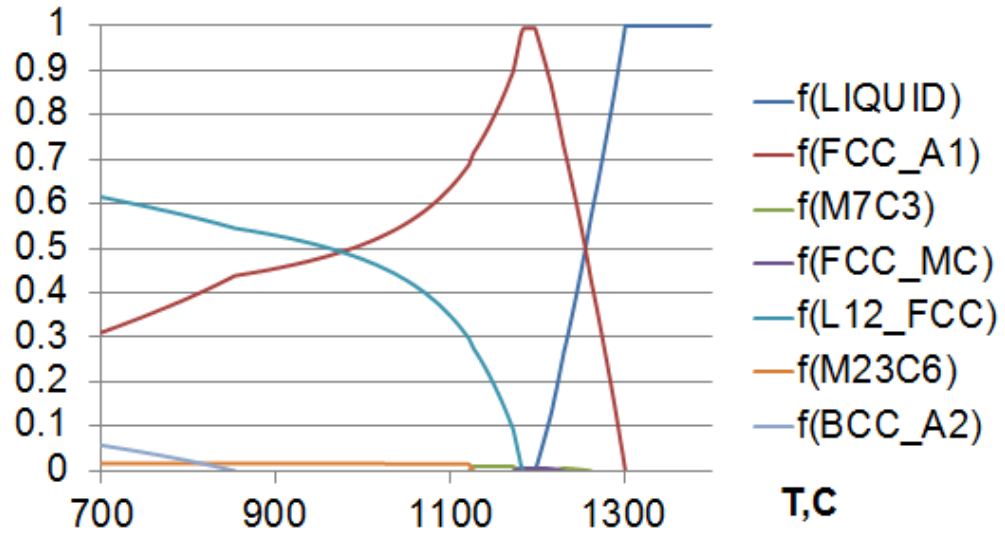
Figure 16: Temperature - Composition diagram for γ/γ'-X750

Phase diagram. 10 wt. % Al

Al	Ti	Fe	Nb	Cr	Co	Mn	Si	C	Ni
10.00	2.25	7.20	0.90	14.40	1.48	0.32	0.32	0.07	63.07
18.95	2.40	6.59	0.50	14.16	1.28	0.29	0.57	0.31	54.95
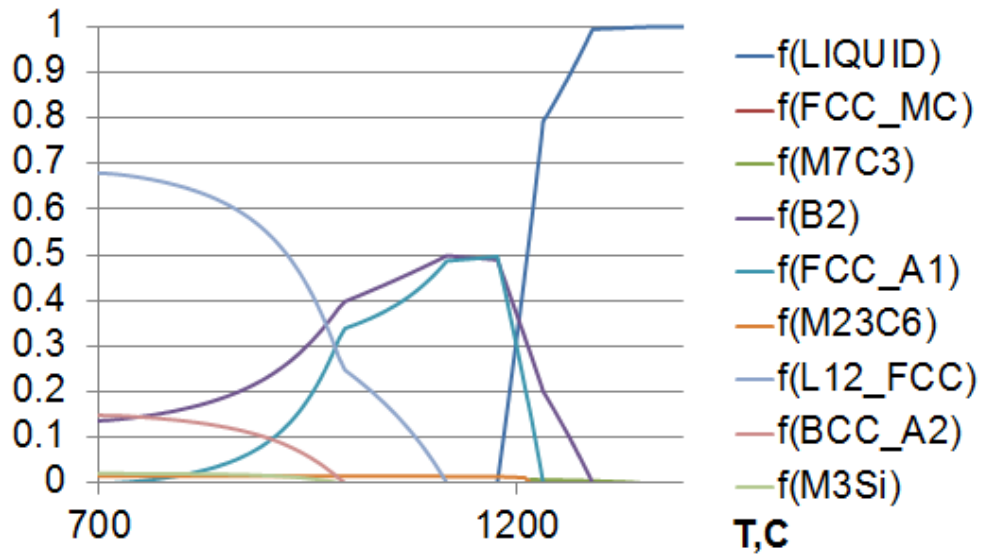
Figure 17: Temperature - Composition diagram for β/γ/γ'-X750

Phase diagram. 20 wt. % Al

Al	Ti	Fe	Nb	Cr	Co	Mn	Si	C	Ni
20.50	2.00	6.40	0.80	12.70	1.30	0.28	0.28	0.06	55.68
35.17	1.93	5.31	0.40	11.31	1.02	0.24	0.46	0.25	43.91
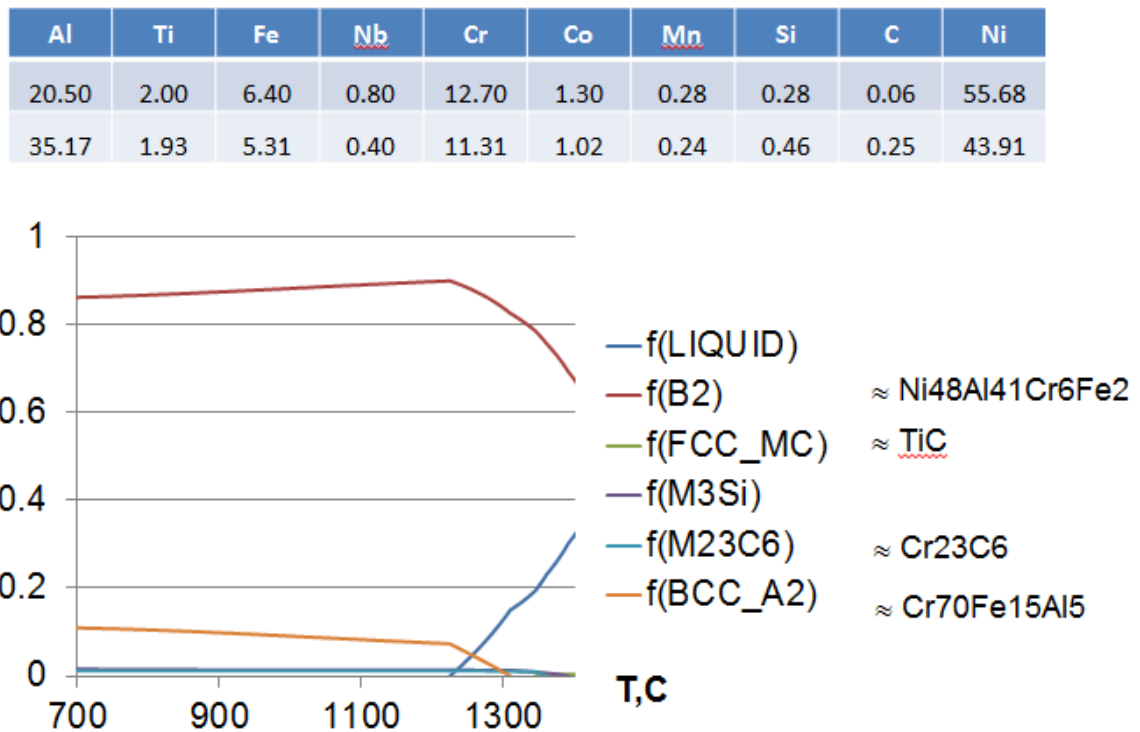
Figure 18: Temperature - Composition diagram for β rich-X750

2.3 Scanning Electron Microscopy Preparation (Molding, Curing, Grinding, and Polishing)

The samples were held between glass slides with rapid curing Beuhler Epothin consisting of 10 parts epoxy resin and 4 parts epoxy hardener by weight. A mount was created by pouring a low temperature (40 deg C) overnight curing epoxy Struers Epofix consisting of 25 parts epoxy resin and 3 parts hardener into a 1'' die. After it was finished curing, the mold was removed from the die. The samples inside the mold were ground with a 220 grit grind wheel and ultrasonically cleaned. The samples were again ground using a

grinding and polishing machine (Struers Labopol-5) with a 9 micrometer, 3 micrometer, and 1 micrometer grind wheel and polished with the wheel's appropriate diamond paste. The mold was then carbon coated using a vacuum thermal evaporator Edwards Auto 306 for preparation in the Scanning Electron Microscope.

2.4 Aluminization Results

The aluminization samples were observed with Scanning Electron Microscopy (SEM) using a Zeiss EVO 50 equipped with Bruker EPMA. The elemental composition was determined from EDS analyzed with Bruker Esprit.

Sample 1: Initial thickness, 600 μm; Final thickness, 710 μm

There was a salient distinction between the outer aluminum rich coating and the base alloy in sample 1. One side appeared like the coating partially homogenized, while the other side appeared like the coating was still aluminizing. For both sides, the aluminization treatment produced a 96.89 micrometer thickness of the outer most aluminum-rich phase ($\delta + \beta$). The inner aluminum-rich phase was harder to contrast, but its thickness was estimated as 34.11 micrometer (β). It should be noted that the aluminum rich coating thickness was remarkably similar to the thickness of the H-X750 sample in the aluminization experiments conducted by Perez-Bergaquist [1].
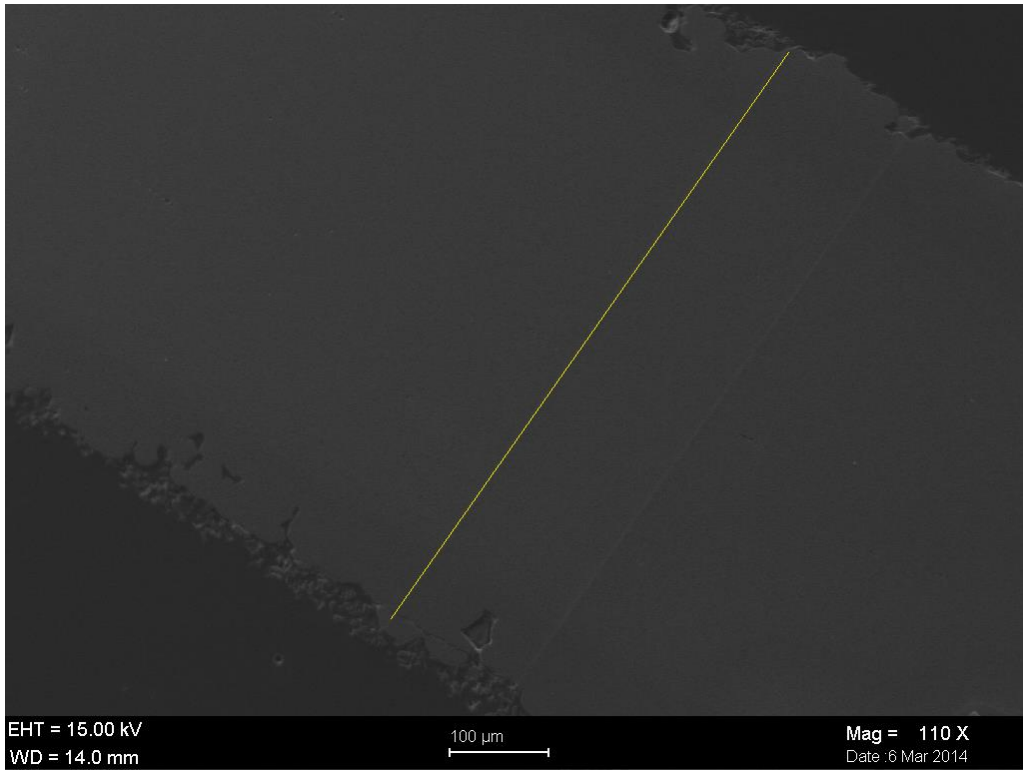
Figure 19: SE Image for the cross section of Sample 1
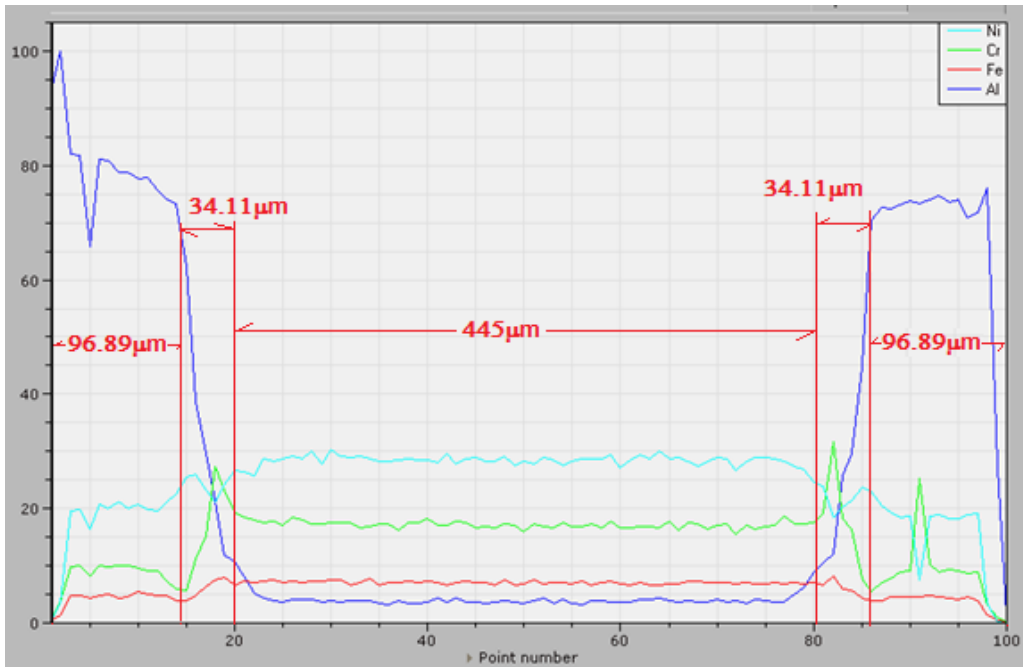
Figure 20: Bruker Line Analysis for the cross section of Sample 1

Sample 2: Initial thickness 400 μm; Final thickness 901.11 μm

The aluminum rich coating penetrated through the entire thickness of the sample.

There were no distinct aluminum rich coating phases like those from sample 1. Grain

boundaries appeared to emerge from the sample, while the sample maintains mostly

uniform phase consistency. The grains ranged in size from 20 micrometer to 100

micrometers.
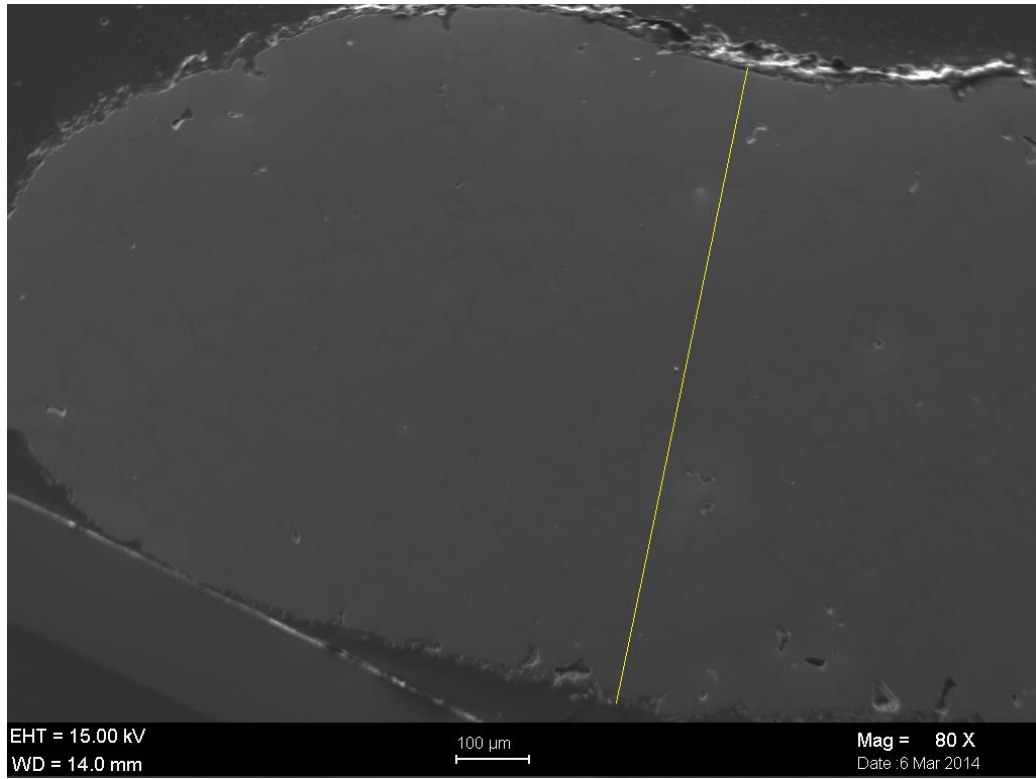
Figure 21: SE Image for the cross section of Sample 2
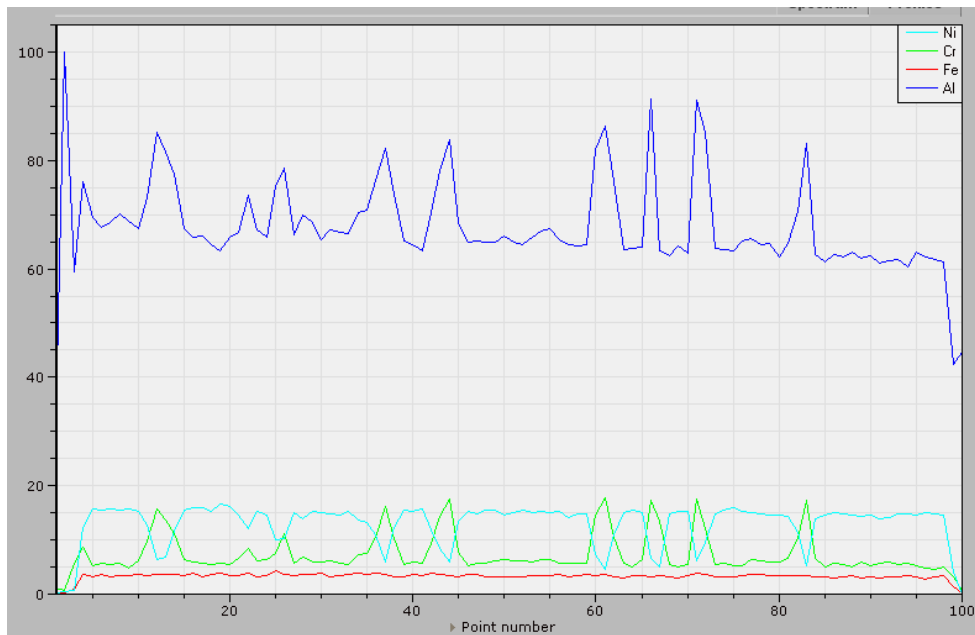
Figure 22: Bruker Line Analysis for the cross section of Sample 2

Sample 3: Initial thickness250 μm; Final thickness 729μm

The aluminum rich coating penetrated through the entire thickness of sample 3. In this sample, the grain boundaries were more prominent. The line profile showed sharper spikes in aluminum across the cross section; the thickness increased more from its original size, which was evidence that more aluminum was added to the substrate with respect to its original mass than Sample 2.
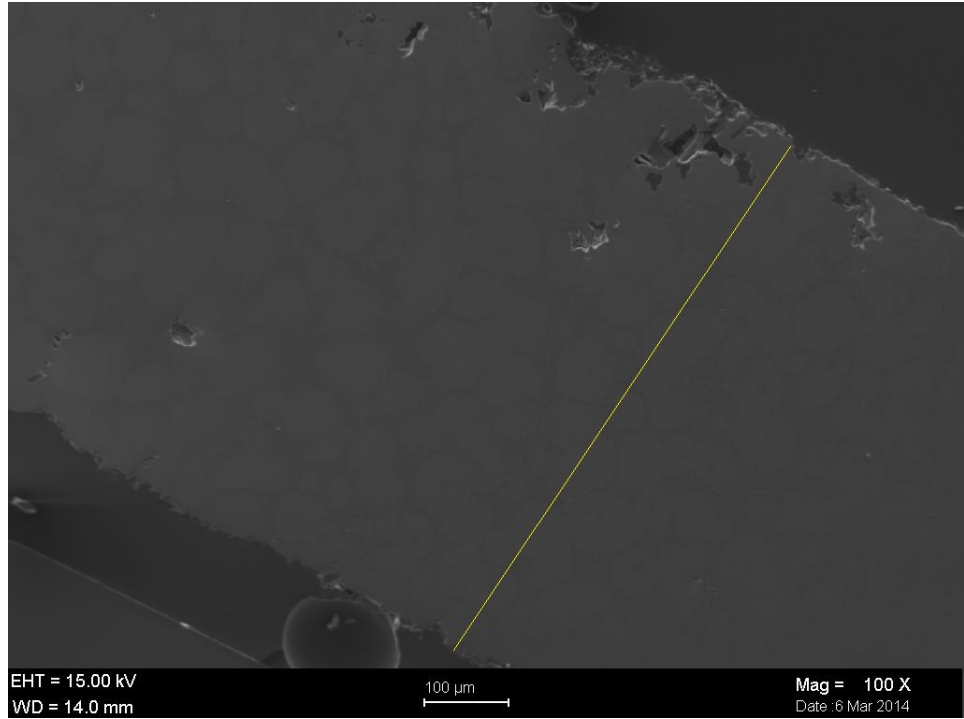
Figure 23: SE Image for the cross section of Sample 3
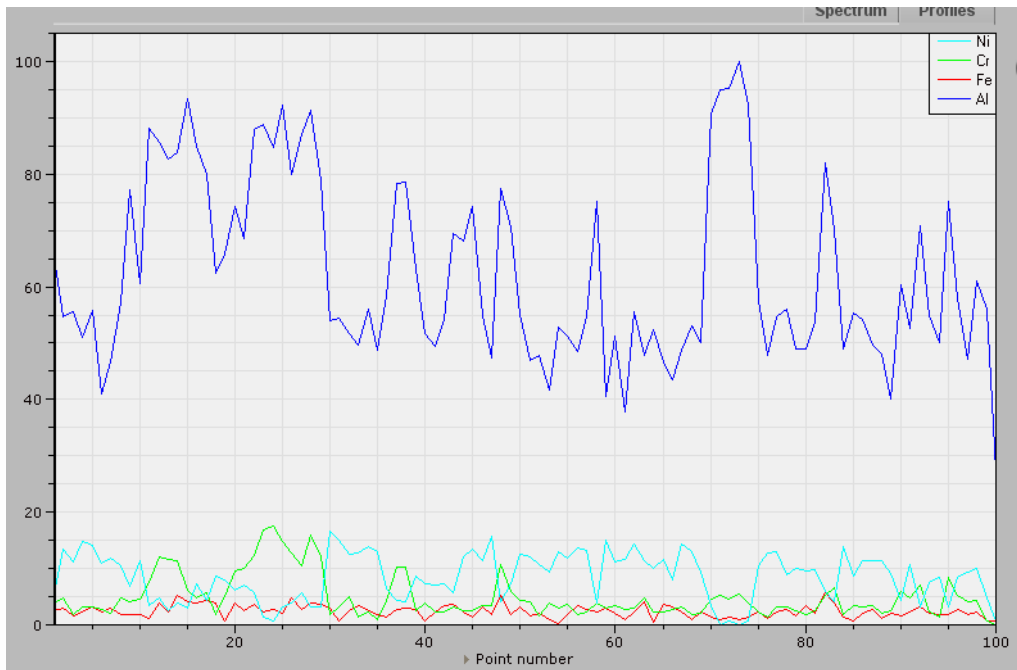
Figure 24: Bruker Line Analysis for the cross section of Sample 3

Sample 4: Initial thickness 100 μm; Final thickness 123.5μm

The short aluminization time sample 4 experienced was enough to produce an

aluminum rich coating. The concentration profiles were lopsided for one side of the

sample versus the other side. Because there was high temperature treatment in the

two-step high activity process, neither side was partially homogenized.
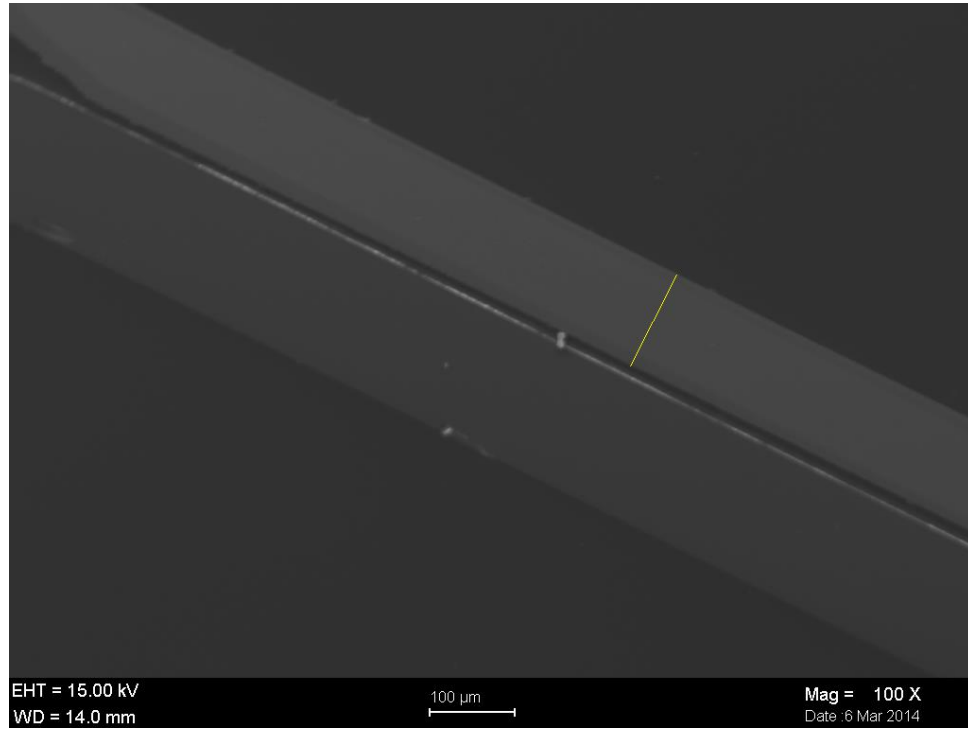
Figure 25: SE Image for the cross section of Sample 4
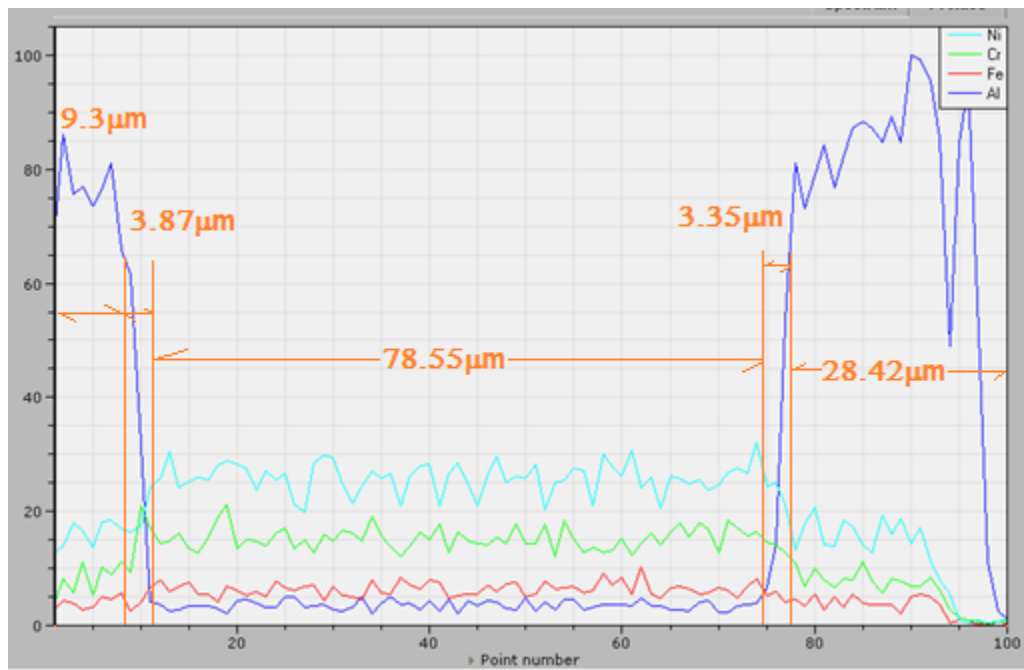
Figure 26: Bruker Line Analysis for the cross section of Sample 4

Sample 5: Initial thickness 100 μm; Final thickness 436 μm

Sample 5 had the lowest nickel, chrome, and iron out of all the samples where the

thickness more than quadrupled in size.   Opposed to grain boundaries forming,

dendrites appear to be growing in the sample as a result of the aluminization. More

aluminum was added to this sample per its original mass than any of the other samples.
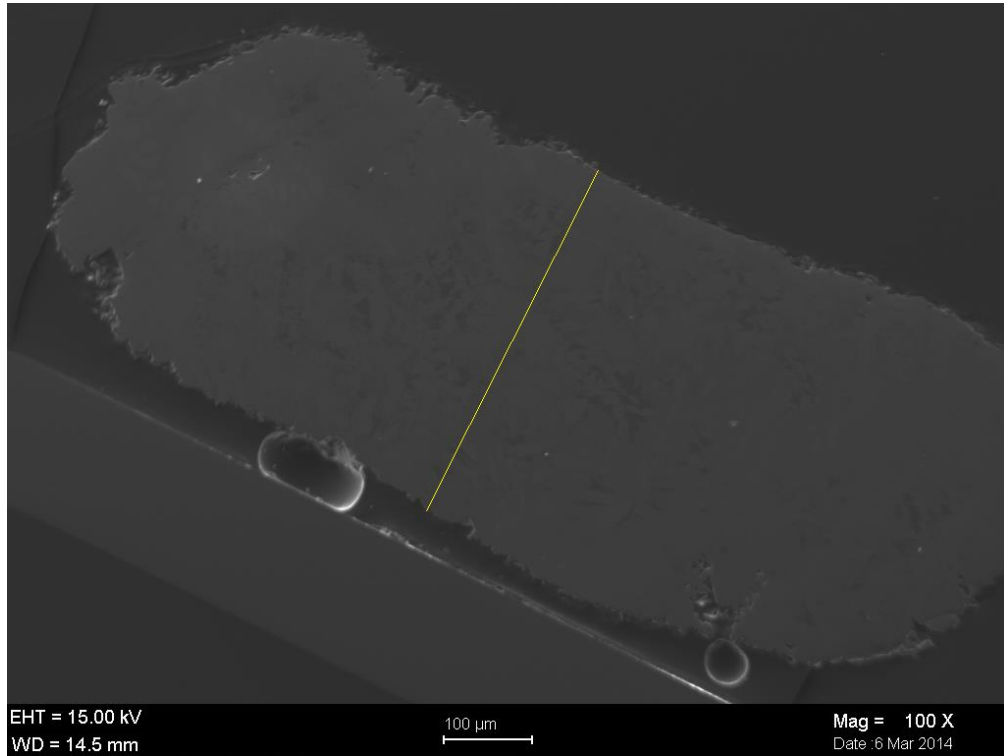
Figure 27: SE Image for the cross section of Sample 5
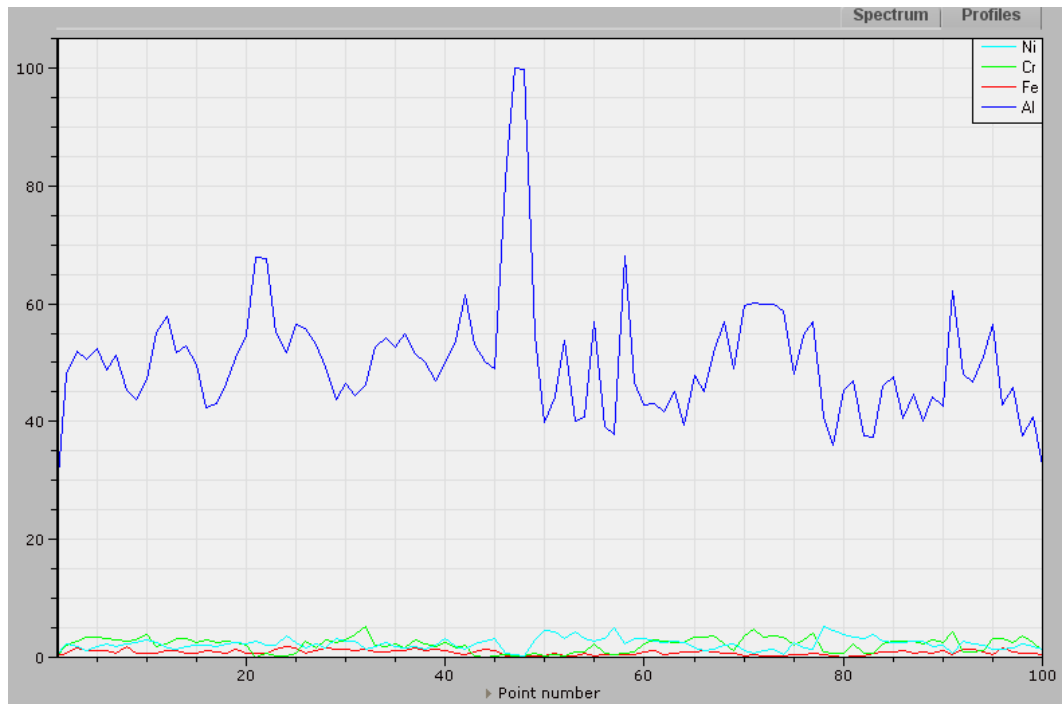
Figure 28: Bruker Line Analysis for the cross section of Sample 5

2.5 Aluminization Discussion

Due to the penetration of aluminum-rich alloy through the entire thickness, Samples 2, 3, and 5 were rejected from any further analysis. A long diffusion would have little effect producing the ideal (γ/γ') microstructure because too much aluminum has penetrated the alloy. Since Samples 1 and 4 may potentially possess a (γ/γ') steady state a long diffusion analysis was performed for these two samples. The long diffusion process for Sample 1 is discussed in Chapter 5 and Sample 4 in Chapter 6.

CHAPTER 3

PROPERTIES OF ALUMINUM-RICH COATINGS

3.1 Properties of Aluminum-Rich Coatings

The bonded aluminum-rich diffusion coatings created by pack cementation have different physical properties than that of (γ) matrix like crystallography, density, and diffusivity. This chapter will discuss these properties and explain why it is important. The higher stoichiometric aluminum rich coating ($\in$) will not be discussed because it does not form during aluminization as it is unstable at high temperatures.

3.1.1 Crystallography

The crystallography of Ni-Al alloys are either face centered cubic (FCC) or body centered cubic (BCC) structures. (γ), (γ/γ'), and (γ') substrate are all face centered cubic (FCC) crystal structures from room temperature to its melting point and (β) and (δ) are both body centered cubic (BCC).

(γ) is Nickel-rich. It is FCC and a disordered phase. It forms a continuous matrix where other phases and transition elements reside and has a single lattice parameter.

(γ'), Ni_3Al is FCC and an ordered $L1_2$ precipitate phase, which is coherent with (γ) and rich in elements like Titanium, Aluminum, Tantalum, and Niobium. It has a single lattice

parameter and four elements per unit cell where aluminum atoms lie in the corners and nickel atoms lie on the faces.

Overall strengthening increases with greater volume fractions of (γ'). Strengthening is primarily attributed to precipitation hardening from strong pair coupling and weak pair coupling, and to a lesser extent solid solution strengthening, and grain boundary strengthening. (γ') strengthens the material by inhibiting motion of dislocations. Dislocations must travel in pairs through (γ') in order to glide through the crystal whereas a single dislocation can glide through (γ) on its own without traveling in pairs. [1][2]

Stoichiometric (δ) Ni_2Al_3 is a trigonal crystal having two lattice parameters and a varying axial ratio ranging from 1.2096 to 1.2161. The crystal is described as a deformed BCC CsCl structure having five atoms per unit cell: three aluminum atoms and two nickel atoms. (δ) is brittle, segregated, and full of microshrinkage pores. [34] 33 percent of nickel sites are vacant in stoichiometric (δ) Ni_2Al_3, however the vacancies are planar and ordered. Every third sheet of nickel atoms perpendicular to the cube diagonal of the NiAl structure is absent.
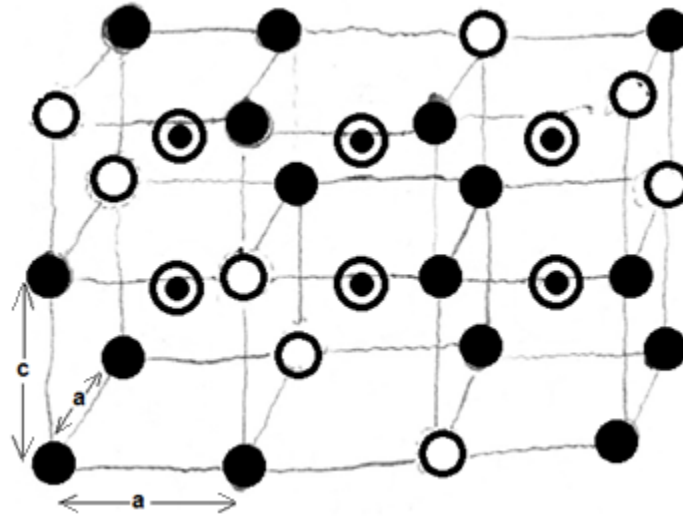
Figure 29 – Ni$_2$Al$_3$ Crystal Structure, Solid is Nickel, Bullseye is Aluminum, Transparent is

vacant

Stoichiometric (β) NiAl is a BCC CsCl type structure having a single lattice parameter and

axial ratio of 1.225. In the unit cell, Nickel atoms occupy the center and Aluminum

atoms occupy cube corners or vice versa. The phase has two atoms per unit cell

consisting of one nickel and one aluminum atom.

Carbides may also reside in matrix, which have the form of M$_{23}$C$_6$, M$_6$C (M - Ni, Co, Cr,

Fe, Ti). Carbides were added during fabrication to control grain size during hot rolling;

they occasionally extend as discontinuous chains in aluminized coatings. Presence of

these carbides can act like natural markers for the motion of the boundary layer that

occurs as a result of diffusion also known as the Kirkendall effect.

Due to the size of the carbon atoms and the carbon coating from the thermo evaporative layer, the presence of carbon in the aluminized samples could not be accurately detected by Energy Dispersive X-Ray Spectroscopy (EDS).

3.1.2 Density

The relationship between density and the concentration of Aluminum for Nickel rich Ni-Al alloy is linear. When the concentration becomes Aluminum rich, a discontinuity occurs in the density diagram. For hyperstoichiometric (β), increasing Nickel fits the same amount of atoms into a smaller lattice. In the unit cell, Aluminum sites are simply replaced by Nickel sites. For hypostoichiometric (β), the cubic structure becomes increasingly anti symmetric. Nickel sites are not simply replaced by Aluminum, but are replaced by vacancies as well.

Evidence of this was shown by Taylor [34]. The observed density and calculated density deviated in hypostoiciometric regions of (β) NiAl due to the replacement of Nickel sites with vacancies.

(13)
$$\rho \ (calculated) = \frac{nM}{Na^3}$$

(n) is the number of atoms per unit cell, (N) is Avagadro's number

(a) is the lattice parameter, and (M) is the atomic weight.

Table 5: Observed Density vs. Calculated Density for (β) NiAl [34]

Al At. %	Lattice (Å)	Ob. Density (g/cm^3)	Calc. Density (g/cm^3)	# atoms/cell
39.9	2.8581	6.5	6.5	2.00
42.3	2.8646	6.4	6.35	2.01
45.5	2.8726	6.16	6.16	2.00
46.8	2.8766	6.07	6.07	2.00
48.55	2.8799	5.95	5.97	1.99
50.21	2.8812	5.91	5.90	2.00
50.42	2.8814	5.90	5.89	2.00
51.1	2.8789	5.88	5.87	2.00
51.6	2.8750	5.76	5.88	1.96
53.4	2.8668	5.52	5.84	1.89
54.75	2.8615	5.35	5.82	1.84

The graph below shows points on the Ni-Al density diagram taken from two sources in literature [34][60] as shown by dots in blue. Gaps in the diagram were replaced by interpolated points shown by the dots in red. On the Nickel side, the graph shows continuity, but is disrupted on the Aluminum side from site replacement by vacancies. The equation for the two linear lines is provided by equation 14 and 15.
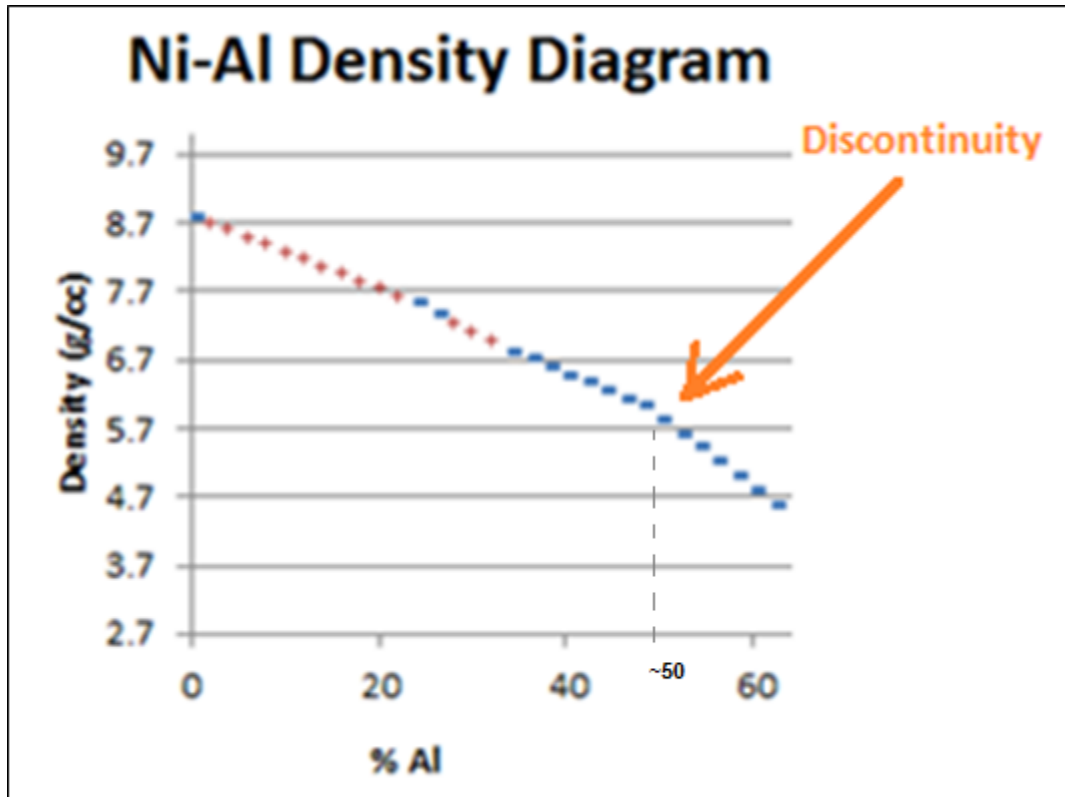
Figure 30: Ni-Al density diagram

(14)
$$\rho \left(\frac{g}{cm^3}\right) = 0.1048C + 0.5984 \; for \; 38\% < C < 50\% \; Nickel$$

(15)
$$\rho \left(\frac{g}{cm^3}\right) = 0.0575C + 3.0325 \; for \; C > 50\% \; Nickel$$

3.1.3 Diffusivity, Self-Diffusivity, and Interdiffusivity

3.1.3.1 Diffusivity

Diffusivity relates the flux or the number of atoms crossing a unit area per unit time and

its concentration gradient for a migrating species in a homogeneous solution. It is a

proportional constant dependent on temperature by the Arrhenius relationship and has units in [length]^2 [time]^-1

3.1.3.2 Self-Diffusivity

Self-diffusion is the diffusion coefficient when the chemical potential gradient is zero. It can be measured by tracking isotopes of the same material assuming that there is no difference in diffusive effect between the trace isotope and stable isotope. For FCC and BCC alloys, self-diffusive jumps occur mostly by the vacancy mechanism because it takes the least amount of energy to move from site to site. During aluminization, site migration occurs less frequently by the interstitial mechanism in BCC alloys and less frequently by the interstitialcy mechanism in FCC alloys. Even though there are more sites to migrate, the interstitial and interstitialcy self-diffusion activation energies are large.

These atomic jumps are described by Brownian motion. The atoms migrate stochastically at the angstrom level, but are continuous at the macroscale. The attempt frequency for these atomic jumps (v) is a function of the harmonic constant (β) and mass of the migrating atom. In theory, the harmonic constant (β) has some temperature dependence.

(16)
$$v = \frac{1}{2\pi}\sqrt{\frac{\beta}{m}}$$

3.1.3.2.1 Site Migration in FCC

For an FCC structure there are 12 nearest neighbors; the nearest neighbor distance is:

$\frac{a}{\sqrt{2}}$. Site migration occurs along [110], but is nonrandom, which compels the diffusion of

vacancies to be uncorrelated. For a tracer atom when there is a vacancy jump, the

second jump will most likely return the tracer atom to its original place as opposed to

jumping into another neighboring vacancy or waiting for another vacancy to arrive.

(17) $$\Gamma = 12\Gamma'$$

(18) $$\Gamma' = v e^{\frac{S^m}{k}} e^{\frac{-H^m}{kT}}$$
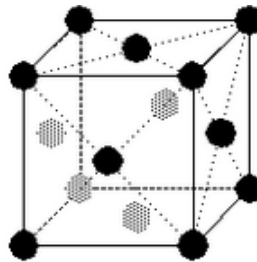
Figure 31: Atomic sites in an FCC crystal

To complete the jump, the vacancy defect must initially be formed, and the atom must

exceed the energy barrier for particle jumping. The jump frequency (Γ) forms the basis

for the entropy and enthalpy of migration.

The entropies of formation and migration in the diffusion equation are represented by

(D°). The activation energy is represented by the sum of the enthalpy of formation and

migration (H^m and H^f). On a wide scale, the vacancy mechanism in FCC crystal shows

diffusive behavior by having characteristics of the Arrhenius diffusion equation 22.

(19)
$$D_V = \frac{\Gamma r^2}{6} = \frac{\Gamma a^2}{12}$$

(20)
$$XD_V = e^{S^f/k}e^{-\frac{H^f}{kT}}\frac{\Gamma a^2}{12}$$

(21)
$$D_v^* = \frac{X\Gamma a^2 f}{12} = a^2 v D^° e^{\frac{-(H^m+H^f)}{kT}}$$

(22)
$$D = D_0 e^{\left(\frac{-Q}{R*T}\right)}$$

3.1.3.3 Interdiffusivity

For two materials in contact, the first material diffuses into the second material, and the

second material diffuses into the first material. If both materials are completely

miscible, the mixing process will distribute atoms of both materials until the system

reaches an equilibrium state where all atoms are distributed randomly. Interdiffusion

measures the mutual diffusion of two materials simultaneously diffusing into each other

through a membrane.

It is possible to measure interdiffusivity using the Darken equation where $D_{Ni}*$ and $D_{Al}*$ are self-diffusivities of Nickel and Aluminum in a homogeneous Ni-Al alloy. [11], [23], [27], [51].

(23)
$$\tilde{D} = (D_{Ni}{}^*X_{Al} + D_{Al}{}^*X_{Ni})\left(\frac{\partial \ln(a_{Ni})}{\partial \ln X_{Ni}}\right)$$

Interdiffusivities can be determined from concentration profiles by the Boltzmann-Matano technique.   This method can determine the interdiffusivity from a concentration profile where volumes are sufficiently constant.   Any changes in the overall specimen volume must be insignificant. [23]

In order to calculate the integral in the Boltzmann-Matano equation, the origin must be chosen such that the left and right integrals are equal. This position is known as the Matano interface. When $c = c_\infty$, the derivative in the Boltzmann-Matano equation goes to infinity, where the integral goes to zero. Close to these boundaries the method incurs large errors. [22]   The Boltzmann-Matano equation is only moderately accurate; it best approximates at concentrations away from the boundaries. At the Matano interface the interdiffusivity for sample 1 measured was 1.43 x 10^{-13} m^2/sec.

(24)
$$\int_0^{c_\infty} x \, dC = 0$$

(25)
$$\frac{-1}{2t}\frac{dx}{dC}\int_0^{C_1} x \, dC = \tilde{D}_{C=C_1}$$

51
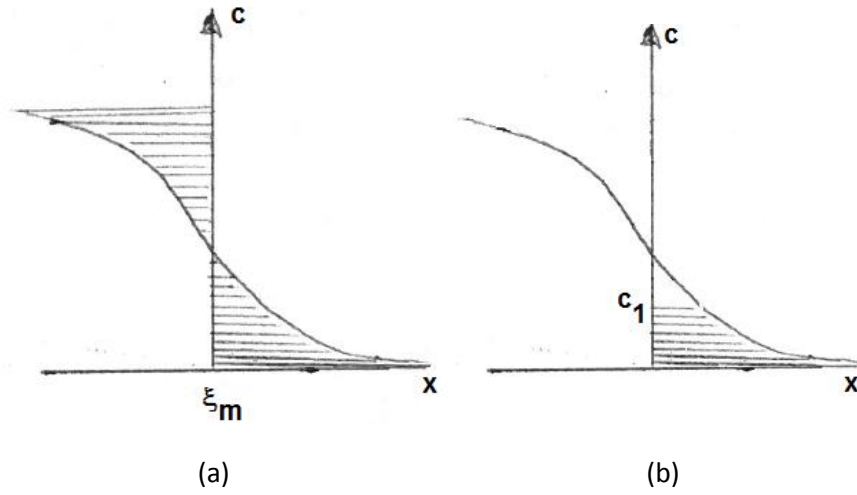
Figure 32: Evaluation of concentration-distance curve using Boltzmann-Matano technique, (a) evaluation of the Matano Interface, (b) evaluation of integral for interdiffusivity at c_1

CHAPTER 4

DIFFUSION ON A WIDE SCALE

4.1 Phase Growth of Bonded Aluminum-Rich Coatings during Aluminization

For both high activity and low activity aluminization, the bonded aluminum-rich coatings are formed by diffusional mechanisms starting at the initial interface between the pack and the substrate surface. Driving forces of diffusion and phase boundary movement are connected to random walks and activated processes discussed from the previous section on site migration, which on a massive scale the statistical nature is described by the diffusion equations for Fick's law. This can be used to understand how bonded aluminum-rich coatings thicken by mass diffusion, develop intermediate phases, and permeate throughout the thickness of the substrate.

4.1.1 Evolution of Bonded Aluminum-Rich Coatings in Aluminization

The evolution of bonded aluminum-rich coatings is characterized by mass diffusion corresponding to mass transfer within each individual phase and mass flux corresponding to boundary movement, phase growth, or phase dissolution.
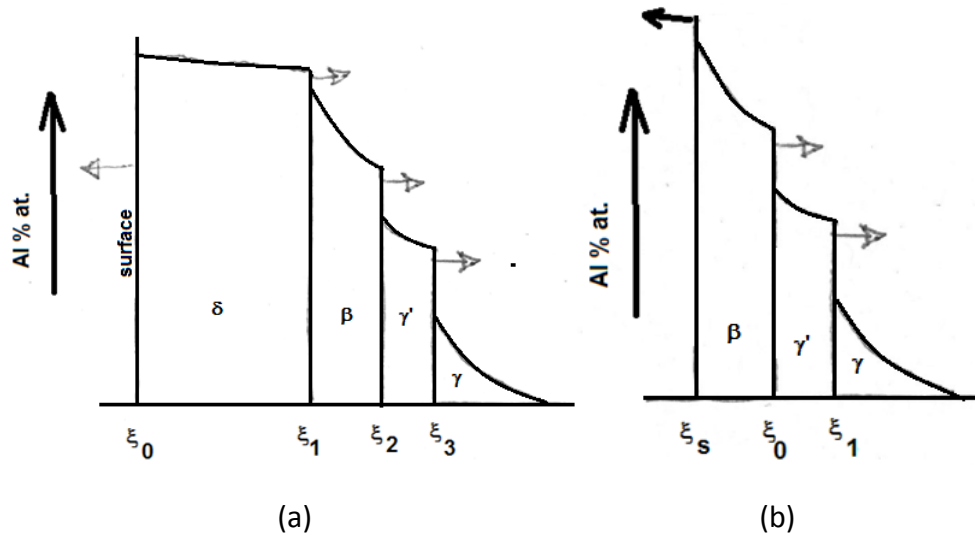
Figure 33: Schematic representation of an aluminum concentration field developed for aluminizing of nickel in (a) a high activity process, (b) a low activity process.

A two phase system is simple and shows the essence of the boundary layer movement behavior and is a good approximation for a low activity process.

For a two phase system, there is a single boundary separating the two phases. The rate at which the concentration field changes within its respective phase is proportional to the second spatial derivative of the concentration field corresponding to Fick's second law.

(26)
$$\frac{\partial C_{Al}}{\partial t} = \frac{\partial}{\partial x}\left(\tilde{D}_\delta \frac{\partial C_{Al}}{\partial x}\right) \; for \; 0 < x < \xi$$

(27)
$$\frac{\partial C_{Al}}{\partial t} = \frac{\partial}{\partial x}\left(\tilde{D}_\gamma \frac{\partial C_{Al}}{\partial x}\right) \; for \; x > \xi$$

Boundary movement behavior is governed by the interaction of fluxes on both sides of

the boundary. The boundary is marked by a discontinuity in concentration gradient

partitioning one phase from another. Velocity of the boundary can be described by the

difference between the fluxes of each phase before the boundary and after the

boundary. The only way a phase boundary is allowed to collide with another phase

boundary is by annihilating the other phase.

(28)
$$\frac{\partial \xi}{\partial t} = \left. \frac{J_\delta|_{x=\xi^+} - J_\gamma|_{x=\xi^-}}{C_{\delta-\gamma} - C_{\gamma-\delta}} \right|_{x=\xi}$$
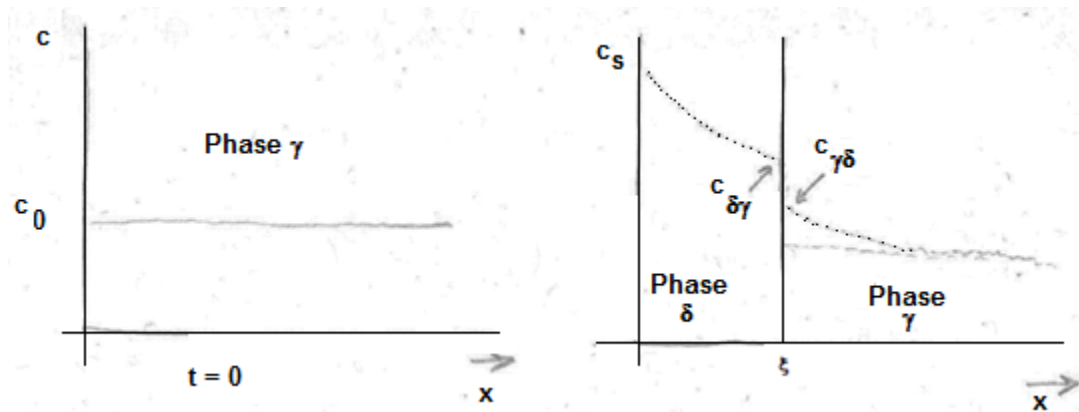
Figure 34: Diffusion in two-phase system (a) concentration in g for t = 0, (b)
concentration in δ (x < ξ) and in phase γ (x > ξ) at t > 0.

The boundary layer movement for a three layer diffusion system is similar to a two layer

diffusion system. In a three layer diffusion system, an intermediate (β) phase forms by

movement of the RFON and RFIN. During aluminization, both the (δ) and (β) phases

continuously grow in this process. During the phase movement, the phase boundary

will move parabolic, stagnant then parabolic, or stagnant. [12]

(29)
$$\frac{\partial C_{Al}}{\partial t} = \frac{\partial}{\partial x}\left(\tilde{D}_\delta \frac{\partial C_{Al}}{\partial x}\right) \; for \; 0 < x < \xi_1$$

(30)
$$\frac{\partial C_{Al}}{\partial t} = \frac{\partial}{\partial x}\left(\tilde{D}_\beta \frac{\partial C_{Al}}{\partial x}\right) \; for \; \xi_1 < x < \xi_2$$

(31)
$$\frac{\partial C_{Al}}{\partial t} = \frac{\partial}{\partial x}\left(\tilde{D}_\gamma \frac{\partial C_{Al}}{\partial x}\right) \; for \; L > \xi_2$$

(32)
$$\frac{\partial \xi_0}{\partial t} = \frac{-J_\delta}{(1 - C_s)}\bigg|_{x=\xi_0}$$

(33)
$$\frac{\partial \xi_1}{\partial t} = \frac{J_\delta|_{x=\xi_{1-}} - J_\beta|_{x=\xi_{1+}}}{C_{\delta-\beta} - C_{\beta-\delta}}\bigg|_{x=\xi_1}$$

(34)
$$\frac{\partial \xi_2}{\partial t} = \frac{J_\beta|_{x=\xi_{2-}} - J_\gamma|_{x=\xi_{2+}}}{C_{\gamma-\beta} - C_{\beta-\gamma}}\bigg|_{x=\xi_2}$$

(35)
$$\frac{\partial \xi_2}{\partial t} \geq \frac{\partial \xi_1}{\partial t} > \frac{\partial \xi_0}{\partial t}$$

Stagnant growth is present at the beginning of the growth of (δ)-Ni$_2$Al$_3$. The time of this

transient period is t_0.   During this transient period t_0, aluminum is building up at the

surface because the alloy is suddenly subjected to an applied surface concentration.

Once it reaches a value of equilibrium, the phase boundary penetrates the surface. [21]

The growth is largely dependent on its own diffusional fluxes and is parabolic.

$$(36) \qquad\qquad\qquad\qquad \xi_i = 2K_i(\widetilde{D}_\delta t)^{1/2}$$

$$(37) \qquad\qquad\qquad\qquad x_\delta = K_T * (t - t_0)^{1/2}$$

4.1.2 Proof of Parabolic Behavior

Proof of this parabolic behavior is found with numerical methods, but also analytically.

The following analytical methods both use two diffusion sources to show this behavior.

The first method involves a short time approximation which uses a method of Laplace

transforms to approximate diffusion at an interface with two real space sources. The

second method involves a long time approximation which uses an arbitrary solution to

calculate diffusion with two mirrored symmetric sources: one in imaginary space and

one in real space.
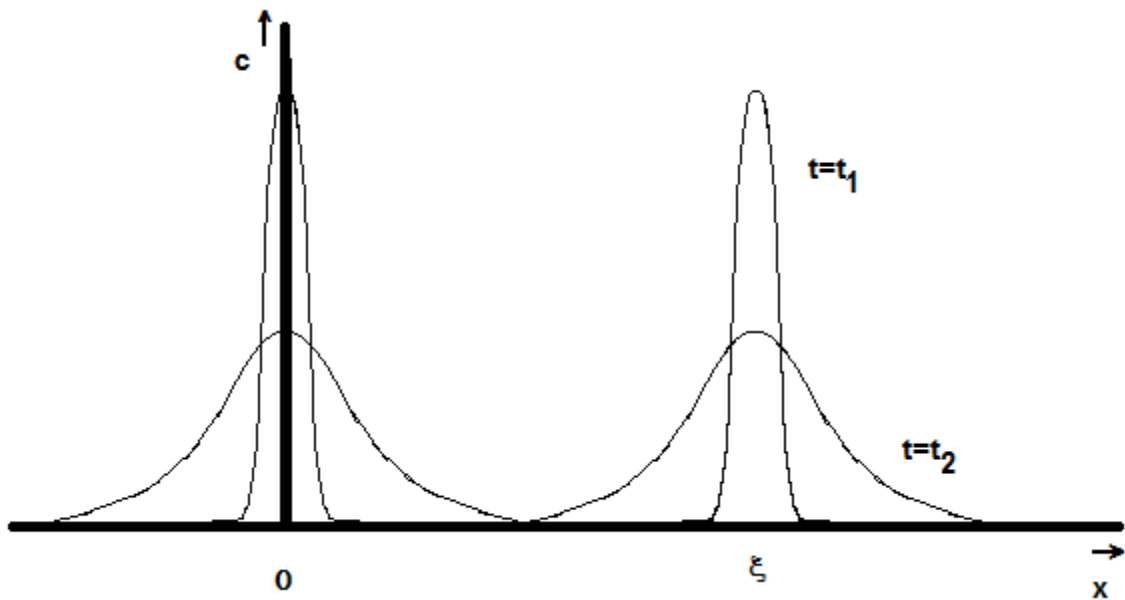
Figure 35: Short time approximation using two sources in real space

For short time approximations, using two sources at $x = 0$ and $x = \xi$, the time dependent concentration field can be approximated. Using a Laplace transform, the time dependent concentration field is transformed to a parameter 'p' dependent concentration field where parameter 'p' is a pseudo time variable with imaginary and real components.   The boundary conditions are transferred from c(x,t) to c_hat(x,p) using a Laplace Transform.

(38)
$$\frac{\partial C}{\partial t} = \frac{\partial}{\partial x}\left(\widetilde{D}_i \frac{\partial C}{\partial x}\right) \; for \; \xi_i < x < \xi_{i+1}$$

(39)
$$\mathcal{L}\left\{\frac{\partial C}{\partial t}\right\} = p\mathcal{L}\{C\} - c(x, t = 0)$$

(40)
$$\mathcal{L}\{C\} = \hat{c}(x,p) = \int_0^\infty e^{-pt} c(x,t) dt$$

The boundary conditions for the source and physical domain is approximated by the following:

(41)
$$c(x = 0, t) = c_0$$

(42)
$$\frac{\partial C}{\partial x}(x = \infty, t) = 0$$

(43)
$$c(x, t = 0) = 0 \ for \ 0 \leq x \leq \infty^{**}$$

Boundary conditions at $x = 0$ and $x = \infty$ form the basis of the solution of the two equations with two unknowns. Since one constant is zero, the pseudo solution c_hat(x,p) can be transferred back to the solution in real time.

(44)
$$\mathcal{L}\left\{\frac{\partial^2 \hat{c}}{\partial x^2}\right\} = \frac{\partial^2 \hat{c}(x,p)}{\partial x^2}$$

(45)
$$q = \sqrt{\frac{p}{D}}$$

(46)
$$\hat{c}(x,p) = a_1 e^{qx} + a_2 e^{-qx}$$

(47)
$$\frac{\partial \hat{c}}{\partial x}(x = \infty, p) = qa_1 e^{qx} - qa_2 e^{-qx}$$

(48)
$$\hat{c}(x, p) = \frac{c_0}{p} e^{-qx}$$

(49)
$$\frac{\partial^2 \hat{c}}{\partial x^2} - \frac{p}{D}\hat{c} = \frac{c(x, t = 0)}{D} = 0$$

(50)
$$\frac{\partial \hat{c}}{\partial x}(x = \infty, p) = 0$$

(51)
$$\hat{c}(x = 0, p) = \frac{c_0}{p} \int_0^\infty e^{-pt} dt = \frac{c_0}{p} = a_1 + a_2$$

(52)
$$qa_1 e^{qx} = 0 \; because \; e^{-q\infty} is \; zero$$

For a single source c_0 at $x = 0$, the solution is the following:

(53)
$$c(x, t) = c_0 erfc\left(\frac{x}{\sqrt{4Dt}}\right)$$

Diffusion of a phase layer at the surface can be approximated by the difference of two sources at $x = 0$ and $x = \xi$. This is valid for $x > \xi$ and $t < \frac{\left(\frac{\xi}{2}\right)^2}{4D}$

(54)
$$c(x,t) = \frac{c_0}{2}erf\left(\frac{x}{\sqrt{4Dt}}\right) - \frac{c_0}{2}erf\left(\frac{x-\xi}{\sqrt{4Dt}}\right)$$

This equation estimates movement of the boundary equation for short times which

closely follows: $\xi \approx \sqrt{2.56Dt}$. For a single layer: $\frac{\partial \xi}{\partial t} = \frac{-D}{1-c_0}\frac{\partial c}{\partial x}$

For longer times, symmetrical sources or mirror sources provide a better approximation

to a semi-finite system. The symmetrical sources must lie beyond the physical domain

and have to obey the boundary condition that $\frac{\partial c}{\partial x} = 0$ at $x = 0$ and $x = L$. If C is an

arbitrary solution, it satisfies the differential equation.

(55)
$$C = \frac{A}{\sqrt{t}}e^{\frac{-x^2}{4Dt}}$$

(56)
$$\frac{\partial C}{\partial t} = \frac{\partial}{\partial x}\left(\tilde{D}_i\frac{\partial C}{\partial x}\right) \ for \ \xi_i < x < \xi_{i+1}$$

The reflection at a boundary satisfies the condition for zero flow at the boundary and is

approximately zero at $x = L$ for all time. A solution exists assuming that there is no

mass flow, $\frac{\partial c}{\partial x} = 0 \ at \ x = 0$ and $\frac{\partial c}{\partial x} \approx 0 \ at \ x = L$.

(57)
$$C(x,t) = \frac{A}{\sqrt{t}}e^{\frac{-(x-\frac{\xi}{2})^2}{4Dt}} + e^{\frac{-(x+\frac{\xi}{2})^2}{4Dt}} \qquad where \ A = \frac{\int_{-\infty}^{\infty}C \ dx}{\sqrt{\pi D}}$$
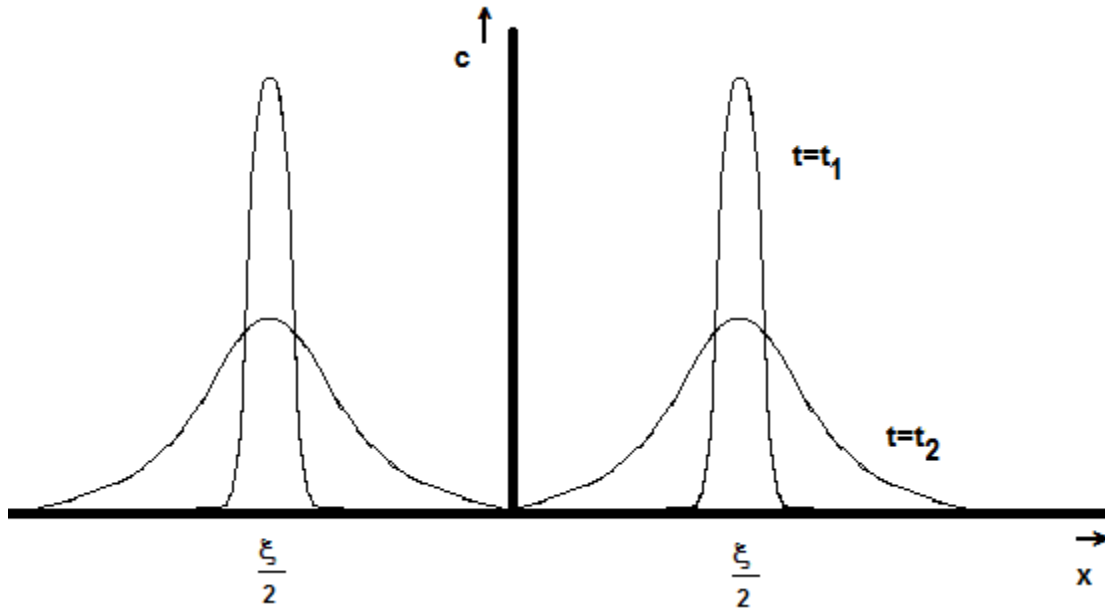
Figure 36: Long time approximation using symmetrical sources

For symmetrical sources, the gradient ensures that at $x = 0$ the boundary condition

holds. As for the boundary condition at $x = L$, $\frac{\partial c}{\partial x}$ goes to zero at $t > \frac{(L-\xi)^2}{4D}$. At this

point the solution becomes accurate because the boundary condition mostly holds. In

this case, movement of the boundary for long times closely follows: $\xi \approx \sqrt{4Dt}$.

4.1.3 Empirical Method

As phase boundary movement can be described by a parabolic equation, its boundary

movement can be solved for using an empirical method for two distinct phases. The

movement of the phase boundary for two phase systems can be determined by finding

the root of equation 59. [48] An example is given to compare the kinetic mass constant

in Appendix B with the density relationship using the following parameters. Section 2.1.1.1 discusses the relationship with mass diffusion.

$$D_L = 9.46 \ x \ 10^{-12} \frac{m^2}{s} \ D_R = 1.65 \ x \ 10^{-15} \frac{m^2}{s} \ \beta = 2.3764489 \ x \ 10^{-7} \frac{m}{s^{\frac{1}{2}}},$$

$$B_L = 0.55, B_R = 0.08, B_{LR} = 0.482, B_{RL} = 0.362.$$

(58)
$$\xi = 2\beta\sqrt{t}$$

(59)
$$(B_{LR} - B_{RL})\beta\sqrt{\pi} - \frac{\sqrt{D_L}(\langle B_L \rangle - B_{LR})}{1 + erf\left(\frac{\beta}{\sqrt{D_L}}\right)} e^{\frac{-\beta^2}{D_L}} + \frac{\sqrt{D_R}(B_{RL} - \langle B_R \rangle)}{1 - erf\left(\frac{\beta}{\sqrt{D_R}}\right)} e^{\frac{-\beta^2}{D_R}} = 0$$

4.2 Fixed-Grid Numerical Method

A fixed-grid method is discussed and presented. Fixed grid schemes use successive over-relaxation (SOR) which is a variant of the Gauss-Seidel method for solving a linear system of equations. SOR calculates steady state based on a predictor c_j equal to the average around the updating grid point. As c_j is updated, the concentration fields move further in time in accordance with the finite difference approximation of Fick's second law (equation 62).

In fixed grid methods, the phase boundary traverses between adjacent points. The position of the interface does not fall on a grid point, but falls between two grid points.

This interface is equivalent to the phase discontinuity in Figure 34b. The amount the

interface falls between two grid points is accounted by a fractional parameter "p" that

varies between 0 and 1.   Lagrangian interpolating polynomials are used to approximate

the concentration gradient and second derivative on both sides of the boundary. [67]

The calculation of both the first and second derivative changes as the interface moves

across the midway point from one grid point to another grid point. [48]   On the

aluminum rich side, for fractional parameters less than 0.5, the finite difference

calculation includes the second and third nearest nodes and omits the nearest node.

For fractional parameters greater than 0.5, the finite difference calculation includes the

nearest first and second node and omits the third node. On the nickel rich side, for

fractional parameters less than 0.5, the finite difference calculation includes the nearest

first and second node. For fractional parameters greater than 0.5, the finite difference

calculation includes the second and third nearest node and omits the nearest node. The

exclusion of the nearest nodes in the calculation of the finite difference approximation

of the first and second derivative on both sides of the boundary is due to singularities.

The nearest node and the boundary concentration provide too much information in a

small space. This change stabilizes the calculation of the finite difference

approximation.

The difference in flux on both sides of the boundary is proportional to the derivative of

the movement of the boundary with respect to time. The movement of the phase

boundary is calculated by approximating the integral using a Riemann sum, or the

trapezoid rule. The central difference scheme used for the first and second derivative approximation has a truncation error equivalent to $\mathcal{O}(\Delta x^2 + \Delta t^2)$. The trapezoidal rule used to calculate the integral is $\mathcal{O}(\Delta x^2)$.

(60)
$$c_j = c_j + \omega(\tilde{c}_j - c_j)$$

(61)
$$\tilde{c}_j = \frac{c_{j-1} + c_{j+1}}{2}$$

(62)
$$c_j = \frac{D(\Delta t)}{(\Delta x)^2}(c_{j-1} + 2 * c_j + c_{j+1})$$

(63)
$$\omega = \frac{2D(\Delta t)}{(\Delta x)^2} \leq \frac{1}{2}$$

(64)   If p > 0.5

$$\left(\frac{\partial b^R}{\partial x}\right)_\xi = \frac{1}{\Delta x}\left[\frac{(2p-5)b^{R/L}}{(2-p)(3-p)} + \frac{(3-p)b_{m+2}}{2-p} - \frac{(2-p)b_{m+3}}{3-p}\right]$$

(65)   If p < 0.5

$$\left(\frac{\partial b^R}{\partial x}\right)_\xi = \frac{1}{\Delta x}\left[\frac{(2p-3)b^{R/L}}{(1-p)(2-p)} + \frac{(2-p)b_{m+1}}{1-p} - \frac{(1-p)b_{m+2}}{2-p}\right]$$

(66)   If p > 0.5

$$\left(\frac{\partial b^L}{\partial x}\right)_\xi = \frac{1}{\Delta x}\left[\frac{pb_{m-2}}{(1+p)} - \frac{(1+p)b_{m-1}}{p} + \frac{(1+2p)b^{L/R}}{p(1+p)}\right]$$

(67)   If p < 0.5

$$\left(\frac{\partial b^L}{\partial x}\right)_\xi = \frac{1}{\Delta x}\left[\frac{(1+p)b_{m-3}}{(2+p)} - \frac{(2+p)b_{m-2}}{1+p} - \frac{(3+2p)b^{L/R}}{(1+p)(2+p)}\right]$$

(68)   If p > 0.5

$$\left(\frac{\partial^2 b}{\partial x^2}\right)_{m+1} = \frac{2}{(\Delta x)^2}\left[\frac{b^{R/L}}{(2-p)(3-p)} - \frac{b_{m+2}}{2-p} + \frac{b_{m+3}}{3-p}\right]$$

(69)   If p < 0.5

$$\left(\frac{\partial^2 b}{\partial x^2}\right)_{m+1} = \frac{2}{(\Delta x)^2}\left[\frac{b^{R/L}}{(1-p)(2-p)} - \frac{b_{m+1}}{1-p} + \frac{b_{m+2}}{2-p}\right]$$

(70)   If p < 0.5

$$\left(\frac{\partial^2 b}{\partial x^2}\right)_{m-1} = \frac{2}{(\Delta x)^2}\left[\frac{b^{L/R}}{(1+p)(2+p)} - \frac{b_{m-2}}{1+p} + \frac{b_{m-3}}{2+p}\right]$$

(71)   If p > 0.5

$$\left(\frac{\partial^2 b}{\partial x^2}\right)_{m-1} = \frac{2}{(\Delta x)^2}\left[\frac{b^{L/R}}{p(1+p)} - \frac{b_{m-1}}{p} + \frac{b_{m-2}}{1+p}\right]$$

$$(72) \qquad \frac{\Delta\xi}{\Delta t} \approx \frac{\partial\xi}{\partial t} = \frac{2(J^{R/L} - J^{L/R})}{(b^{R/L} - b^{L/R})}$$

$$(73) \qquad \xi_t = \xi_{t-1} + \left[\frac{(\partial\xi_t - \partial\xi_{t-1})}{2\partial t} + \frac{\partial\xi_{t-1}}{\partial t}\right]\Delta t$$
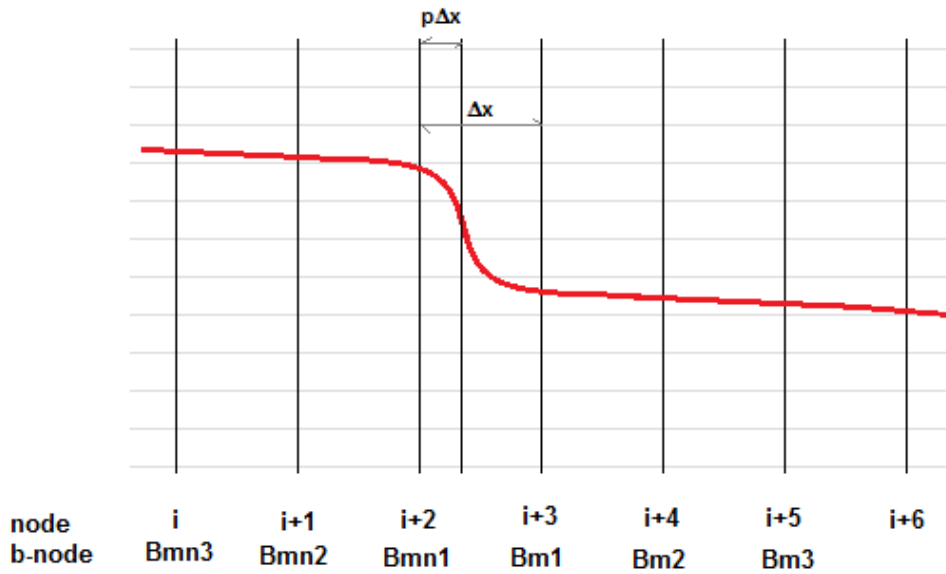
Figure 37: Phase boundary movement for p < 0.5, use equation 65, 67, 69, and 70
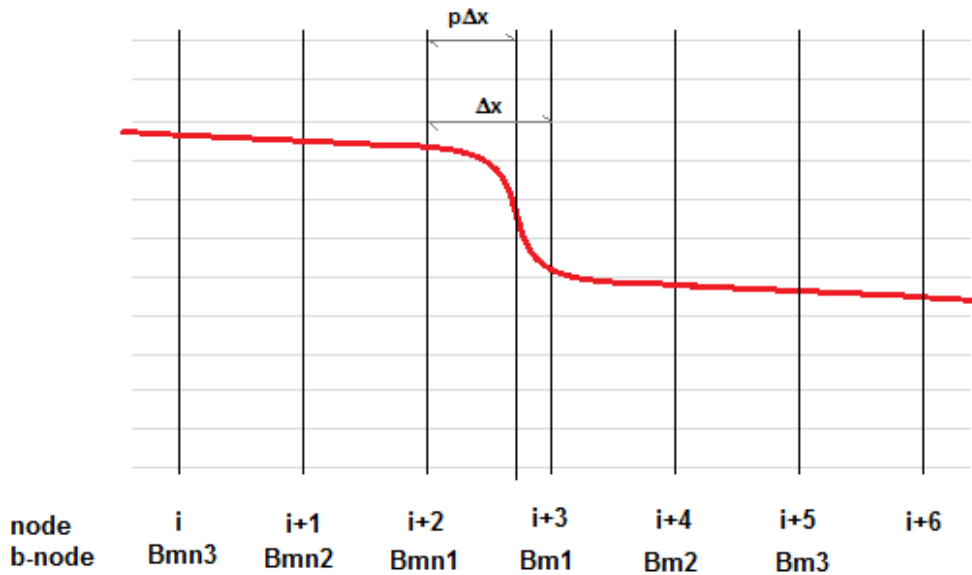
Figure 38: Phase boundary movement for p > 0.5, use equation 64, 66, 68, and 71
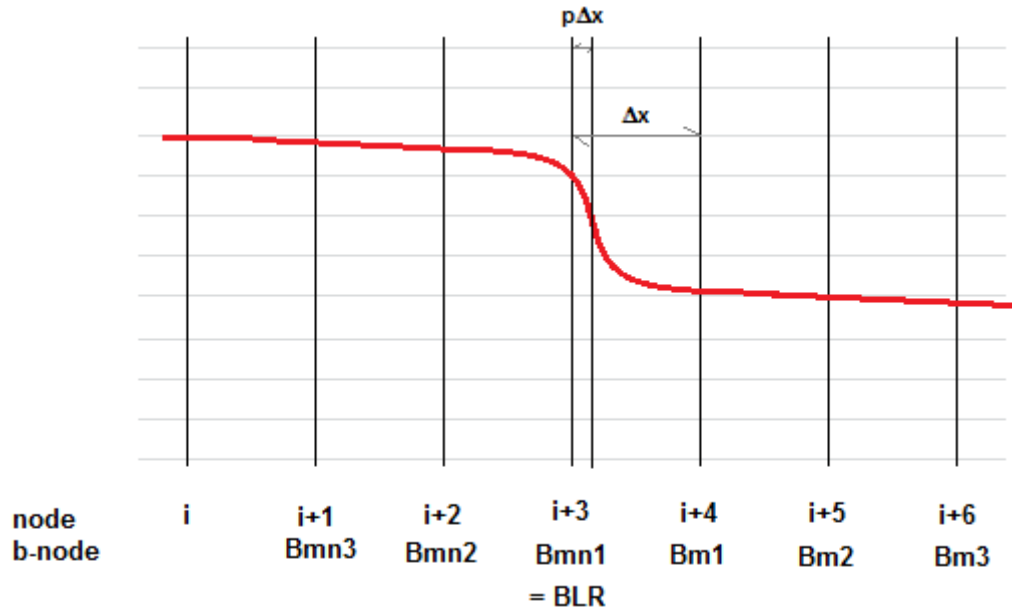
Figure 39: Variable node shift for phase boundary movement; p < 0.5

Boundary conditions for the ISS change for aluminization and homogenization. For aluminization, the ISS is fixed to the surface concentration. For homogenization, the ISS is equivalent to its neighboring grid point. This approximates the boundary condition $\frac{\partial c}{\partial x} = 0.$

The results produced a numerical scheme where the boundary layer not only moved continuously starting from time zero, but also moved parabolically which is consistent with the approximation by diffusion sources (Figure 41).   [47]
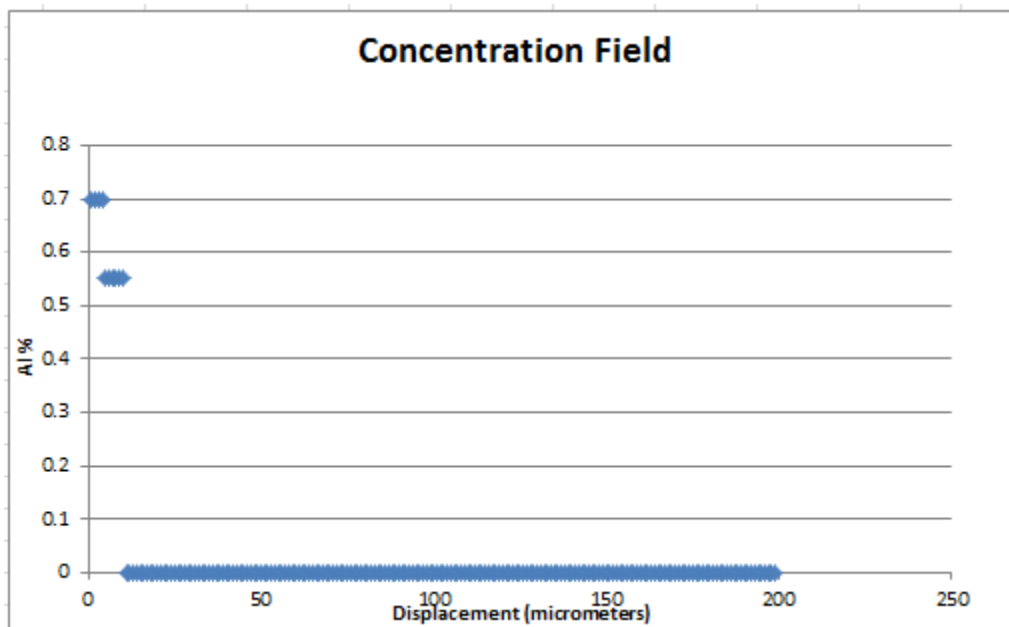
(a)
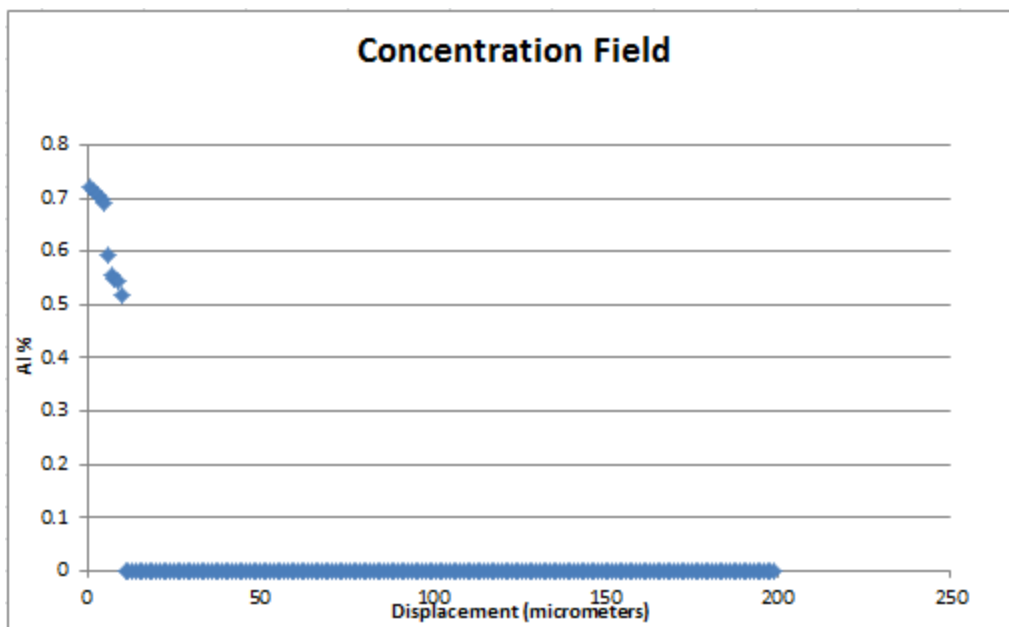
(b)
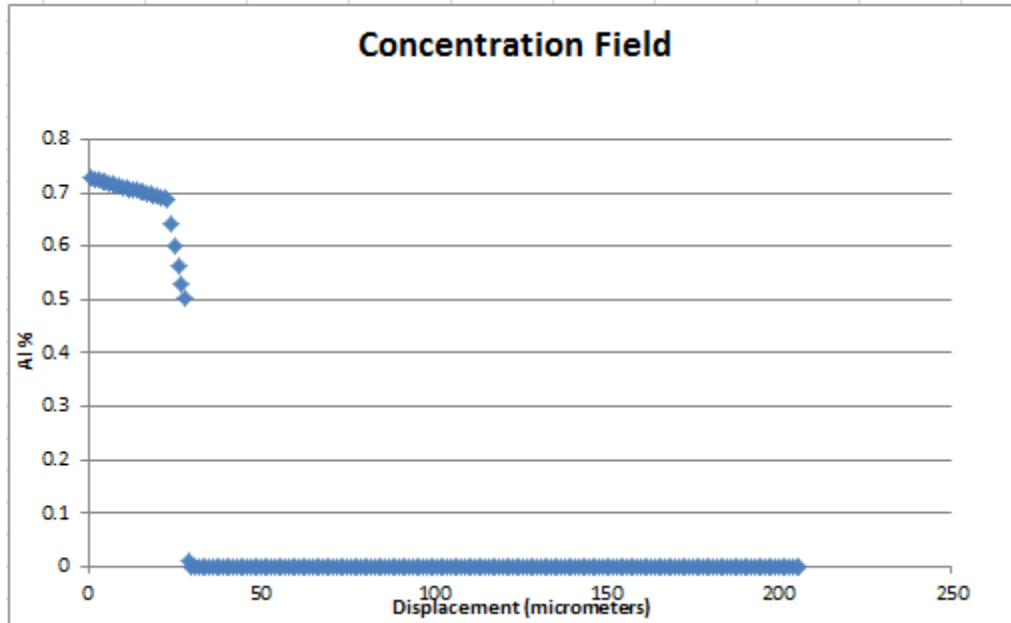
(c)
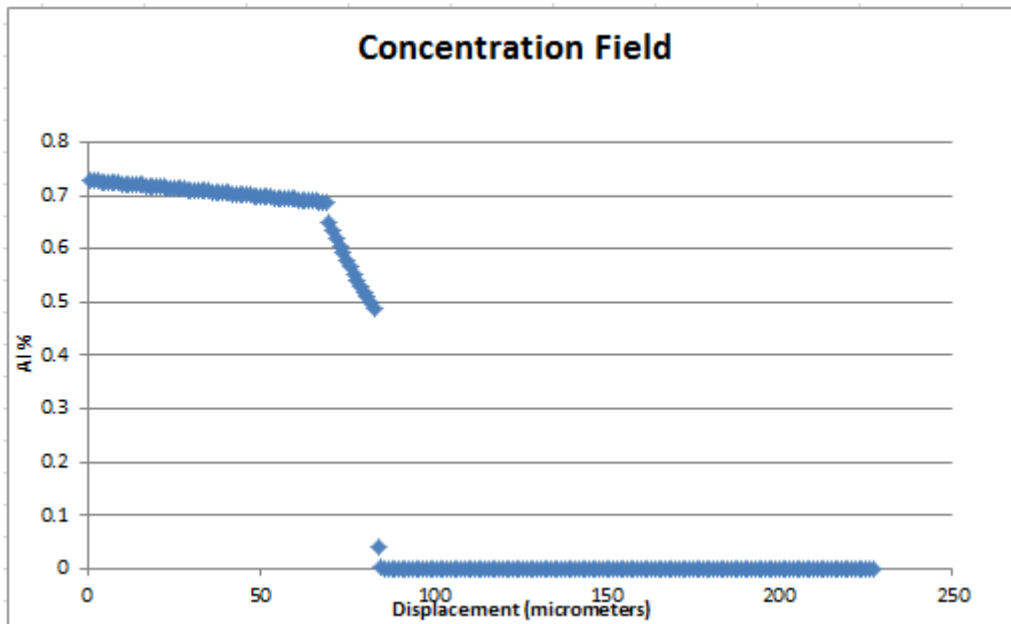
(d)

Figure 40: Zhou and North Numerical Solution [47] with a Moving Interface for 400 micron sample aluminization a) t=0, b) t = 1.5 sec, c) t = 150 sec, d) t = 1500 sec
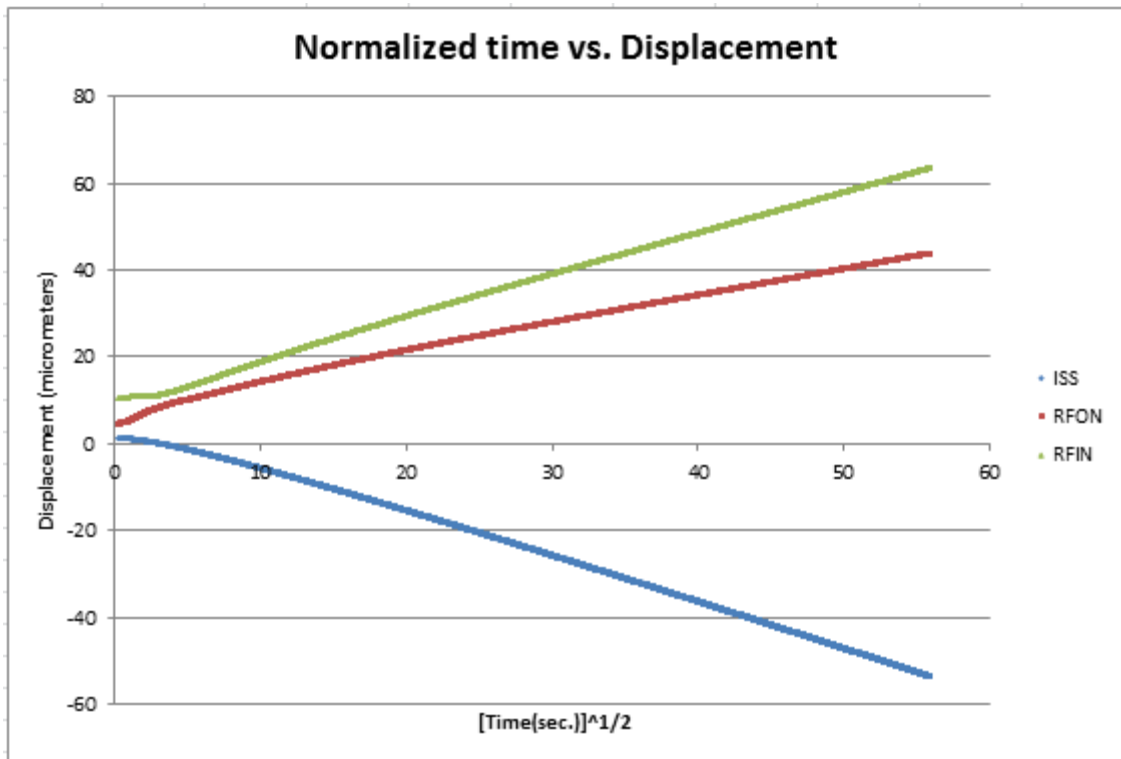
Figure 41: Normalized time vs. displacement for aluminization

(a)

(b)

(c)

(d)

(e)

73
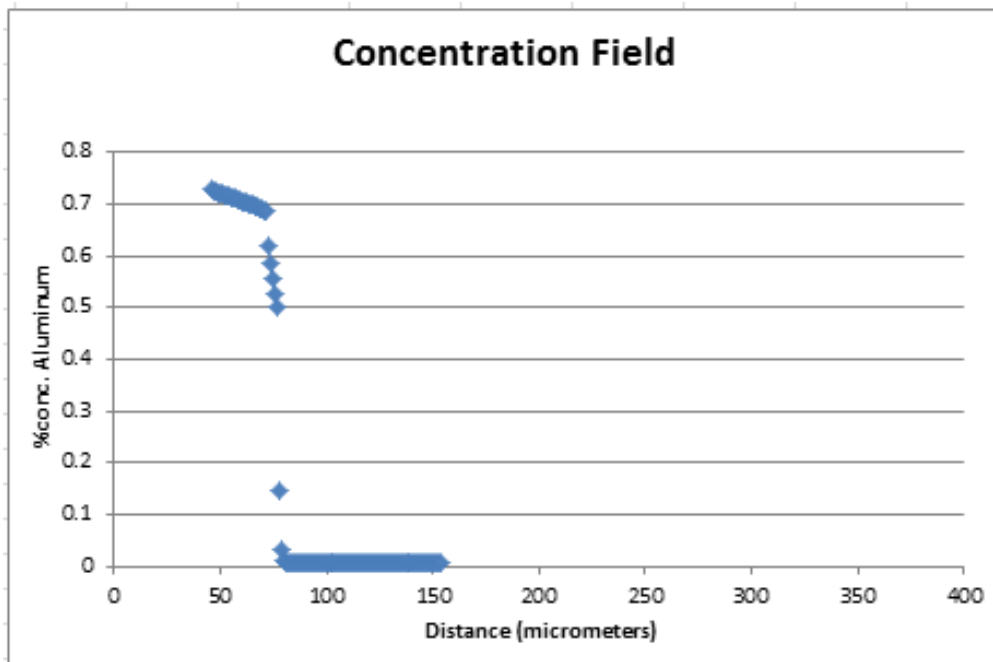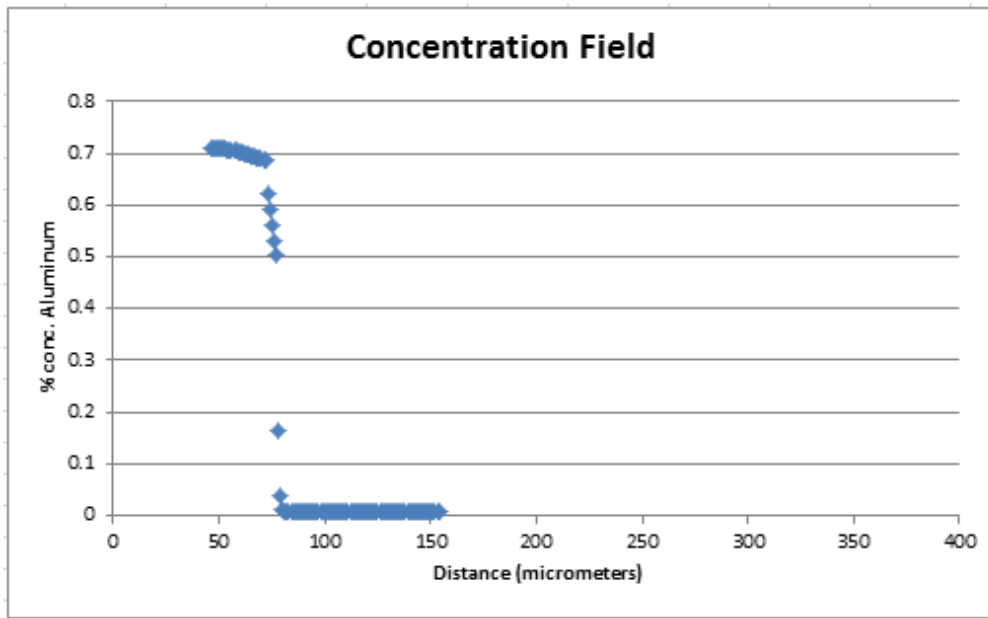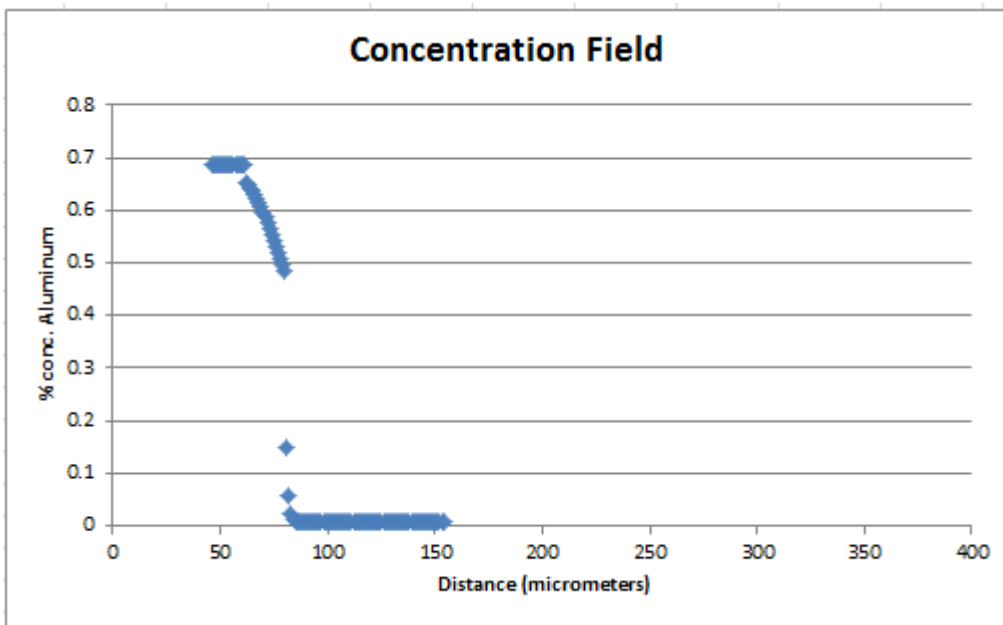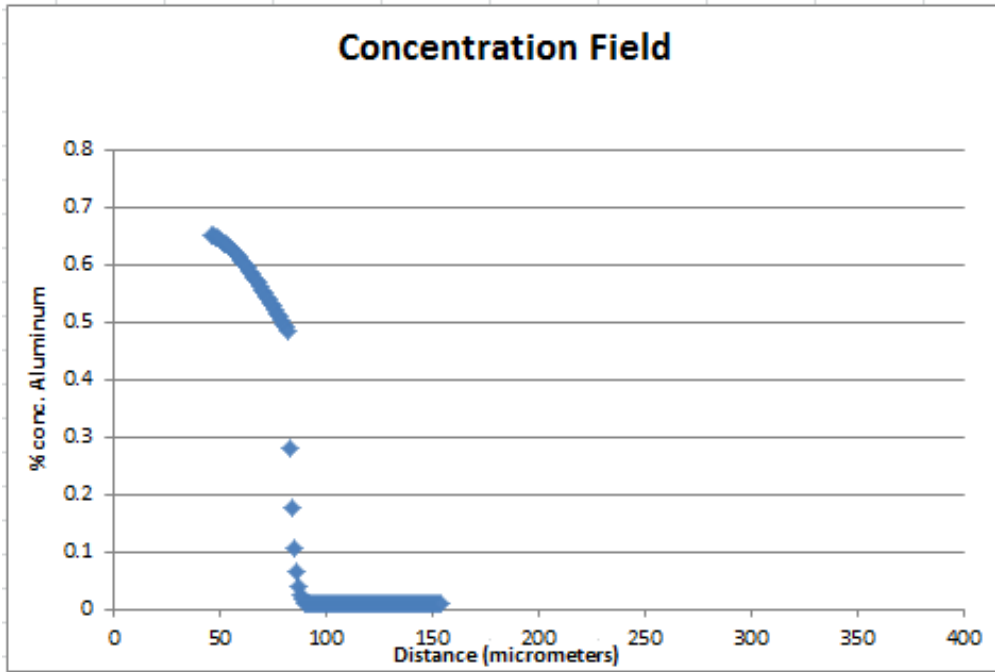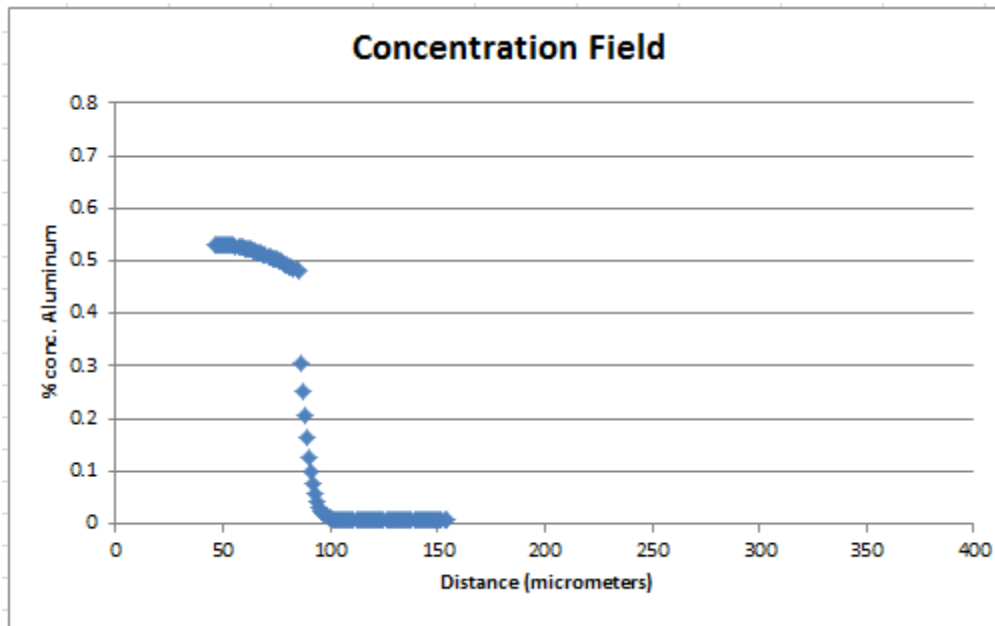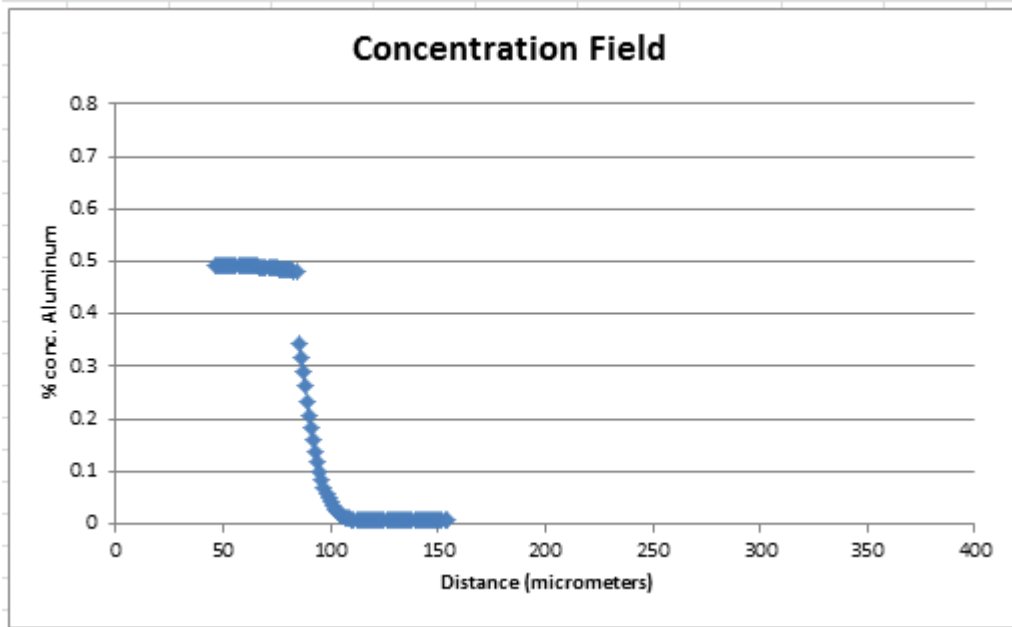
(f)
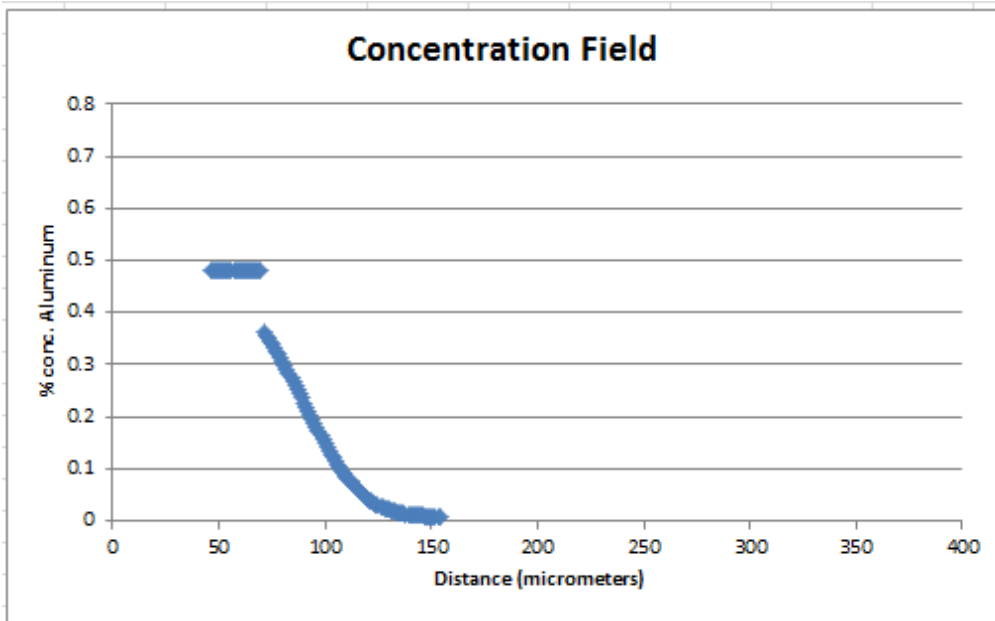
(g)
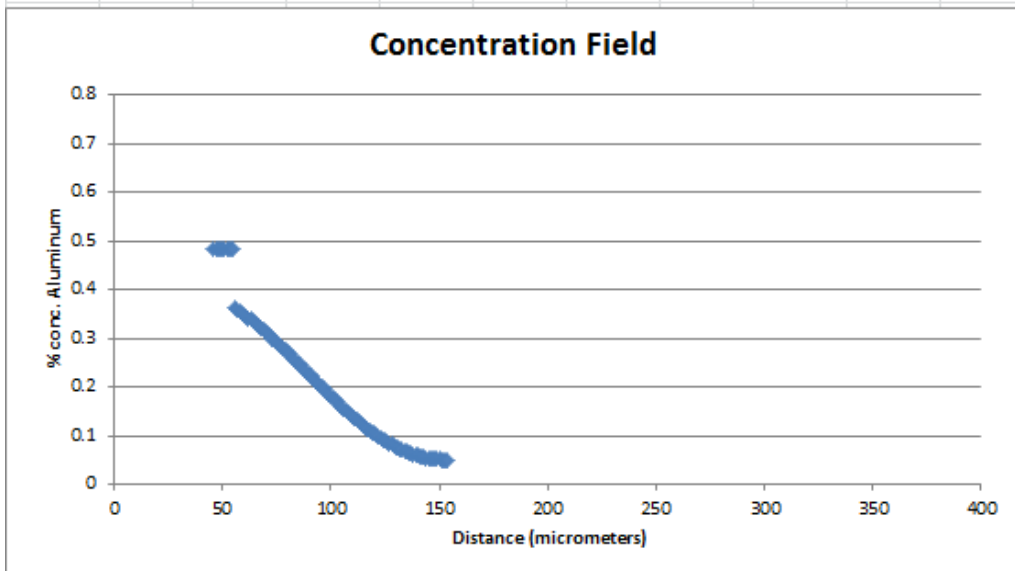
(h)
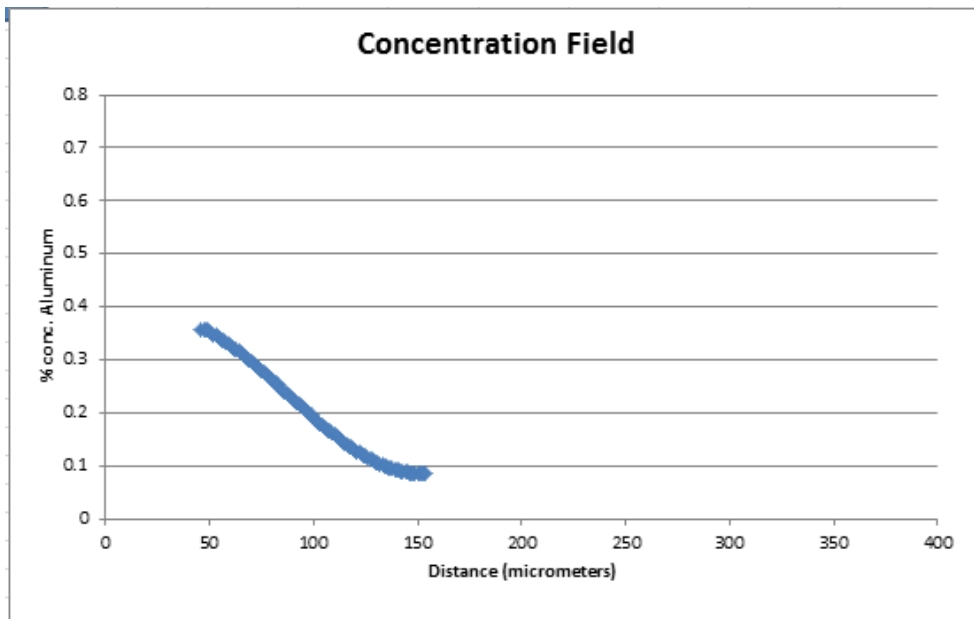
(i)
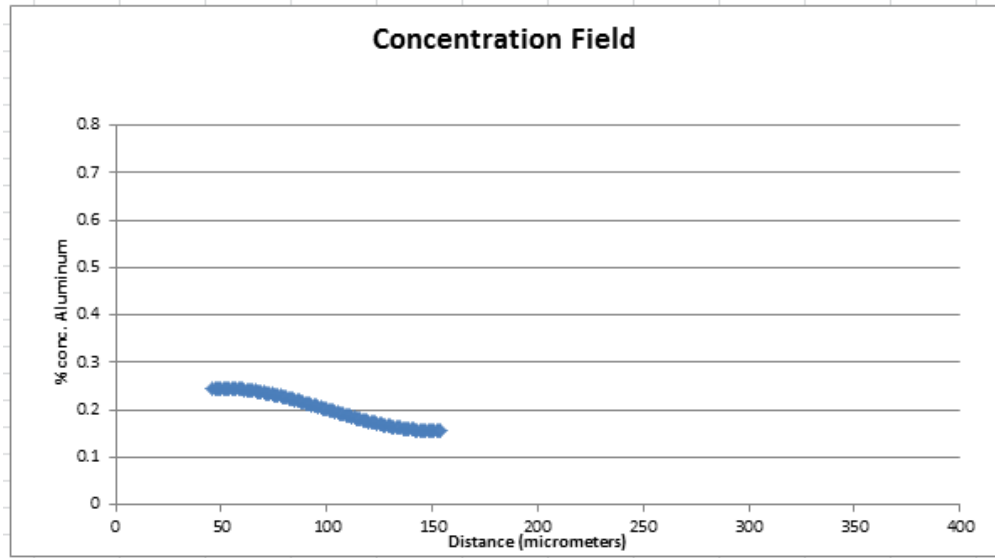
(j)

Figure 42: Zhou and North Numerical Solution [47] with a Moving Interface for homgoenization a) 0 sec, b) 3.75 sec, c) 270 sec, d) 460 sec, e) 1820 sec., f) 5420 sec, g) 33320 sec, h) 54450 sec, i) 64193 sec, j) 108000 sec

4.2.1 Discussion

Using trial and error, L = 600 μm, a 52 minute aluminization time, an 8 minute homogenization time, and the code from Appendix D, the three diffusion constants D_1 = 12.9058 μm²/s, D_2 = 0.5318 μm²/s , D_3 = 0.017375 μm²/s provided coatings similar to sample 1. 52 minutes was chosen as the aluminization time because the overall thickness of the sample increases by approximately 100 μm at that point and it gives a remaining 8 minute homogenization time that adjusts the thicknesses of the aluminum-rich coatings to that of sample 1 within 12 μm.

The same three diffusion constants and L = 100 μm using a 3 minute aluminization time provided coatings similar to sample 4 within 5 μm. This sample was then homogenized

76

numerically until only one phase existed. This occurred at 17.8 hours (Figure 42i).   The

sample was further homogenized to remove any concentration gradients, which was

considered sufficient by 30 hours (Figure 42j).

The diffusivities D_1 and D_3 in the numerical method were in the same log scale and very

close to the diffusivities used in the empirical method from Appendix C, although the

empirical method did not have an interdiffusive phase (β) because the variables in the

empirical method are only for two phases.

It should be noted that the phase boundary discontinuities in the code from Appendix D

were taken from the pure Nickel samples in [21]. While the boundary discontinuities

should be different for Nickel superalloy, the overall phase boundary movement should

be parabolic in either case. Samples 2, 3, and 5 were not considered for this analysis

due to the aluminum-rich phase penetrating the entire thickness of the alloy.

4.3 Evolution of Bonded Aluminum-Rich Coatings by Homogenization

Like aluminization, boundary movement behavior is governed by the interaction of

fluxes and concentrations on both sides of the boundary. Eventually these fluxes vanish

as mass is no longer diffused from one phase to another. The boundary reverses

direction where the flux of the substrate alloy dominates.

If the right amount of aluminum-rich coating is added to the surface, with a long

homogenization treatment the (γ/γ') phase will permeate throughout the thickness of

the alloy. In this case, for an alloy with a coating sequence that is like sample 1 or

sample 4 the boundary layers move the following way.

ξ_0, the ISS does not move at all throughout homogenization process because there is no

external mass diffusion; therefore, $\partial c / \partial x$ is zero at the endpoints.

ξ_1, the RFON may experience slow growth from residual gradients that were a result

from aluminization treatment. When these residual gradients diminish, the (δ/β) layer

changes from growth to dissolution. ξ_1 reverses direction and moves parabolically

toward the closest surface.   From the inside, (δ/β) decomposes to (β).

ξ_2, the RFIN initially experiences slow growth from residual gradients that were a result

from aluminization treatment. When these residual gradients diminish, the (β) layer

changes from growth to dissolution. ξ_2 reverses direction and moves parabolically

toward the closest surface removing (β) and replacing it with (γ/γ').

4.3.1 Boundary Movement Reversal

There is an analytical method to calculating the period of time that a phase changes

from growth to dissolution. This method is based on numerical experiments by Hickl and

Heckel [21]. In this method, the period of time where (δ) changes from growth to

dissolution is t_δ. This value (t_δ) is dependent on layer thickness and diffusivity which is

measured from the start of the homogenization step.

Using a_δ = 0.11, the results from the analytical method was comparable to the numerical

method. The analytical method was more accurate for boundary movement reversal for

the RFIN which had a larger t_δ than the RFON which had smaller t_δ.

(74)
$$t_\delta = a_\delta * \frac{X_\delta{}^2}{\widetilde{D}_\delta}$$

Table 6: Constant a_δ from [21]

$a_\delta =$	Valid for temperatures:
0.23	At 870 deg C
0.19	At 930 deg C
0.11	At 1000 deg C

4.4 Separation of Variables Method with Fourier Series

The separation of variables method is a standard method to solving partial differential

equations. In this method it is assumed that the variables are separable such that

$c(x,t)$ is separated into its explicit and general solutions $C_1(x)$ and $C_2(t)$ which are

related by the eigenvalues λ_n. [22] [23] [27] [51]

The imaginary sources beyond the physical domain are characterized by an arithmetic

series of sinusoids known as the Fourier Series. This series represents sources outside

the physical domain. The summation for each term with each respective eigenvalue

from $n = 0$ to ∞ is equal an exact solution for $c(x,t)$ within the physical domain.

This method is useful for measuring concentration gradients for alloys without phase

boundaries.

(75)
$$\frac{\partial C_{Al}}{\partial t} = D\nabla^2 C_{Al}$$

(76)
$$\frac{1}{C_2} * \frac{dC_2}{dt} = \frac{D}{C_1} * \frac{d^2C_1}{dx^2} = -D\lambda$$

(77)
$$\frac{d^2C_1}{dx^2} = -\lambda * C_1$$

(78)
$$\frac{dC_2}{dt} = -\lambda * D * C_2$$

(79)
$$\lambda = \frac{n^2 * \pi^2}{L^2}$$

(80)
$$C_1(x) = A * \sin(x\sqrt{\lambda}) + B \cos(x\sqrt{\lambda})$$

(81)
$$C_2(t) = D' * \exp(-\lambda Dt)$$

(82)
$$c(x,t) = M + \sum_{i=1}^{\infty} C_1(x)C_2(t)$$

(83)
$$c(x,t) \approx c_{av} + (c_{coat} - c_{av})exp\left(-\frac{\pi^2 Dt}{l^2}\right)$$

$C_1(x)$ is an even series due to symmetry, so constant A is usually zero.
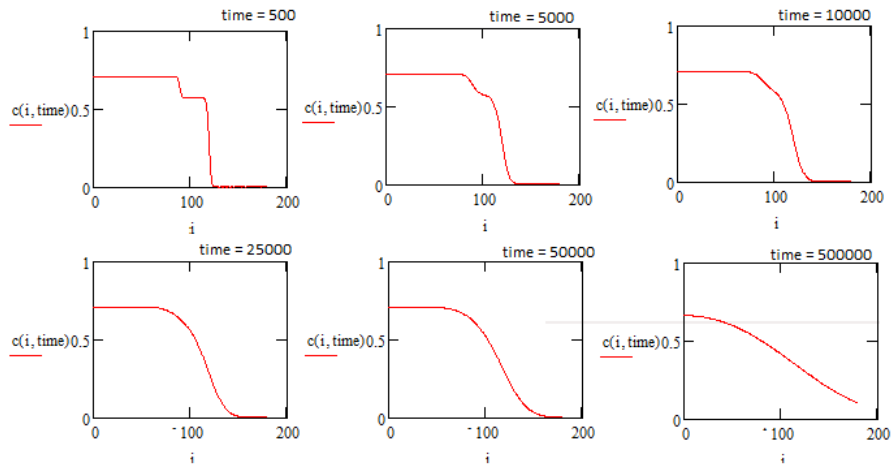
Figure 43: Concentration field with constant diffusivity using a Fourier series with 150 terms
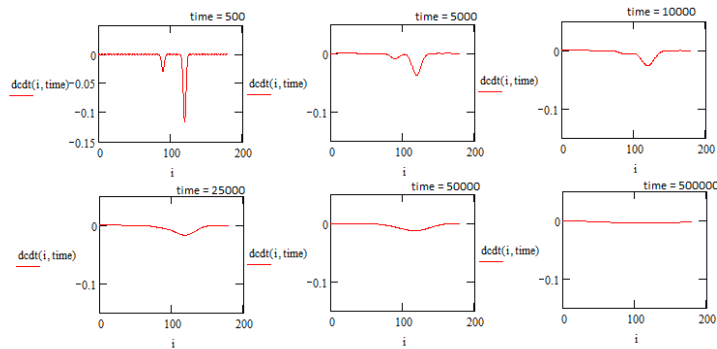
Figure 44: $\partial c / \partial x$ field; Boundary condition is zero at the 0 and L for all time

CHAPTER 5

LONG DIFFUSION FOR SAMPLE 1

5.1 Introduction

A long diffusion process was attempted for sample 1, but homogenization was not realized at the end of the process. Impurities seen in the alloy may have tampered with the diffusion process. The sample was analyzed anyway in order to observe the presence of a (γ/γ') microstructure assuming that the diffusion is as one-dimensional as possible. The following describes the details of the long diffusion process.

5.2 Sample 1 Preparation

Prior to the long diffusion process, sample 1 was contained in an epoxy filling from the aluminization experiment. The epoxy was ground away using a 200 grit diamond grind wheel powered by a Dremel. The sample was put into a solution of Methylene Chloride for 24 hours to strip any excess epoxy off the surface. The width was filed down 0.5 mm using SiC sandpaper on each side so that the flux was one dimensional during the long diffusion process (transparent areas, Figure 45). The back was also filed down to keep the process as ideal as possible (transparent areas, Figure 45).
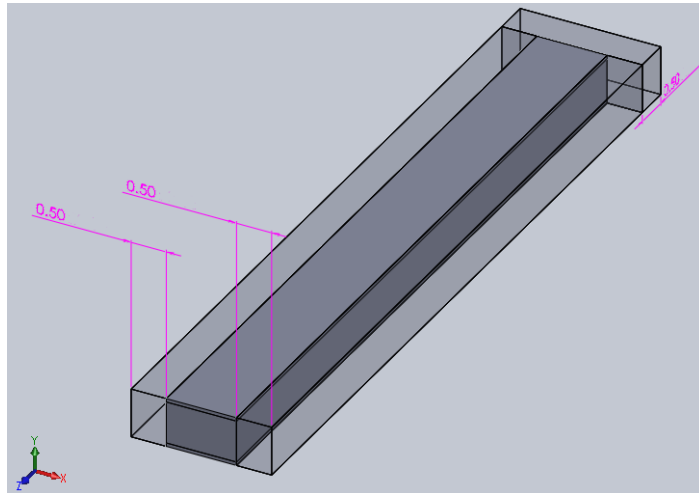
Figure 45: Filing schematic; transparent volumes were filed away

The long diffusion process consisted of applying a heat treatment and subsequent anneal for 8 hours at 1100 deg. C under flowing argon. The remaining 142 hours applied heat treatment at 1100 deg. C in an evacuated ampoule. The reason for the discontinuous heat treatment was that the heat treatment was interrupted during the long diffusion process.

The sample was loaded and sealed in a quartz ampoule at an absolute pressure of 0.86 atm at room temperature. 0.86 atm was the capacity of the vacuum pump the glassblower used. At 1100 deg C, the pressure increases to approximately 4 atm, which gives a hoop stress of 3.242 MPa. The tensile strength for quartz glass is 48.3MPa. The failure surface crack length c for a typical ceramic is defined by the relationship from equation 84 where K_{IC} is $2 \frac{MN}{m^{3/2}}$ [46]. This stress allows for a safety factor of 240 flaws smaller than 0.546 mm, which would easily be observed.

$$c = \left(\frac{K_{IC}}{\sigma_F}\right)^2 \frac{1}{\pi}$$

The dimensions of the quartz ampoule measured (18mm o.d., 16 mm i.d. x 203.2 mm L).

A small amount of tantalum was sealed in with the sample outside the alumina crucible

to absorb any remaining oxygen.

5.3 Experiment Results
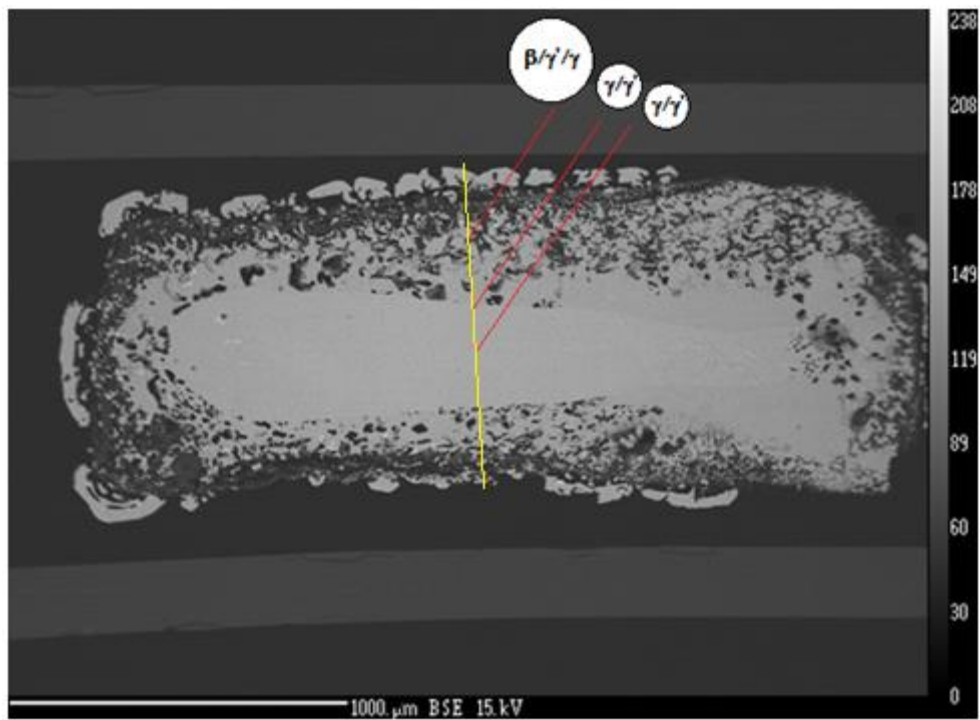
Figure 46: BSE image for Sample 1, homogenized for 150 hours at 1100 deg C
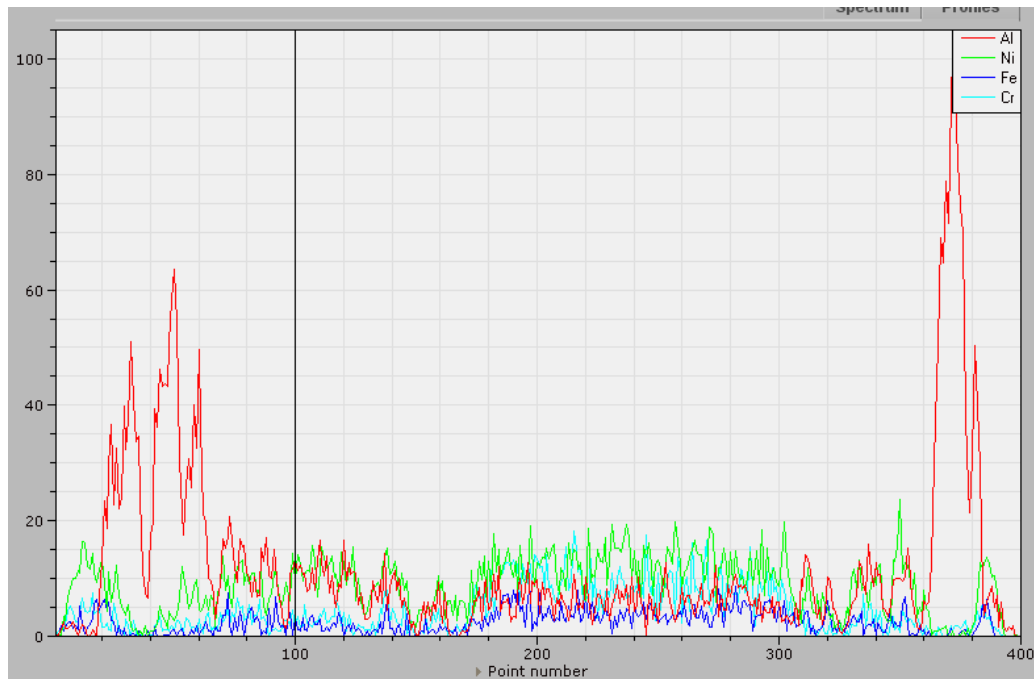
Figure 47: Sample 1 Bruker Analysis Line scan

Sample 1 was ground, mounted, and polished using the same technique the aluminized

samples went through. The surface of Sample 1 contained impurities. Some darker

colored inclusions were aluminum-rich which could be Al_2O_3; however, other darker

colored inclusions showed no Al, Cr, Ni, or Fe at all suggesting it could be epoxy,

porcelain, dirt, or other impurities. If the epoxy were not completely dissolved by the

Methylene Chloride soak, under the long diffusion at high temperature pyrolosis

products are mostly vapors (hydrocarbons), but some carbon would be left behind.

The thickness of the sample increased to approximately 880 micrometers during the

long diffusion, but a lighter colored inner metallic thickness measured approximately

670 micrometers. Sample 1 was weighed before the long diffusion as 0.121g and after

as 0.117g which was almost equal within the uncertainty of the mass balance.
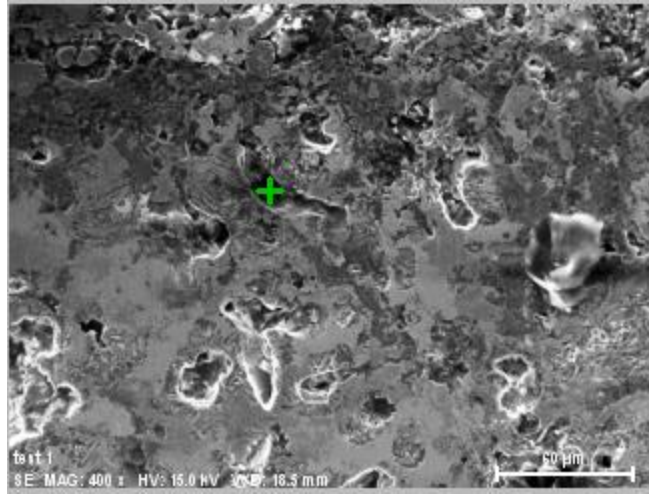
Figure 48: SE Image of Sample 1 inclusion composition probe
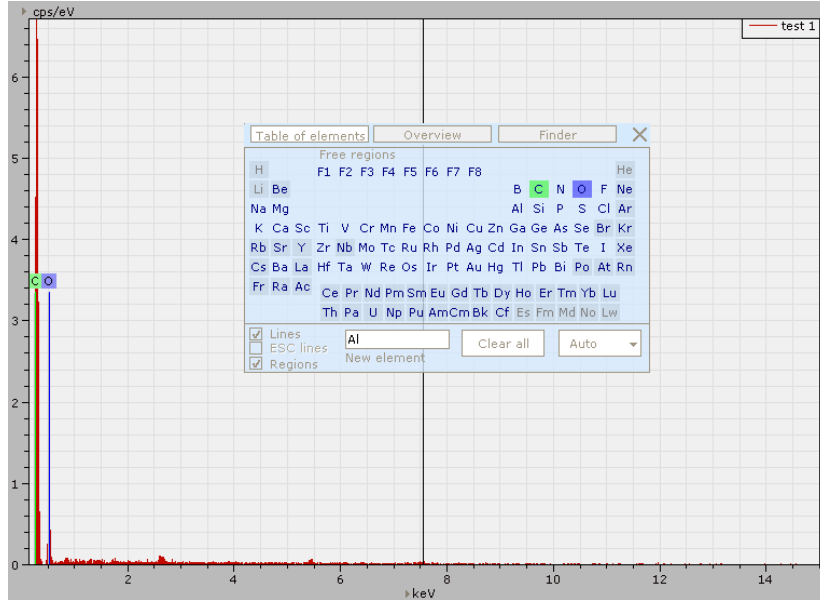
Figure 49: Bruker point analysis for inclusion in Sample 1

From the Energy-dispersive X-Ray Spectroscopy (EDS), a compositional analysis was conducted in light shaded metallic areas. Using the Pandat diagrams, the outer aluminum-rich coating by weight consisted of (β/γ/γ') as determined by the average concentration of 12.34 +/- 1.86 Al% wt., 6.669 +/- 2.702 Cr% wt., 5.566 +/- 0.919 Fe% wt., 71.8 +/- 4.769 Ni% wt. In the center, (γ/γ') was prevalent with an average concentration of 6.52 +/- 2.75 Al% wt., 12.68 +/- 5.15 Cr% wt., 8.3147 +/- 2.08 Fe %wt., 71.93 +/- 5.00 Ni% wt.

5.4 Beam Parameters

SE images were taken on the Zeiss EVO 50. BSE images were taken on a Cameca SX-100. EDS composition analysis was taken on the Cameca SX-100 which used a 20 nA, 15kV (CeB_6 Cathode) 250nm beam. For a pure Ni case, the excitation volume was constrained to about 800nm, while for a pure Al case, the excitation volume was constrained to 2.5 microns. The Anderson and Hasler analytical expression for the x-ray range is useful for most elements in approximating this excitation volume. [83] E_0 can range from 0 to 30 keV; in this example it was approximately 20 keV. E_c for $Al_{K\alpha}$ was 1559.6 eV, E_c for $Ni_{K\alpha}$ was 8333 eV. E_c for $Ni_{L\alpha}$ was 1008.6 eV as listed in the binding energies for elements. [84] The beam excitation range was much smaller than the microstructural features observed and was able to distinguish the different phases in figure 46.
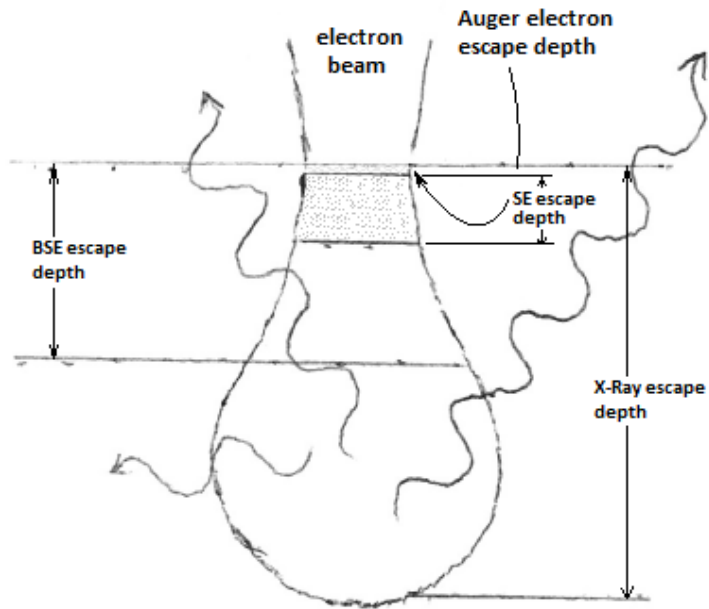
Figure 50: Auger, SE, BSE, and X-Ray Resolution Schematic [85]

(85)

$$R_x = \frac{0.064\left(E_0^{1.68} - E_c^{1.68}\right)}{\rho}$$

$R_x - Spatial\ Resolution\ (\mu m),\ E_0 - Accelerating\ Voltage\ (keV),$

$E_c - Excitation\ Energy\ (keV),\ \rho - density\ \left(\dfrac{g}{cm^3}\right)$
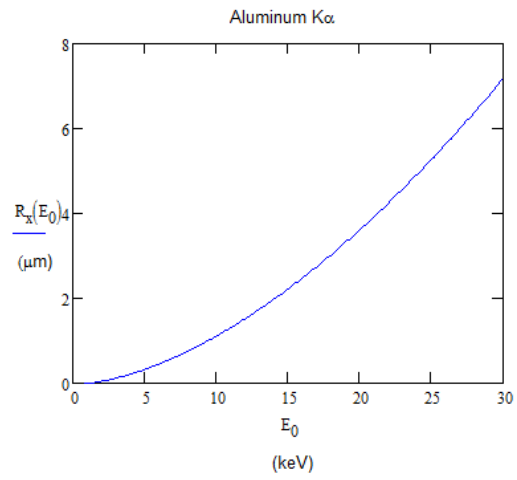
Figure 51: Anderson-Hasler Diagram for Al Kα
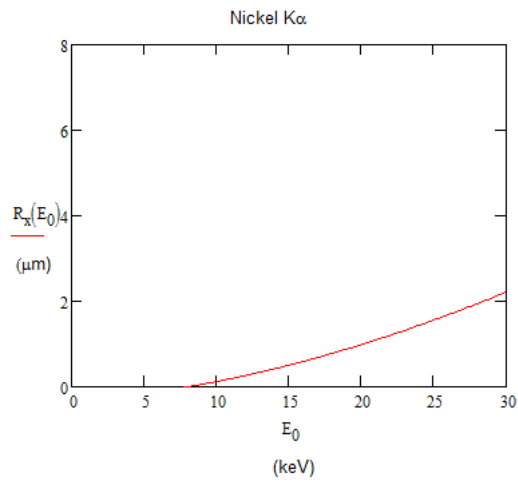
Figure 52: Anderson-Hasler Diagram for Ni Kα
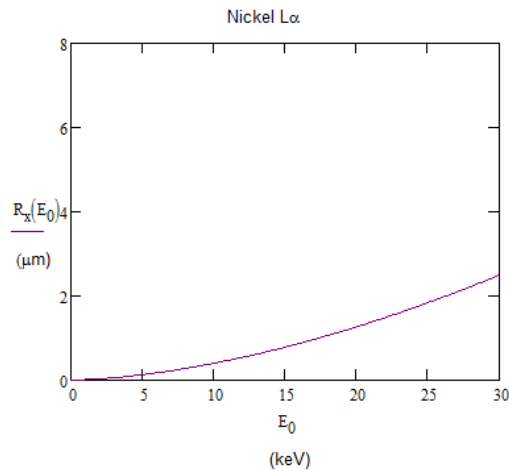
Figure 53: Anderson-Hasler Diagram for Ni Lα

5.5 Metallographic Technique

An etching solution was employed in order to obtain good contrast between

microstructures.   The (γ/γ') microstructure was revealed using Marble's etchant (10 g.

$CuSO_4$, 50mL H_2O, 50mL HCl) by submersion of the alloy samples for 30 seconds. [81]

The microstructure revealed by the etchant in Sample 1 closely resembled what the EDS

predicted. The (β/γ/γ') phase was very dendritic reminiscent of the dendrites revealed

in the over aluminized sample 5. The precipitates in the (γ/γ') microstructure appeared

like they were oriented in the same direction even in different areas of the alloy.

Average precipitate size was measured as 0.32151 +/- 0.063278 μm.
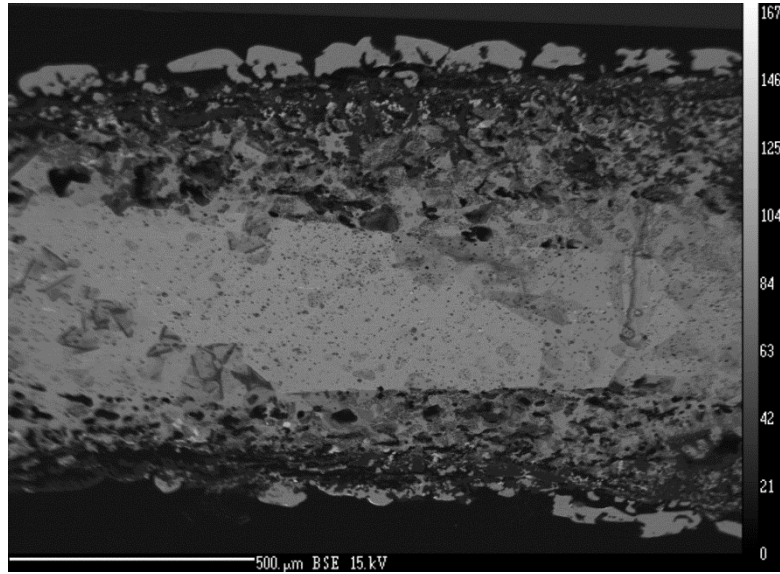
Figure 54: Sample 1 etched in Marble's etchant
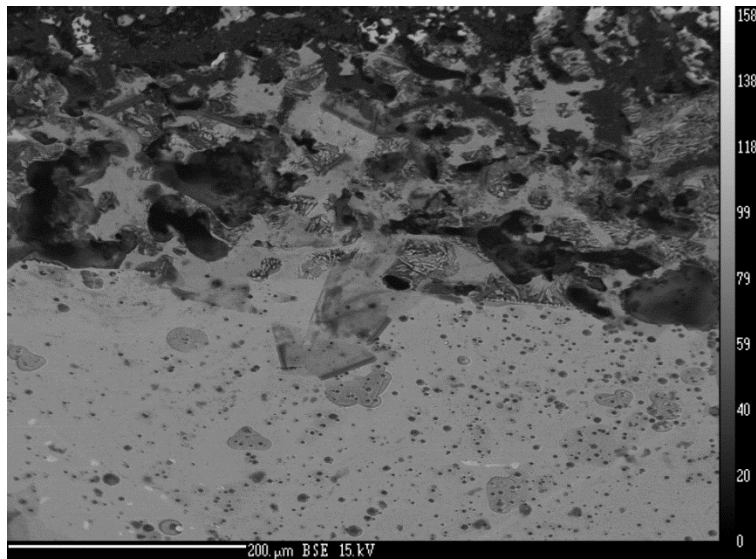
Figure 55: Sample 1 etched in Marble's etchant
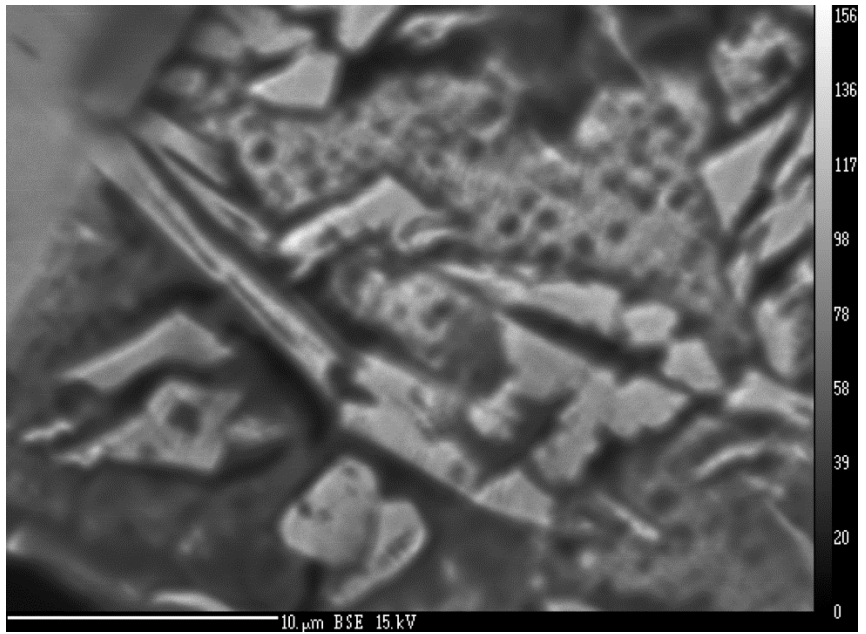
Figure 56: β/γ/γ' present in Sample 1
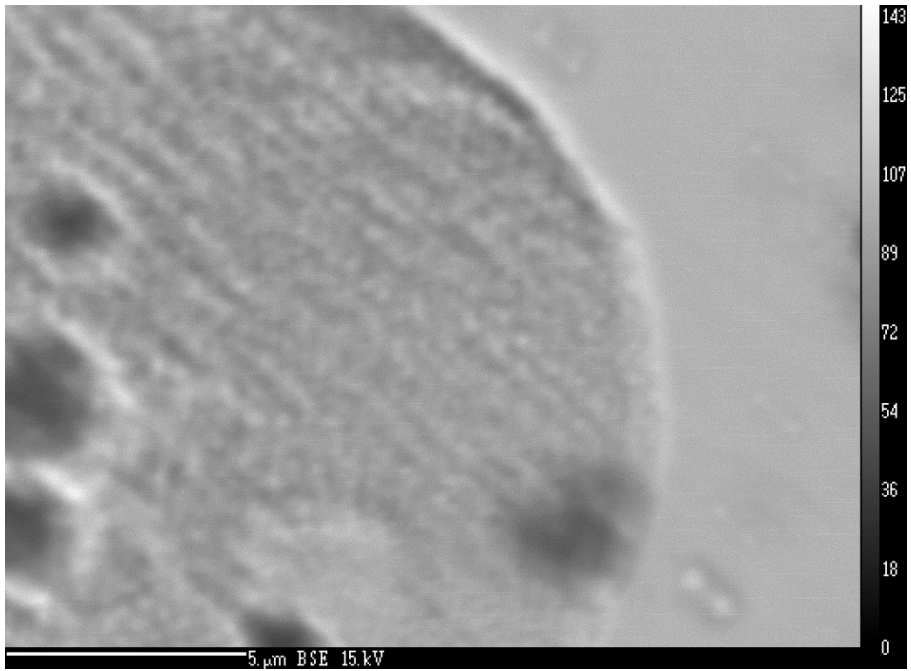
Figure 57: γ/γ' Sample 1 in BSE
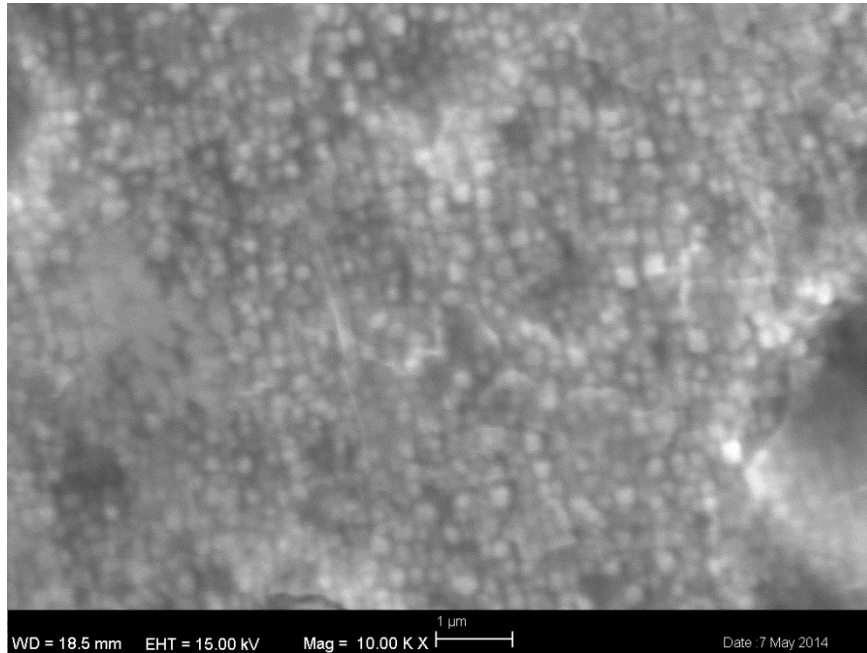
Figure 58: Close up of γ/γ′ Sample 1 in SE

5.6 Discussion

Sample 1 was not considered a homogenization process due to the concentration

gradient and inclusions present. The Bruker line analysis showed higher aluminum

concentrations 110 to 150 μm from the surface. After the long diffusion, the thickness

of the inner metal was slightly smaller than the thickness from the aluminization process

(670 μm vs. 710 μm). The impurities present in the material are likely non-metallic due

to the darker coloration. Epoxy inclusions are possible since Carbon has no known

melting point and a very high temperature sublimation point. These inclusions may

have penetrated the alloy similar to how inclusions can penetrate a low activity process

when the surface is dirty. The forces involved in this process may be due to the

Kirkendall effect where vacancies are being destroyed at the surface while some are created in the base alloy. As a result, the impurities move inward within the base alloy.

The impurities tracking the perimeter of the sample made the overall thickness increase. This complicates the ideal diffusion process as overall thickness should stay constant due to the boundary condition $\frac{\partial c}{\partial x}\bigg|_{x=\xi_0} = 0$ because no mass is transferred.

The presence of two disparate phase fields ($\beta/\gamma/\gamma'$) and (γ/γ') and their concentration gradient suggest that 150 hours may have been insufficient in homogenizing the alloy. Impurities may have slowed the flux of aluminum to the sample increasing the time to permeate the aluminum-rich phase throughout the alloy.

CHAPTER 6

HOMOGENIZATION FOR SAMPLE 4

6.1 Introduction

The evolution of bonded aluminum-rich coatings in homogenization is the same process as an aluminization process except different boundary conditions. In homogenization, no mass is transferred through the outer most surface; therefore, any mass diffusion is exclusively achieved by diffusion between the coating and alloy. The objective of homogenization process is to eliminate concentration gradients obtaining a uniform concentration of donor element throughout the alloy.

6.2 Sample 4 Preparation

Prior to homogenization, sample 4 was contained in an epoxy filling from the aluminization experiment. The epoxy was ground away using a diamond grind wheel powered by a Dremel. The sample was put into a solution of Methylene Chloride for 24 hours to strip any excess epoxy off the surface. There was no filing on any side of sample 4.

The homogenization process consisted of applying a heat treatment and subsequent anneal for 30 hours at 1100 deg. C in the evacuated ampoule. 30 hours was chosen in accordance with the results from the numerical analysis from 4.2.1.

The sample was loaded and sealed in a quartz ampoule at an absolute pressure of 0.86 atm at room temperature. The dimensions of the quartz ampoule measured (18mm O.D., 16 mm I.D. x 203.2 mm L). A small amount of tantalum was sealed in with the sample outside the alumina crucible to absorb any remaining oxygen.

6.3 Experiment Results

Sample 4 was ground, mounted, and polished using the same technique sample 1 went through and the aluminized samples prior.

For sample 4, there were no concentration gradients in any of the white colored areas across the thickness indicating that the aluminum-rich coating penetrated through the thickness of sample 4; however, a chromium-rich phase was also present throughout the alloy.

From the EDS, a compositional analysis was conducted for the four main elements Ni, Al, Cr, Fe using eight evenly spaced data points in white colored areas. The beam used for the EDS analysis was the same beam used in sample 1. Sample 4 had an average composition 3.28 +/- 0.313 %wt. Al, 8.213 +/- 4.93 %wt. Cr, 8.76 +/- 0.414 %wt. Fe, 79.26 +/- 6.433 %wt. Ni.

The phase of darker grey colored area was a Chromium rich phase with a composition 0.1144 +/- 0.127 %wt. Al, 76.76 +/- 4.845 %wt. Cr, 4.69 +/- 0.822 %wt. Fe, 7.94 +/- 3.00 %wt. Ni.

(γ/γ') microstructure was found in sample 4; however, its presence was much limited.

The EDS probed an area in sample 4 where (γ/γ') was believed to be present and its

composition measured 4.622 %wt. Al, 5.901 %wt. Cr, 7.866 %wt. Fe, 75.301 %wt. Ni.

There overall length of the sample was about 118 micrometers which changed very little

from its aluminized overall length.
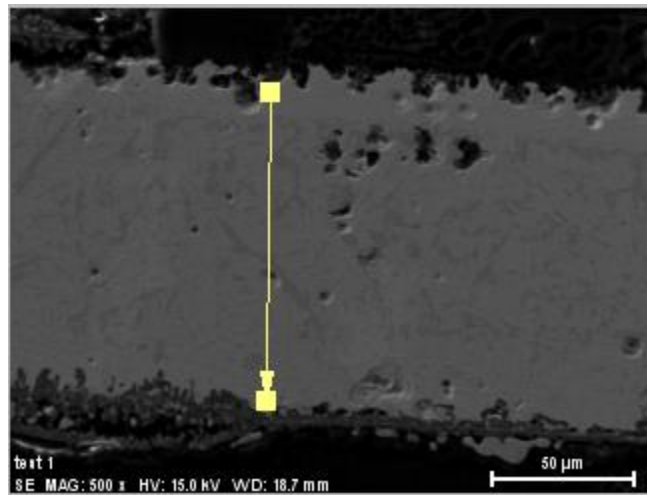
Figure 59: SE image for Sample 4, homogenized for 30 hours at 1100 deg C

Figure 60: Bruker line analysis for Sample 4

6.4 Metallographic Technique

Marble's etchant was employed on sample 4, but had less effect than sample 1 had. The same technique was employed for sample 4 by submersion in the etching solution for 30 seconds. [81]
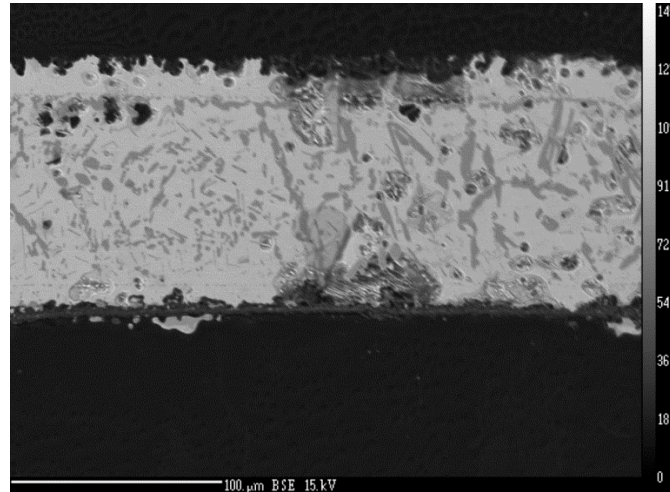
Figure 61: Sample 4 etched in Marble's etchant

6.5 Discussion

The aluminum penetrated the entire thickness of sample 4, but chromium-rich phases of M_7C_3 and $M_{23}C_6$ were present in the alloy. The chromium-rich phases in the sample are present at the grain boundaries and form as discontinuous carbon chains. Remartinez et. al. [82] determined that the chromium-rich grain boundary carbides form after aging treatments which are designed to improve yield strength. Cr-depletion in this form is associated intergrainular stress corrosion cracking.

Table 7: Chemical composition of Cr-rich Grain Boundary Carbides

Element	Al	Si	Nb	Ti	Cr	Fe	Ni	P or S
Wt%	0.13	0.48	0.63	0.21	88.99	2.14	7.39	Not detectable

The uniform thickness of aluminum revealed by the EDS showed that 30 hours was

successful at homogenizing the sample. While the aluminum penetrated the thickness

of sample 4, the metallography revealed that the addition was not enough to form (γ/γ')

pervasively.

CHAPTER 7

SOURCES OF ERROR

Geometry of the aluminum used in the aluminization experiment differed from other experiments mentioned in literature [1], [12], [14] where aluminum powder was used. When the pack powder is scooped out, the density of donor element in pack mixture can differ in each scoop and the geometry of the aluminum sourced can affect this. A different donor element pack density may alter the mass deposition parabolic constant (k_g).

The thermocouple used to measure temperature in the vertical tube furnace measured the temperature from a thermowell and not directly inside the quartz tube. The actual temperature inside the quartz tube will slightly lead the temperature measured by the thermocouple during heating and slightly lag for cooling.

The scale used to weigh samples has a tolerance of $1/100^{th}$ of a gram which was in many cases more than 5 percent the weight of the sample. Samples may need to be thinner and have more surface area so that the 5 percent weight is greater than the tolerance that can be weighed.

In the numerical method, the aluminum rich phases do not materialize from zero thickness starting at the surface instead they emerge as an initial finite thickness. This

assumption may underestimate the interdiffusivity constant used to calculate the

concentration field and interface movement.

Confidence in the element composition measured by the EDS is 95%.

CHAPTER 8

CONCLUSIONS

This research from this study demonstrated the basis for determining the parameters for the concentration field and boundary layer movement from the aluminization and homogenization process. The following is a summary of the key points from this research.

- The mass diffusion rate constant was determined using the tabulated information from [72] in Appendix A and the donor element pack density from the experiment. The kinetic constant for boundary layer movement was solved for using the density of the aluminum-rich coating and compared with the empirical solution from [48]. The kinetic constants determined from the different methods were comparable suggesting that the mass diffusion is related to the boundary layer movement by density. Both equations are parabolic.

- Diffusivities (D_1, D_2, and D_3) from the numerical method in Appendix C were determined using trial and error to fit the phase thicknesses from the aluminized Sample 1. The diffusivities determined by this method were used to approximate the homogenization time for sample 4. D_1 and D_3 from the numerical method were very close to the two diffusivities used in the empirical method.

- 30 hours was enough time for complete homogenization in sample 4. Prediction of phase boundary movement by the numerical method was useful in determining homogenization time.

- 150 hours was not enough time for complete homogenization in sample 1, although the inclusions present may weaken this point. Inclusions and voids may explain a longer homogenization time.

- SEM and EMPA observations of the aluminized and homogenized samples were successful at identifying disparate phases of alloy using the Pandat diagrams as revealed by the metallographic etchant.

CHAPTER 9

RECOMMENDATIONS FOR FUTURE WORK

There was a considerable amount of research that was not pursued for this project. Much of that had to do with the long time to commit to a project and resources on hand. The following is a list of work that was researched but not pursued.

- X-Ray diffraction of the dark colored impurities in sample 1 would reveal the crystallography. This could give more information on the composition of the impurities.

- The same experiment using a low activity process could be conducted to determine mass gains and boundary layer movement behavior.

- Aluminization and homogenization on 3D objects like turbine blades, forge-pressed workpieces, or micrometer sized parts.

- Calculating mass added solely from the numerical method using the density field for H-X750 alloy.

- Evidence of interstialcy antisite defects is seen by the behavior of anelastic strains in γ' Ni$_3$Al precipitates. [3][49] Due to the movement of antisite defects, these anelastic strains trigger internal friction that produces a hysteresis in an oscillating stress. These strains are often recoverable. [23] The constant strain experiments from Schaller et al. [49] revealed damping characteristics in the flow stresses of constant strain experiments of γ' Ni$_3$Al crystal. He suggested that damping is triggered by loss free decay of vibrations in a torsional

pendulum. [49][3] A similar test could be conducted with aluminized Nichrome wire.

- Perez-Bergaquist [1] coarsened average particle diameter in her γ/γ' sample using Ostwald Ripening. For aerospace applications γ/γ' precipitate strengthened alloys have precipitates ranging from 350nm to 600nm. [69] The strengthening mechanisms involved in precipitate strengthening are particularly dependent on volume fraction and average particle size. A subsequent experiment could determine the benefit of coarsening to strengthening in particle hardened alloys.

- An embedded atom Monte Carlo simulation could be used to calculate interatomic site migrations between (γ), (γ'), (β), and (δ) phase boundaries.

- A phase field model could be used to simulate interactions between phase boundaries to produce a two phase result like (γ/γ').

- A high-temperature yield and ultimate strength tensile test for precipitation strengthened alloys.

- Creep-mechanism diagrams could be produced for H-X750 alloy to differentiate Dislocation Glide, Power Law, Coble, and Nabarro Herring creep regions from the stress and temperature in the operation region. This test would require many samples of γ/γ' precipitate strengthened alloy with the same volume fraction and number of particles or particle diameter.

APPENDIX A

PARTIAL PRESSURE, GAS DIFFUSION, AND RATE CONSTANT DATA FOR NH$_4$Cl PACKS

FROM [72] WITH ALUMINUM DENSITY OF 40 mg/cm^3

Equilibrium Partial Pressure of gases in atm in 4%wt. NH$_4$Cl Activated pure Al packs					
		Temperature (deg C)			
Gas	Activity	800	900	1000	1093
PAlCl	1	1.13E-02	2.86E-02	4.89E-02	7.91E-02
PAlCl$_2$	1	9.25E-02	1.23E-01	1.37E-01	1.36E-01
PAlCl$_3$	1	7.17E-02	4.27E-03	2.37E-02	1.12E-02
PHCl	1	4.96E-04	5.60E-04	5.83E-04	5.75E-04
PH$_2$	1	0.8239	0.8053	0.7896	0.7725

Partial Pressure of gases in atm in 4%wt. NH$_4$Cl Activated pure Al packs					
		Temperature (deg C)			
Gas	Activity	800	900	1000	1093
PAlCl	0.5	7.49E-03	1.95E-02	3.42E-02	5.71E-02
PAlCl$_2$	0.5	8.07E-02	1.14E-01	1.34E-01	1.42E-01
PAlCl$_3$	0.5	8.25E-02	5.38E-02	3.26E-02	1.68E-02
PHCl	0.5	6.55E-04	7.62E-04	8.17E-04	8.30E-04
PH$_2$	0.5	0.8238	0.8053	0.7895	0.7724

Partial Pressure of gases in atm in 4%wt. NH$_4$Cl Activated pure Al packs					
		Temperature (deg C)			
Gas	Activity	800	900	1000	1093
PAlCl	0.1	2.77E-03	7.59E-03	1.41E-02	2.50E-02
PAlCl$_2$	0.1	5.50E-02	8.65E-02	1.41E-01	1.37E-01
PAlCl$_3$	0.1	1.04E-01	7.99E-02	5.71E-02	3.55E-02
PHCl	0.1	1.21E-03	1.48E-03	1.68E-03	1.82E-03
PH$_2$	0.1	0.8236	0.805	0.7893	0.7721

Partial Pressure of gases in atm in 4%wt. NH$_4$Cl Activated pure Al packs					
		Temperature (deg C)			
Gas	Activity	800	900	1000	1093
PAlCl	0.01	6.33E-03	1.82E-03	3.57E-03	6.79E-03
PAlCl$_2$	0.01	2.88E-02	4.96E-02	7.30E-02	1.00E-01
PAlCl$_3$	0.01	1.24E-01	1.10E-01	9.24E-02	7.07E-02
PHCl	0.01	2.76E-03	3.56E-03	4.26E-03	4.93E-03
PH$_2$	0.01	0.8217	0.8044	0.7885	0.7711

Partial Pressure of gases in atm in 4%wt. NH$_4$Cl Activated pure Al packs					
		Temperature (deg C)			
Gas	Activity	800	900	1000	1093
PAlCl	1.00E-04	3.04E-05	9.02E-05	1.85E-04	3.74E-04
PAlCl$_2$	1.00E-04	6.63E-03	1.22E-02	1.95E-02	3.06E-02
PAlCl$_3$	1.00E-04	1.37E-01	1.34E-01	1.28E-01	1.18E-01
PHCl	1.00E-04	1.32E-02	1.76E-02	2.19E-02	2.70E-02
PH$_2$	1.00E-04	0.8199	0.7999	0.7829	0.7689

Interdiffusion Coefficient for Gaseous Species -cm^2/sec				
	Temperature (deg C)			
Gas	800	900	1000	1093
H$_2$-AlCl	3.36	3.84	4.35	4.83
H$_2$-AlCl$_2$	2.76	3.15	3.56	3.96
H$_2$-AlCl$_3$	2.4	2.75	3.1	3.45
H$_2$-HCl	2.89	3.31	3.74	4.16

Theoretical Aluminum Rate Gaseous Rate Constant - g^2 cm^4 hr^-1				
	Temperature (deg C)			
Surface Comp	800	900	1000	1093
45	1.00E-03	2.15E-03	3.20E-03	4.60E-03
50	8.60E-04	1.55E-03	2.30E-03	2.80E-03
55	6.80E-04	1.12E-03	1.75E-03	1.80E-03
60	4.90E-04	8.20E-04	1.25E-03	1.55E-03
61	4.20E-04	6.80E-04	9.80E-04	1.15E-03

Theoretical Aluminum Rate Solid Rate Constant - g^2 cm^4 hr^-1				
	Temperature (deg C)			
Surface Comp	800	900	1000	1093
45	1.60E-07	5.10E-07	2.50E-06	1.50E-05
50	1.65E-07	5.70E-07	2.65E-06	1.55E-05
55	1.80E-06	8.50E-06	3.20E-05	1.15E-04
60	1.75E-05	5.70E-05	3.20E-05	1.75E-03
61	3.70E-05	1.25E-04	5.80E-05	2.40E-03

APPENDIX B

MATHCAD DENSITY RELATIONSHIP

$PA1C1 := 1.13 \cdot 10^{-2} \cdot atm$

$PA1C12 := 9.25 \cdot 10^{-2} \cdot atm$

$PA1C13 := 7.17 \cdot 10^{-2} \cdot atm$

$PHC1 := 4.96 \cdot 10^{-4} \cdot atm$

$PpA1C1 := 6.33 \cdot 10^{-3} \cdot atm$

$PpA1C12 := 2.88 \cdot 10^{-2} \cdot atm$

$PpA1C13 := 1.24 \cdot 10^{-1} \cdot atm$

$PpHC1 := 2.76 \cdot 10^{-3} \cdot atm$

$DA1C1 := 3.36 \cdot \frac{cm^2}{sec}$

$DA1C12 := 2.76 \cdot \frac{cm^2}{sec}$

$DA1C13 := 2.4 \cdot \frac{cm^2}{sec}$

$DHC1 := 2.89 \cdot \frac{cm^2}{sec}$

$M := 26 \frac{gm}{mol}$

$\rho := \frac{15}{1000} \frac{gm}{cm^3}$

$R := 8.314 \frac{J}{mol \cdot K}$

$T := (800 + 273) \cdot K$

$\Sigma D \Delta P := [DA1C1 \cdot (PA1C1 - PpA1C1) + DA1C12 \cdot (PA1C12 - PpA1C12) + DA1C13 \cdot (PA1C13 - PpA1C13) + DHC1 \cdot (PHC1 - PpHC1)]$

$$Kg := \frac{2\rho \cdot M}{R \cdot T} \cdot \frac{0.79}{4} \cdot \Sigma D \Delta P$$

$Kg = 3.808 \times 10^{-4} \frac{gm^2}{cm^4 \cdot hr}$

$Kg = 1.058 \times 10^{-7} \frac{gm^2}{cm^4 \cdot s}$

$\frac{\sqrt{Kg}}{d} = 7.711 \times 10^{-7} \frac{m}{s^{0.5}}$

$d := 4.2174 \cdot \frac{gm}{cm^3}$ Density

Compared with Empirical Equation by Zhou And North

$\beta := \left(2.3764489 \cdot 10^{-7} \frac{m}{s^{.5}}\right)$ $x := 2 \cdot \beta$ $x = 4.753 \times 10^{-7} \frac{m}{s^{0.5}}$ close

APPENDIX C

MATHCAD FOR EMPIRICAL EQUATION

$CP := 0.55$

$CM := 0.08$

$CXP := 0.482$

$CXM := 0.362$

$Dp := 9.46 \cdot 10^{-12}$ m^2/sec

$Dm := 1.65 \cdot 10^{-15}$ m^2/sec

$\beta := 2.3764889445283 \cdot 10^{-7}$ m*s^-.5

$$g(\beta) := (CXP - CXM) \cdot \beta \cdot \sqrt{\pi} - \frac{\sqrt{Dp} \cdot (CP - CXP) \cdot e^{\frac{-\beta^2}{Dp}}}{1 + erf\left(\frac{\beta}{\sqrt{Dp}}\right)} + \frac{\sqrt{Dm} \cdot (CXM - CM) \cdot e^{\frac{-\beta^2}{Dm}}}{1 - erf\left(\frac{\beta}{\sqrt{Dm}}\right)}$$

$g(\beta) = 8.476 \times 10^{-20}$ small, close to zero

APPENDIX D

VBA NUMERICAL METHOD CODE

'Diffusion With Movable Boundary

'By Sean Reilly

'All Rights Reserved (c) 2014

'

'This is how the macro works

'You must run "Resetvalues()" before you start "DiffusionWithMovableBoundary()"

'Make sure that the variable "L" is the same for both "Resetvalues()" and "DiffusionWithMovableBoundary()"

'When you change the variable alu to 1 it means you are aluminizing, 0 is homogenizing

'You must start aluminizing first, then homogenize

'When you aluminize, the variable "start" is the aluminize time in minutes

'When you homogenize, the variable "start" is the homogenize time + aluminize time in minutes

'D1, D2, D3 are interdiffusivities for phase 1, 2, and 3

'dt is the time step

'For any $D*dt/dx^2 < 0.5$ otherwise the macro will not work

'dx = 1 micrometer btw

'If one phase runs into another the macro will not work

'Starting about row 500 is the concentration field in column E, the density field is column H

'This macro was based on the kinetic model by Zhou and North at the University of Toronto

'Their paper is here Zhou, Y., North, T., "Kinetic Modeling of Diffusion Controlled, Two-Phase Moving Interface Problems", Modeling Simul. Mater. Sci. Eng. I (1993) 505-516

'Enjoy!!

```vbnet
Sub DiffusionWithMovableBoundary()

Dim inta As Double

Dim intb As Double

Dim intc As Double


Dim bdone As Integer

Dim cdone As Integer



Dim ainterface As Integer

Dim ainterfaceold As Integer

Dim binterface As Integer

Dim binterfaceold As Integer

Dim cinterface As Integer

Dim cinterfaceold As Integer


Dim m As Integer

Dim n As Integer


Dim alu As Integer

Dim start As Long


Dim q As Double

Dim p As Double

Dim r As Double
```

```
Dim JARL As Double

Dim JBRL As Double

Dim JBLR As Double

Dim JCRL As Double

Dim JCLR As Double


Dim ARL As Double

Dim Am1 As Double

Dim Am2 As Double

Dim Am3 As Double


Dim BRL As Double

Dim BLR As Double

Dim Bm1 As Double

Dim Bm2 As Double

Dim Bm3 As Double

Dim Bmn1 As Double

Dim Bmn2 As Double

Dim Bmn3 As Double


Dim dB2dt As Double

Dim dB1dt As Double


Dim dA2dt As Double

Dim dA1dt As Double
```

```
Dim dt As Double

Dim Ad2cdx2atm1 As Double

Dim Bd2cdx2atmn1 As Double
Dim Bd2cdx2atm1 As Double

Dim D1 As Double
Dim D2 As Double
Dim D3 As Double

Dim afloat As Double
Dim bfloat As Double

Dim length As Double

Dim K1 As Double
Dim K2 As Double

Dim mass As Double

Dim j1 As Long

bdone = 0
cdone = 0
m = 1
dA1dt = 0
```

```
dB1dt = 0

dC1dt = 0

length = 100

mass = 0

j1 = 0

'''''''''''''''''''''''''''''''''''

'''''''''''''''''''''''''''''''''''

alu = 1 ' aluminization/homogenization'

start = 3 '2.8 '52.1'54.45 '51.45 '51.5 '51.4 '51.2 '51.6   ' In Minutes

'''''''''''''''''''''''''''''''''''

'''''''''''''''''''''''''''''''''''

intc = ActiveCell.Offset(1, 5)

cinterface = Int(intc)

intb = ActiveCell.Offset(1, 3)

binterface = Int(intb)

inta = ActiveCell.Offset(1, 1)

ainterface = Int(inta)


dt = 0.025 ' In Seconds


For j = 1 To ((1 / dt) * 60 * start)

mass = 0


D1 = 12.9058  'in micrometer^2/sec

D2 = 0.5318 'in micrometer^2/sec

D3 = 0.017375 'in micrometer^2/sec
```

```
Cells(1, 1).Select

j = ActiveCell.Offset(0, 5)

'If alu = 0 Then

inta = ActiveCell.Offset(1, 1)



If alu = 0 Then adone = 1



If intb <= inta Then

bdone = 1

ElseIf intb >= length Then

bdone = 1

Else

bdone = 0

End If



If intb < (Int(inta) + 1) Then

If intc < Int(inta) + 1 Then

Else

ActiveCell.Offset(499 + ainterface + 1, 4) = ActiveCell.Offset(499 + ainterface + 2, 4) ' + (D1 * dt)
* Ad2cdx2atm1 '((ActiveCell.Offset(499 + i + ainterface - 1, 3) - 2 * ActiveCell.Offset(499 + i +
ainterface - 1, 4) + ActiveCell.Offset(500 + i + ainterface - 1, 4)))

End If

End If



If intb < inta Then

If intc < inta Then
```

```
Else

ActiveCell.Offset(499 + ainterface + 0, 4) = ActiveCell.Offset(499 + ainterface + 1, 4) ' + (D1 * dt)
* Ad2cdx2atm1 '((ActiveCell.Offset(499 + i + ainterface - 1, 3) - 2 * ActiveCell.Offset(499 + i +
ainterface - 1, 4) + ActiveCell.Offset(500 + i + ainterface - 1, 4)))

End If

End If


If intc < Int(inta) + 1 Then

ActiveCell.Offset(499 + binterface + 1, 4) = ActiveCell.Offset(499 + binterface + 2, 4) ' + (D1 * dt)
* Ad2cdx2atm1 '((ActiveCell.Offset(499 + i + ainterface - 1, 3) - 2 * ActiveCell.Offset(499 + i +
ainterface - 1, 4) + ActiveCell.Offset(500 + i + ainterface - 1, 4)))

End If

If intc < inta Then

ActiveCell.Offset(499 + binterface + 0, 4) = ActiveCell.Offset(499 + binterface + 1, 4) ' + (D1 * dt)
* Ad2cdx2atm1 '((ActiveCell.Offset(499 + i + ainterface - 1, 3) - 2 * ActiveCell.Offset(499 + i +
ainterface - 1, 4) + ActiveCell.Offset(500 + i + ainterface - 1, 4)))

End If


If intc <= inta Then

cdone = 1

ElseIf intc >= length Then

cdone = 1

Else

cdone = 0

End If


If alu = 1 Then

For i = 1 To 50

If ActiveCell.Offset(501 - i, 1) = "surf-B" Then

ainterface = 2 - i
```

```vba
End If

Next

Else

ainterface = ActiveCell.Offset(2, 3)

End If



If bdone = 0 Then

If binterface > 0 Then

For i = 1 To 118

If ActiveCell.Offset(500 + i, 1) = "beta-B" Then

binterface = i

Exit For

End If

Next

Else

For h = 1 To 50

If ActiveCell.Offset(500 - h, 1) = "beta-B" Then

binterface = -h

End If

Next

End If

End If



If cdone = 0 Then

If cinterface > 0 Then
```

```vba
For i = 1 To 118

If ActiveCell.Offset(500 + i, 1) = "gamma-B" Then

cinterface = i

Exit For

End If

Next

Else

For h = 1 To 50

If ActiveCell.Offset(500 - h, 1) = "gamma-B" Then

cinterface = -h

End If

Next


End If

End If


ainterfaceold = ActiveCell.Offset(2, 5)

ActiveCell.Offset(2, 5) = ActiveCell.Offset(2, 3)

binterfaceold = ActiveCell.Offset(3, 5)

'ActiveCell.Offset(3, 5) = ActiveCell.Offset(3, 3)

cinterfaceold = ActiveCell.Offset(4, 5)



o = ActiveCell.Offset(1, 3) - binterface ' ActiveCell.Offset(3, 3)

p = ActiveCell.Offset(1, 5) - cinterface

r = ActiveCell.Offset(1, 1) - ainterface
```

```
ARL = ActiveCell.Offset(499 + ainterface, 3)

Am1 = ActiveCell.Offset(499 + ainterface, 4)

Am2 = ActiveCell.Offset(500 + ainterface, 4)

Am3 = ActiveCell.Offset(501 + ainterface, 4)
'Stop


BRL = ActiveCell.Offset(500 + binterface, 3)

Bm1 = ActiveCell.Offset(500 + binterface, 4)

Bm2 = ActiveCell.Offset(501 + binterface, 4)

BLR = ActiveCell.Offset(499 + binterface, 3)

Bmn1 = ActiveCell.Offset(499 + binterface, 4)

Bmn2 = ActiveCell.Offset(498 + binterface, 4)

CRL = ActiveCell.Offset(500 + cinterface, 3)

Cm1 = ActiveCell.Offset(500 + cinterface, 4)

Cm2 = ActiveCell.Offset(501 + cinterface, 4)

CLR = ActiveCell.Offset(499 + cinterface, 3)

Cmn1 = ActiveCell.Offset(499 + cinterface, 4)

Cmn2 = ActiveCell.Offset(498 + cinterface, 4)



If binterface < length - 1 Then

Bm3 = ActiveCell.Offset(502 + binterface, 4)

ElseIf binterface = length - 1 Then

Bm1 = BRL

Bm2 = Bm1

Bm3 = Bm2

Else
```

```
Bm2 = BRL

Bm3 = Bm2

End If


If cinterface < length - 1 Then

Cm3 = ActiveCell.Offset(502 + cinterface, 4)

ElseIf cinterface = length - 1 Then

Cm1 = CRL

Cm2 = Cm1

Cm3 = Cm2

Else

Cm2 = CRL

Cm3 = Cm2

End If


If binterface - ainterface > 1 Then

Bmn3 = ActiveCell.Offset(497 + binterface, 4)

ElseIf binterface = ainterface - 1 Then

Bmn1 = BLR

Bmn2 = Bmn1

Bmn3 = Bmn2

Else

Bmn2 = BLR

Bmn3 = Bmn2

End If
```

If cinterface - ainterface > 1 Then

Cmn3 = ActiveCell.Offset(497 + cinterface, 4)

'Stop

ElseIf cinterface = ainterface + 1 Or cinterface = ainterface Then

Cmn1 = CLR

Cmn2 = Cmn1

Cmn3 = Cmn2

'Stop

Else

Cmn2 = CLR

Cmn3 = Cmn2

'Stop

End If

'Stop

If r < 0.5 Then

dARdx = ((2 * r - 3) * ARL / ((1 - r) * (2 - r))) + ((2 - r) * Am1 / (1 - r)) - ((1 - r) * Am2 / (2 - r))

'dBRdx = (BRL - Bm1) / (1 - o) '

Else

dARdx = ((2 * r - 5) * ARL / ((2 - r) * (3 - r))) + ((3 - r) * Am2 / (2 - r)) - (2 - r) * Am3 / (3 - r)

'dBRdx = (BRL - Bm2) / (2 - o) '

End If

If r > 0.5 Then

Ad2cdx2atm1 = (2 * Am3 / (3 - r)) - (2 * (Am2) / (2 - r)) + (2 * ARL / ((2 - r) * (3 - r)))

Else

Ad2cdx2atm1 = (2 * Am2 / (2 - r)) - (2 * Am1 / (1 - r)) + (2 * ARL / ((1 - r) * (2 - r))) '(Bm2 - 2 * Bm1 + BRL)

End If

"""

"""

"""

If o > 0.5 Then

dBLdx = (o * Bmn2 / (1 + o)) - ((1 + o) * Bmn1 / o) + ((1 + 2 * o) * BLR / (o * (1 + o)))

'dBLdx = (Bmn1 - BLR) / o

Else

dBLdx = ((1 + o) * Bmn3 / (2 + o)) - ((2 + o) * Bmn2 / (1 + o)) + ((3 + 2 * o) * BLR / ((1 + o) * (2 + o)))

'dBLdx = (Bmn2 - BLR) / (1 + o) '(2 * o - 3) * BRL / ((1 - o) * (2 - o)) + (2 - o) * Bm1 / (1 - o) - (1 - o) * Bm2 / (2 - o) '(-3 * BRL + 4 * Bm1 - Bm2)

End If

If o < 0.5 Then

dBRdx = ((2 * o - 3) * BRL / ((1 - o) * (2 - o))) + ((2 - o) * Bm1 / (1 - o)) - ((1 - o) * Bm2 / (2 - o))

'dBRdx = (BRL - Bm1) / (1 - o) '

Else

dBRdx = ((2 * o - 5) * BRL / ((2 - o) * (3 - o))) + ((3 - o) * Bm2 / (2 - o)) - (2 - o) * Bm3 / (3 - o)

'dBRdx = (BRL - Bm2) / (2 - o) '

End If

If o > 0.5 Then

Bd2cdx2atm1 = (2 * Bm3 / (3 - o)) - (2 * (Bm2) / (2 - o)) + (2 * BRL / ((2 - o) * (3 - o)))

Else

Bd2cdx2atm1 = (2 * Bm2 / (2 - o)) - (2 * Bm1 / (1 - o)) + (2 * BRL / ((1 - o) * (2 - o))) '(Bm2 - 2 * Bm1 + BRL)

End If

If o <= 0.5 Then

Bd2cdx2atmn1 = (((2 * Bmn3 / ((2 + o))) - ((2 * Bmn2) / (1 + o))) + ((2 * BLR / ((1 + o) * (2 + o)))))

Else

Bd2cdx2atmn1 = (2 * ((Bmn2 / (1 + o)))) - (2 * Bmn1 / (o)) + (2 * BLR / ((o) * (1 + o))) '(Bmn2 - 2 * Bmn1 + BLR)

End If

''

''

If p > 0.5 Then

dCLdx = (p * Cmn2 / (1 + p)) - ((1 + p) * Cmn1 / p) + ((1 + 2 * p) * CLR / (p * (1 + p)))

'dBLdx = (Bmn1 - BLR) / o

Else

dCLdx = ((1 + p) * Cmn3 / (2 + p)) - ((2 + p) * Cmn2 / (1 + p)) + ((3 + 2 * p) * CLR / ((1 + p) * (2 + p)))

'dBLdx = (Bmn2 - BLR) / (1 + o) '(2 * o - 3) * BRL / ((1 - o) * (2 - o)) + (2 - o) * Bm1 / (1 - o) - (1 - o) * Bm2 / (2 - o) '(-3 * BRL + 4 * Bm1 - Bm2)

End If

If p < 0.5 Then

dCRdx = ((2 * p - 3) * CRL / ((1 - p) * (2 - p))) + ((2 - p) * Cm1 / (1 - p)) - ((1 - p) * Cm2 / (2 - p))

'dBRdx = (BRL - Bm1) / (1 - o) '

Else

dCRdx = ((2 * p - 5) * CRL / ((2 - p) * (3 - p))) + ((3 - p) * Cm2 / (2 - p)) - (2 - p) * Cm3 / (3 - p)

'dBRdx = (BRL - Bm2) / (2 - o) '

End If

If p > 0.5 Then

Cd2cdx2atm1 = (2 * Cm3 / (3 - p)) - (2 * (Cm2) / (2 - p)) + (2 * CRL / ((2 - p) * (3 - p)))

Else

Cd2cdx2atm1 = (2 * Cm2 / (2 - p)) - (2 * Cm1 / (1 - p)) + (2 * CRL / ((1 - p) * (2 - p))) '(Bm2 - 2 * Bm1 + BRL)

End If

If p <= 0.5 Then

Cd2cdx2atmn1 = (((2 * Cmn3 / ((2 + p))) - ((2 * Cmn2) / (1 + p))) + ((2 * CLR / ((1 + p) * (2 + p)))))

Else

Cd2cdx2atmn1 = (2 * ((Cmn2 / (1 + p)))) - (2 * Cmn1 / (p)) + (2 * CLR / ((p) * (1 + p))) '(Bmn2 - 2 * Bmn1 + BLR)

End If

JARL = -D1 * dARdx

JBLR = -D1 * dBLdx

JBRL = -D2 * dBRdx

JCLR = -D2 * dCLdx

JCRL = -D3 * dCRdx

If r > 0.5 Then

dA1dt = -JARL / (1 - ARL)

Else

dA1dt = -JARL / (1 - ARL)

End If

If bdone = 0 Then

ActiveCell.Offset(499 + binterface, 3) = BLR

125

```vba
ActiveCell.Offset(500 + binterface, 3) = BRL

BLR = ActiveCell.Offset(499 + binterface, 3)

BRL = ActiveCell.Offset(500 + binterface, 3)

If o > 0.5 Then

dB2dt = (JBLR - JBRL) / (BLR - BRL) '+ Bmn1 - Bm2)

Else

dB2dt = (JBLR - JBRL) / (BLR - BRL) '+ Bmn2 - Bm1)

End If

Else

dB2dt = 0

End If


If cdone = 0 Then

ActiveCell.Offset(499 + cinterface, 3) = CLR

ActiveCell.Offset(500 + cinterface, 3) = CRL

CLR = ActiveCell.Offset(499 + cinterface, 3)

CRL = ActiveCell.Offset(500 + cinterface, 3)

If p > 0.5 Then

dC2dt = (JCLR - JCRL) / (CLR - CRL) '+ Cmn1 - Cm2)

Else

dC2dt = (JCLR - JCRL) / (CLR - CRL) ' + Cmn2 - Cm1)

End If

Else

dC2dt = 0

End If
''''''''''''''''''''''''''''''''''''''''''''

''''''''''''''''''''''''''''''''''''''''''''
```

```vba
'''  Define Density(x,t)

'''

''''''''''''''''''''''''''''''''''''''''''''''''

''''''''''''''''''''''''''''''''''''''''''''''''

Dim DeRL As Double

Dim EeLR As Double

Dim EeRL As Double

Dim FeLR As Double

Dim FeRL As Double


'Stop

For i = 1 To binterface - ainterface + 1

If i = 1 Then

'If alu = 1 Then

If (1 - ActiveCell.Offset(499 + i + ainterface - 1, 4)) * 100 < 49 Then

ActiveCell.Offset(499 + i + ainterface - 1, 7) = 0.1048 * ((1 - ActiveCell.Offset(499 + i + ainterface
- 1, 4)) * 100) + 0.5984 'ActiveCell.Offset(499 + i + ainterface - 1, 4) + (D1 * dt) * Ad2cdx2atm1
'((ActiveCell.Offset(499 + i + ainterface - 1, 3) - 2 * ActiveCell.Offset(499 + i + ainterface - 1, 4) +
ActiveCell.Offset(500 + i + ainterface - 1, 4)))

'ActiveCell.Offset(499 + i + ainterface - 1, 7) = 0.0575 * ((1 - ActiveCell.Offset(499 + i + ainterface
- 1, 4)) * 100) + 3.0325

Else

ActiveCell.Offset(499 + i + ainterface - 1, 7) = 0.0575 * ((1 - ActiveCell.Offset(499 + i + ainterface
- 1, 4)) * 100) + 3.0325

End If

If (1 - ActiveCell.Offset(499 + i + ainterface - 1, 3)) * 100 < 49 Then

If alu = 1 Then

ActiveCell.Offset(499 + i + ainterface - 1, 6) = 0.1048 * ((1 - ActiveCell.Offset(499 + i + ainterface
- 1, 3)) * 100) + 0.5984 'ActiveCell.Offset(499 + i + ainterface - 1, 4) + (D1 * dt) * Ad2cdx2atm1
'((ActiveCell.Offset(499 + i + ainterface - 1, 3) - 2 * ActiveCell.Offset(499 + i + ainterface - 1, 4) +
ActiveCell.Offset(500 + i + ainterface - 1, 4)))
```

'ActiveCell.Offset(499 + i + ainterface - 1, 6) = 0.0575 * ((1 - ActiveCell.Offset(499 + i + ainterface - 1, 3)) * 100) + 3.0325

DeRL = ActiveCell.Offset(499 + i + ainterface - 1, 6)

Else

ActiveCell.Offset(499 + i + ainterface - 1, 6) = ActiveCell.Offset(499 + i + ainterface - 1, 7)

DeRL = ActiveCell.Offset(499 + i + ainterface - 1, 6)

End If

Else

If alu = 1 Then

ActiveCell.Offset(499 + i + ainterface - 1, 6) = 0.0575 * ((1 - ActiveCell.Offset(499 + i + ainterface - 1, 3)) * 100) + 3.0325

DeRL = ActiveCell.Offset(499 + i + ainterface - 1, 6)

Else

ActiveCell.Offset(499 + i + ainterface - 1, 6) = ActiveCell.Offset(499 + i + ainterface - 1, 7)

DeRL = ActiveCell.Offset(499 + i + ainterface - 1, 6)

End If

End If

ElseIf i > 1 And i < binterface - ainterface + 1 Then

If (1 - ActiveCell.Offset(499 + i + ainterface - 1, 4)) * 100 < 49 Then

ActiveCell.Offset(499 + i + ainterface - 1, 7) = 0.1048 * ((1 - ActiveCell.Offset(499 + i + ainterface - 1, 4)) * 100) + 0.5984 'ActiveCell.Offset(499 + i + ainterface - 1, 4) + (D1 * dt) * Ad2cdx2atm1 '((ActiveCell.Offset(499 + i + ainterface - 1, 3) - 2 * ActiveCell.Offset(499 + i + ainterface - 1, 4) + ActiveCell.Offset(500 + i + ainterface - 1, 4)))

'ActiveCell.Offset(499 + i + ainterface - 1, 7) = 0.0575 * ((1 - ActiveCell.Offset(499 + i + ainterface - 1, 4)) * 100) + 3.0325

Else

ActiveCell.Offset(499 + i + ainterface - 1, 7) = 0.0575 * ((1 - ActiveCell.Offset(499 + i + ainterface - 1, 4)) * 100) + 3.0325

End If

'Stop

ActiveCell.Offset(499 + i + ainterface - 1, 6) = ""

ElseIf i = binterface - ainterface + 1 Then

If (1 - ActiveCell.Offset(499 + i + ainterface - 1, 4)) * 100 < 49 Then

ActiveCell.Offset(499 + i + ainterface - 1, 7) = 0.1048 * ((1 - ActiveCell.Offset(499 + i + ainterface - 1, 4)) * 100) + 0.5984 'ActiveCell.Offset(499 + i + ainterface - 1, 4) + (D1 * dt) * Ad2cdx2atm1 '((ActiveCell.Offset(499 + i + ainterface - 1, 3) - 2 * ActiveCell.Offset(499 + i + ainterface - 1, 4) + ActiveCell.Offset(500 + i + ainterface - 1, 4)))

'ActiveCell.Offset(499 + i + ainterface - 1, 7) = 0.0575 * ((1 - ActiveCell.Offset(499 + i + ainterface - 1, 4)) * 100) + 3.0325

Else

ActiveCell.Offset(499 + i + ainterface - 1, 7) = 0.0575 * ((1 - ActiveCell.Offset(499 + i + ainterface - 1, 4)) * 100) + 3.0325

End If

'Stop

If (1 - ActiveCell.Offset(499 + i + ainterface - 1, 4)) * 100 < 49 Then

ActiveCell.Offset(499 + i + ainterface - 1, 6) = 0.1048 * ((1 - ActiveCell.Offset(499 + i + ainterface - 1, 3)) * 100) + 0.5984 'ActiveCell.Offset(499 + i + ainterface - 1, 4) + (D1 * dt) * Ad2cdx2atm1 '((ActiveCell.Offset(499 + i + ainterface - 1, 3) - 2 * ActiveCell.Offset(499 + i + ainterface - 1, 4) + ActiveCell.Offset(500 + i + ainterface - 1, 4)))

'ActiveCell.Offset(499 + i + ainterface - 1, 6) = 0.0575 * ((1 - ActiveCell.Offset(499 + i + ainterface - 1, 3)) * 100) + 3.0325

EeLR = ActiveCell.Offset(499 + i + ainterface - 1, 6)

Else

ActiveCell.Offset(499 + i + ainterface - 1, 6) = 0.0575 * ((1 - ActiveCell.Offset(499 + i + ainterface - 1, 3)) * 100) + 3.0325

EeLR = ActiveCell.Offset(499 + i + ainterface - 1, 6)

End If

'Stop

End If

Next

For i = 1 To cinterface - binterface

If i = 1 Then

If (1 - ActiveCell.Offset(binterface + 499 + i, 4)) * 100 < 49 Then

ActiveCell.Offset(binterface + 499 + i, 7) = 0.1048 * ((1 - ActiveCell.Offset(binterface + 499 + i, 4)) * 100) + 0.5984 'ActiveCell.Offset(499 + i + ainterface - 1, 4) + (D1 * dt) * Ad2cdx2atm1 '((ActiveCell.Offset(499 + i + ainterface - 1, 3) - 2 * ActiveCell.Offset(499 + i + ainterface - 1, 4) + ActiveCell.Offset(500 + i + ainterface - 1, 4)))

'ActiveCell.Offset(binterface + 499 + i, 7) = 0.0575 * ((1 - ActiveCell.Offset(binterface + 499 + i, 4)) * 100) + 3.0325

Else

ActiveCell.Offset(binterface + 499 + i, 7) = 0.0575 * ((1 - ActiveCell.Offset(binterface + 499 + i, 4)) * 100) + 3.0325

End If

If (1 - ActiveCell.Offset(binterface + 499 + i, 3)) * 100 < 49 Then

ActiveCell.Offset(binterface + 499 + i, 6) = 0.1048 * ((1 - ActiveCell.Offset(binterface + 499 + i, 3)) * 100) + 0.5984 'ActiveCell.Offset(499 + i + ainterface - 1, 4) + (D1 * dt) * Ad2cdx2atm1 '((ActiveCell.Offset(499 + i + ainterface - 1, 3) - 2 * ActiveCell.Offset(499 + i + ainterface - 1, 4) + ActiveCell.Offset(500 + i + ainterface - 1, 4)))

'ActiveCell.Offset(binterface + 499 + i, 6) = 0.0575 * ((1 - ActiveCell.Offset(binterface + 499 + i, 3)) * 100) + 3.0325

EeRL = ActiveCell.Offset(binterface + 499 + i, 6)

Else

ActiveCell.Offset(binterface + 499 + i, 6) = 0.0575 * ((1 - ActiveCell.Offset(binterface + 499 + i, 3)) * 100) + 3.0325

EeRL = ActiveCell.Offset(binterface + 499 + i, 6)

```vba
End If

'Stop

ElseIf i > 1 And i < cinterface - binterface Then


If (1 - ActiveCell.Offset(binterface + 499 + i, 4)) * 100 < 49 Then

ActiveCell.Offset(binterface + 499 + i, 7) = 0.1048 * ((1 - ActiveCell.Offset(binterface + 499 + i, 4))
* 100) + 0.5984 'ActiveCell.Offset(499 + i + ainterface - 1, 4) + (D1 * dt) * Ad2cdx2atm1
'((ActiveCell.Offset(499 + i + ainterface - 1, 3) - 2 * ActiveCell.Offset(499 + i + ainterface - 1, 4) +
ActiveCell.Offset(500 + i + ainterface - 1, 4)))

'ActiveCell.Offset(binterface + 499 + i, 7) = 0.0575 * ((1 - ActiveCell.Offset(binterface + 499 + i,
4)) * 100) + 3.0325

Else

ActiveCell.Offset(binterface + 499 + i, 7) = 0.0575 * ((1 - ActiveCell.Offset(binterface + 499 + i, 4))
* 100) + 3.0325

End If

'Stop

ActiveCell.Offset(binterface + 499 + i, 6) = ""

ElseIf i = cinterface - binterface Then

If (1 - ActiveCell.Offset(binterface + 499 + i, 4)) * 100 < 49 Then

ActiveCell.Offset(binterface + 499 + i, 7) = 0.1048 * ((1 - ActiveCell.Offset(binterface + 499 + i, 4))
* 100) + 0.5984 'ActiveCell.Offset(499 + i + ainterface - 1, 4) + (D1 * dt) * Ad2cdx2atm1
'((ActiveCell.Offset(499 + i + ainterface - 1, 3) - 2 * ActiveCell.Offset(499 + i + ainterface - 1, 4) +
ActiveCell.Offset(500 + i + ainterface - 1, 4)))

'ActiveCell.Offset(binterface + 499 + i, 7) = 0.0575 * ((1 - ActiveCell.Offset(binterface + 499 + i,
4)) * 100) + 3.0325

Else

ActiveCell.Offset(binterface + 499 + i, 7) = 0.0575 * ((1 - ActiveCell.Offset(binterface + 499 + i, 4))
* 100) + 3.0325

End If

'Stop
```

131

If (1 - ActiveCell.Offset(binterface + 499 + i, 3)) * 100 < 49 Then

ActiveCell.Offset(binterface + 499 + i, 6) = 0.1048 * ((1 - ActiveCell.Offset(binterface + 499 + i, 3)) * 100) + 0.5984 'ActiveCell.Offset(499 + i + ainterface - 1, 4) + (D1 * dt) * Ad2cdx2atm1 '((ActiveCell.Offset(499 + i + ainterface - 1, 3) - 2 * ActiveCell.Offset(499 + i + ainterface - 1, 4) + ActiveCell.Offset(500 + i + ainterface - 1, 4)))

'ActiveCell.Offset(binterface + 499 + i, 6) = 0.0575 * ((1 - ActiveCell.Offset(binterface + 499 + i, 3)) * 100) + 3.0325

FeLR = ActiveCell.Offset(binterface + 499 + i, 6)

Else

ActiveCell.Offset(binterface + 499 + i, 6) = 0.0575 * ((1 - ActiveCell.Offset(binterface + 499 + i, 3)) * 100) + 3.0325

FeLR = ActiveCell.Offset(binterface + 499 + i, 6)

End If

'Stop

End If

Next

'Stop

For i = 1 To length - 1 - cinterface

If i = 1 Then

If (1 - ActiveCell.Offset(cinterface + 499 + i, 4)) * 100 < 49 Then

ActiveCell.Offset(cinterface + 499 + i, 7) = 0.1048 * ((1 - ActiveCell.Offset(cinterface + 499 + i, 4)) * 100) + 0.5984 'ActiveCell.Offset(499 + i + ainterface - 1, 4) + (D1 * dt) * Ad2cdx2atm1 '((ActiveCell.Offset(499 + i + ainterface - 1, 3) - 2 * ActiveCell.Offset(499 + i + ainterface - 1, 4) + ActiveCell.Offset(500 + i + ainterface - 1, 4)))

'ActiveCell.Offset(cinterface + 499 + i, 7) = 0.0575 * ((1 - ActiveCell.Offset(cinterface + 499 + i, 4)) * 100) + 3.0325

Else

ActiveCell.Offset(cinterface + 499 + i, 7) = 0.0575 * ((1 - ActiveCell.Offset(cinterface + 499 + i, 4)) * 100) + 3.0325

End If

End If

If (1 - ActiveCell.Offset(cinterface + 499 + i, 4)) * 100 < 49 Then

ActiveCell.Offset(cinterface + 499 + i, 6) = 0.1048 * ((1 - ActiveCell.Offset(cinterface + 499 + i, 3)) * 100) + 0.5984 'ActiveCell.Offset(499 + i + ainterface - 1, 4) + (D1 * dt) * Ad2cdx2atm1 '((ActiveCell.Offset(499 + i + ainterface - 1, 3) - 2 * ActiveCell.Offset(499 + i + ainterface - 1, 4) + ActiveCell.Offset(500 + i + ainterface - 1, 4)))

'ActiveCell.Offset(cinterface + 499 + i, 6) = 0.0575 * ((1 - ActiveCell.Offset(cinterface + 499 + i, 3)) * 100) + 3.0325

FeRL = ActiveCell.Offset(cinterface + 499 + i, 6)

Else

ActiveCell.Offset(cinterface + 499 + i, 6) = 0.0575 * ((1 - ActiveCell.Offset(cinterface + 499 + i, 3)) * 100) + 3.0325

FeRL = ActiveCell.Offset(cinterface + 499 + i, 6)

End If

'Stop

End If

If i > 1 And i < length - 1 - cinterface Then

If (1 - ActiveCell.Offset(cinterface + 499 + i, 4)) * 100 < 49 Then

ActiveCell.Offset(cinterface + 499 + i, 7) = 0.1048 * ((1 - ActiveCell.Offset(cinterface + 499 + i, 4)) * 100) + 0.5984 'ActiveCell.Offset(499 + i + ainterface - 1, 4) + (D1 * dt) * Ad2cdx2atm1 '((ActiveCell.Offset(499 + i + ainterface - 1, 3) - 2 * ActiveCell.Offset(499 + i + ainterface - 1, 4) + ActiveCell.Offset(500 + i + ainterface - 1, 4)))

'ActiveCell.Offset(cinterface + 499 + i, 7) = 0.0575 * ((1 - ActiveCell.Offset(cinterface + 499 + i, 4)) * 100) + 3.0325

Else

ActiveCell.Offset(cinterface + 499 + i, 7) = 0.0575 * ((1 - ActiveCell.Offset(cinterface + 499 + i, 4)) * 100) + 3.0325

End If

'Stop

ActiveCell.Offset(cinterface + 499 + i, 6) = ""

End If

133

If i = length - 1 - cinterface Then

If (1 - ActiveCell.Offset(cinterface + 499 + i, 4)) * 100 < 49 Then

ActiveCell.Offset(cinterface + 499 + i, 7) = 0.1048 * ((1 - ActiveCell.Offset(binterface + 499 + i, 4)) * 100) + 0.5984 'ActiveCell.Offset(499 + i + ainterface - 1, 4) + (D1 * dt) * Ad2cdx2atm1 '((ActiveCell.Offset(499 + i + ainterface - 1, 3) - 2 * ActiveCell.Offset(499 + i + ainterface - 1, 4) + ActiveCell.Offset(500 + i + ainterface - 1, 4)))

'ActiveCell.Offset(cinterface + 499 + i, 7) = 0.0575 * ((1 - ActiveCell.Offset(binterface + 499 + i, 4)) * 100) + 3.0325

Else

ActiveCell.Offset(cinterface + 499 + i, 7) = 0.0575 * ((1 - ActiveCell.Offset(binterface + 499 + i, 4)) * 100) + 3.0325

End If

'Stop

End If

Next

'''

'''

'''

'Calculate mass

'''

'''

For i = 1 To binterface - ainterface + 1

If i = 1 Then

mass = mass + (0.5 * (ActiveCell.Offset(499 + i + ainterface - 1, 7) - DeRL) * (1 - r)) + DeRL * (1 - r)

ElseIf i > 1 And i < binterface - ainterface + 1 Then

mass = mass + (0.5 * (ActiveCell.Offset(499 + i + ainterface - 1, 7) - ActiveCell.Offset(498 + i + ainterface - 1, 7))) + ActiveCell.Offset(498 + i + ainterface - 1, 7)

'Stop

ElseIf i = binterface - ainterface + 1 Then

mass = mass + (0.5 * (ActiveCell.Offset(499 + i + ainterface - 1, 7) - ActiveCell.Offset(498 + i + ainterface - 1, 7))) + ActiveCell.Offset(498 + i + ainterface - 1, 7)

'Stop

mass = mass + (0.5 * (0.5 * (EeLR + EeRL) - ActiveCell.Offset(499 + i + ainterface - 1, 7))) * o + ActiveCell.Offset(499 + i + ainterface - 1, 7) * o

'Stop

End If

Next

For i = 1 To cinterface - binterface

If i = 1 Then

mass = mass + (0.5 * (ActiveCell.Offset(binterface + 499 + i, 7) - 0.5 * (EeLR + EeRL)) * (1 - o)) + 0.5 * (EeLR + EeRL) * (1 - o)

'Stop

ElseIf i > 1 And i < cinterface - binterface Then

mass = mass + (0.5 * (ActiveCell.Offset(binterface + 499 + i, 7) - ActiveCell.Offset(binterface + 498 + i, 7))) + ActiveCell.Offset(binterface + 498 + i, 7)

'Stop

ElseIf i = cinterface - binterface Then

mass = mass + (0.5 * (ActiveCell.Offset(binterface + 499 + i, 7) - ActiveCell.Offset(binterface + 498 + i, 7))) + ActiveCell.Offset(binterface + 498 + i, 7)

'Stop

mass = mass + (0.5 * (0.5 * (FeLR + FeRL) - ActiveCell.Offset(binterface + 499 + i, 7))) * p + ActiveCell.Offset(binterface + 499 + i, 7) * p

'Stop

End If

Next

'Stop

For i = 1 To length - 1 - cinterface

If i = 1 Then

mass = mass + (0.5 * (ActiveCell.Offset(cinterface + 499 + i, 7) - 0.5 * (FeLR + FeRL)) * (1 - p)) + 0.5 * (FeLR + FeRL) * (1 - p)

'Stop

End If

If i > 1 And i < length - 1 - cinterface Then

mass = mass + (0.5 * (ActiveCell.Offset(cinterface + 499 + i, 7) - ActiveCell.Offset(cinterface + 498 + i, 7))) + ActiveCell.Offset(cinterface + 498 + i, 7)

'Stop

End If

If i = length - 1 - cinterface Then

mass = mass + (0.5 * (ActiveCell.Offset(cinterface + 499 + i, 7) - ActiveCell.Offset(cinterface + 498 + i, 7))) + ActiveCell.Offset(cinterface + 498 + i, 7)

'Stop

End If

Next

''

```vba
''''''''''''''''''''''''''''''''''''''''''

''''''''''''''''''''''''''''''''''''''''''

''''''''''''''''''''''''''''''''''''''''''

''''''''''''''''''''''''''''''''''''''''''


If binterface - ainterface > 1 Then

For i = 1 To binterface - ainterface + 1

If i = 1 Then

If alu = 1 Then

ActiveCell.Offset(499 + i + ainterface - 1, 4) = ActiveCell.Offset(499 + i + ainterface - 1, 4) + (D1 * dt) * Ad2cdx2atm1 '((ActiveCell.Offset(499 + i + ainterface - 1, 3) - 2 * ActiveCell.Offset(499 + i + ainterface - 1, 4) + ActiveCell.Offset(500 + i + ainterface - 1, 4)))

'Stop

Else

ActiveCell.Offset(499 + i + ainterface - 1, 4) = ActiveCell.Offset(499 + i + ainterface, 4)

End If

ElseIf i > 1 And i < binterface - ainterface + 1 Then

ActiveCell.Offset(499 + i + ainterface - 1, 4) = ActiveCell.Offset(499 + i + ainterface - 1, 4) + (D1 * dt) * ((ActiveCell.Offset(500 + i + ainterface - 1, 4) - 2 * ActiveCell.Offset(499 + i + ainterface - 1, 4) + ActiveCell.Offset(498 + i + ainterface - 1, 4)))

ElseIf i = binterface - ainterface + 1 Then

ActiveCell.Offset(499 + i + ainterface - 1, 4) = ActiveCell.Offset(499 + i + ainterface - 1, 4) + (D1 * dt) * Bd2cdx2atmn1

End If

Next

End If


For i = 1 To cinterface - binterface

If i = 1 Then
```

If bdone = 0 Then

ActiveCell.Offset(binterface + 499 + i, 4) = ActiveCell.Offset(binterface + 499 + i, 4) + (D2 * dt) * Bd2cdx2atm1 '((ActiveCell.Offset(binterface + 499 + i, 3) - 2 * ActiveCell.Offset(binterface + 499 + i, 4) + ActiveCell.Offset(binterface + 500 + i, 4)))

Else

ActiveCell.Offset(binterface + 499 + i, 4) = ActiveCell.Offset(binterface + 501 + i, 4)

End If

ElseIf i > 1 And i < cinterface - binterface Then

ActiveCell.Offset(binterface + 499 + i, 4) = ActiveCell.Offset(binterface + 499 + i, 4) + (D2 * dt) * ((ActiveCell.Offset(binterface + 498 + i, 4) - 2 * ActiveCell.Offset(binterface + 499 + i, 4) + ActiveCell.Offset(binterface + 500 + i, 4)))

ElseIf i = cinterface - binterface Then

ActiveCell.Offset(binterface + 499 + i, 4) = ActiveCell.Offset(binterface + 499 + i, 4) + (D2 * dt) * Cd2cdx2atmn1 '((ActiveCell.Offset(binterface + 499 + i, 3) - 2 * ActiveCell.Offset(binterface + 499 + i, 4) + ActiveCell.Offset(binterface + 498 + i, 4)))

End If

Next

For i = 1 To length - 1 - cinterface

If i = 1 Then

If cdone = 0 Then

ActiveCell.Offset(cinterface + 499 + i, 4) = ActiveCell.Offset(cinterface + 499 + i, 4) + (D3 * dt) * Cd2cdx2atm1

Else

ActiveCell.Offset(cinterface + 499 + i, 4) = ActiveCell.Offset(cinterface + 501 + i, 4)

End If

End If

If i > 1 And i < length - 1 - cinterface Then

ActiveCell.Offset(cinterface + 499 + i, 4) = ActiveCell.Offset(cinterface + 499 + i, 4) + (D3 * dt) * ((ActiveCell.Offset(cinterface + 498 + i, 4) - 2 * ActiveCell.Offset(cinterface + 499 + i, 4) + ActiveCell.Offset(cinterface + 500 + i, 4)))

End If

If i = length - 1 - cinterface Then

ActiveCell.Offset(cinterface + 499 + i, 4) = ActiveCell.Offset(cinterface + 497 + i, 4)

End If

Next

If alu = 1 Then

inta = inta + ((dA1dt - dA2dt) * 0.5 + dA2dt) * dt

Else

End If

If bdone = 0 Then

intb = intb + ((dB1dt - dB2dt) * 0.5 + dB2dt) * dt

Else

End If

If cdone = 0 Then

intc = intc + ((dC1dt - dC2dt) * 0.5 + dC2dt) * dt

Else

End If

```
If bdone = 0 Then

ActiveCell.Offset(1, 3) = intb

ActiveCell.Offset(499 + binterface, 3) = ""

ActiveCell.Offset(500 + binterface, 3) = ""

ActiveCell.Offset(501 + binterface, 3) = ""


ActiveCell.Offset(3, 5) = binterface

binterfaceold = ActiveCell.Offset(3, 5)

binterface = Int(intb)

ActiveCell.Offset(3, 3) = binterface


ActiveCell.Offset(2, 5) = ainterface

ainterfaceold = ActiveCell.Offset(2, 5)

ainterface = Int(inta)

ActiveCell.Offset(2, 3) = ainterface

Else

End If


If cdone = 0 Then

ActiveCell.Offset(1, 5) = intc

ActiveCell.Offset(499 + cinterface, 3) = ""

ActiveCell.Offset(500 + cinterface, 3) = ""

ActiveCell.Offset(501 + cinterface, 3) = ""


ActiveCell.Offset(4, 5) = cinterface
```

```
cinterfaceold = ActiveCell.Offset(4, 5)

cinterface = Int(intc)

ActiveCell.Offset(4, 3) = cinterface


'ActiveCell.Offset(2, 5) = ainterface

ainterfaceold = ActiveCell.Offset(2, 5)

ainterface = Int(inta)

ActiveCell.Offset(2, 3) = ainterface

Else

End If



If alu = 1 Then

If Abs(ainterface - ainterfaceold) >= 1 Then

ActiveCell.Offset(499 - 2 + ainterface, 1) = "time"

ActiveCell.Offset(500 - 2 + ainterface, 1) = "B"

ActiveCell.Offset(501 - 2 + ainterface, 1) = "surf-B"

ActiveCell.Offset(500 - 2 + ainterface, 3) = 1

ActiveCell.Offset(501 - 2 + ainterface, 3) = 0.728

ActiveCell.Offset(501 - 2 + ainterface, 4) = 0.728

ActiveCell.Offset(502 - 2 + ainterface, 3) = ""

For i = 1 To binterface - ainterface + 1

ActiveCell.Offset(499 + ainterface + i, 1) = "delta"

Next

For i = 1 To -ainterface + length

ActiveCell.Offset(498 + ainterface + i, 2) = i

Next
```

```
ActiveCell.Offset(501 - ainterface, 3) = ""

End If

Else

End If


If binterface - binterfaceold >= 1 Then  'the interface must be moved

ActiveCell.Offset(498 + binterface, 1) = "delta"

ActiveCell.Offset(499 + binterface, 1) = "delta-B"

ActiveCell.Offset(500 + binterface, 1) = "beta-B"

ActiveCell.Offset(499 + binterface, 3) = BLR

ActiveCell.Offset(500 + binterface, 3) = BRL

ActiveCell.Offset(499 + binterface, 4) = BLR


ElseIf binterface - binterfaceold < 1 And binterface - binterfaceold >= 0 Then

ActiveCell.Offset(499 + binterface, 1) = "delta-B"

ActiveCell.Offset(500 + binterface, 1) = "beta-B"

ActiveCell.Offset(499 + binterface, 3) = BLR

ActiveCell.Offset(500 + binterface, 3) = BRL

Else

ActiveCell.Offset(499 + binterface, 1) = "delta-B"

ActiveCell.Offset(500 + binterface, 1) = "beta-B"

ActiveCell.Offset(501 + binterface, 1) = "beta"

ActiveCell.Offset(501 + binterface, 3) = BRL

ActiveCell.Offset(500 + binterface, 3) = BLR

ActiveCell.Offset(500 + binterface, 4) = BRL

End If
```

```
If cinterface - cinterfaceold >= 1 Then  'the interface must be moved

ActiveCell.Offset(498 + cinterface, 1) = "beta"

ActiveCell.Offset(499 + cinterface, 1) = "beta-B"

ActiveCell.Offset(500 + cinterface, 1) = "gamma-B"

ActiveCell.Offset(499 + cinterface, 3) = CLR

ActiveCell.Offset(500 + cinterface, 3) = CRL

ActiveCell.Offset(499 + cinterface, 4) = CLR


ElseIf cinterface - cinterfaceold < 1 And cinterface - cinterfaceold >= 0 Then

ActiveCell.Offset(499 + cinterface, 1) = "beta-B"

ActiveCell.Offset(500 + cinterface, 1) = "gamma-B"

ActiveCell.Offset(499 + cinterface, 3) = CLR

ActiveCell.Offset(500 + cinterface, 3) = CRL

Else

ActiveCell.Offset(499 + cinterface, 1) = "beta-B"

ActiveCell.Offset(500 + cinterface, 1) = "gamma-B"

ActiveCell.Offset(501 + cinterface, 1) = "gamma"

ActiveCell.Offset(501 + cinterface, 3) = CRL

ActiveCell.Offset(500 + cinterface, 3) = CLR

ActiveCell.Offset(500 + cinterface, 4) = CRL

End If


ActiveCell.Offset(499 + binterface, 1) = "delta-B"

ActiveCell.Offset(500 + binterface, 1) = "beta-B"

ActiveCell.Offset(499 + binterface, 3) = BLR

ActiveCell.Offset(500 + binterface, 3) = BRL
```

```vba
ActiveCell.Offset(499 + cinterface, 1) = "beta-B"

ActiveCell.Offset(500 + cinterface, 1) = "gamma-B"

ActiveCell.Offset(499 + cinterface, 3) = CLR

ActiveCell.Offset(500 + cinterface, 3) = CRL


ActiveCell.Offset(0, 7) = ActiveCell.Offset(0, 7) + dt

ActiveCell.Offset(0, 5) = ActiveCell.Offset(0, 5) + 1


""""""""""""""

'  movement of surface

""""""""""""""

If alu = 1 Then

ActiveCell.Offset(1, 1) = inta '1.5 - ((intb - 4.5) * (1 - 0.54)) + (((intc - intb - 6) * (1 - 0.66)))

'1.5-((ActiveCell.Offset(1, 3) - 4.5) * (1 - 0.54)) + (((ActiveCell.Offset(1, 5) - ActiveCell.Offset(1, 3) - 6) * (1 - 0.66)))

Else

End If


If (ActiveCell.Offset(0, 5) / 1000) - Int(ActiveCell.Offset(0, 5) / 1000) = 0 Then

'ActiveCell.Offset(800 + j1, 4) = mass


'ActiveCell.Offset(800 + j1, 5) = inta

'ActiveCell.Offset(800 + j1, 6) = intb

'ActiveCell.Offset(800 + j1, 7) = intc

'j1 = j1 + 1


Else

End If
```

```vba
'ActiveCell.Offset(800 + j, 4) = dB2dt

dA1dt = dA2dt

dB1dt = dB2dt

dC1dt = dC2dt


Next



End Sub



Sub resetvalues()

Dim length As Integer

Cells.Select

Selection.ClearContents

Range("A1").Select

length = 100



Cells(1, 1).Select

ActiveCell.Offset(1, 0) = "A-interface"

ActiveCell.Offset(1, 1) = 1.5

ActiveCell.Offset(1, 2) = "B-interface"

ActiveCell.Offset(1, 3) = 4.5

ActiveCell.Offset(1, 4) = "C-interface"

ActiveCell.Offset(1, 5) = 10.5



ActiveCell.Offset(2, 2) = "A-int"
```

ActiveCell.Offset(2, 3) = 1

ActiveCell.Offset(2, 4) = "Old A-intfc"

ActiveCell.Offset(2, 5) = 1

ActiveCell.Offset(3, 2) = "B-int"

ActiveCell.Offset(3, 3) = 4

ActiveCell.Offset(3, 4) = "Old B-intfc"

ActiveCell.Offset(3, 5) = 4

ActiveCell.Offset(4, 2) = "C-int"

ActiveCell.Offset(4, 3) = 10

ActiveCell.Offset(4, 4) = "Old C-intfc"

ActiveCell.Offset(4, 5) = 10

ActiveCell.Offset(0, 4) = "Counter"

ActiveCell.Offset(0, 5) = 0

ActiveCell.Offset(0, 6) = "time"

ActiveCell.Offset(0, 7) = 0

ActiveCell.Offset(498, 1) = "time"

ActiveCell.Offset(499, 1) = "B"

ActiveCell.Offset(500, 1) = "surf-B"

```
ActiveCell.Offset(501, 1) = "delta"

ActiveCell.Offset(502, 1) = "delta"


ActiveCell.Offset(503, 1) = "delta-B"

ActiveCell.Offset(504, 1) = "beta-B"


ActiveCell.Offset(505, 1) = "beta"

ActiveCell.Offset(506, 1) = "beta"

ActiveCell.Offset(507, 1) = "beta"

ActiveCell.Offset(508, 1) = "beta"


ActiveCell.Offset(509, 1) = "beta-B"

ActiveCell.Offset(510, 1) = "gamma-B"


For i = 1 To length - 12

ActiveCell.Offset(510 + i, 1) = "gamma"

Next


For i = 1 To length - 1

ActiveCell.Offset(495 + 4 + i, 2) = i

Next


ActiveCell.Offset(495 + 4, 3) = 1

ActiveCell.Offset(500, 3) = 0.728 'delta-B

ActiveCell.Offset(500, 4) = 0.7 'delta

ActiveCell.Offset(501, 4) = 0.7 'delta
```

```
ActiveCell.Offset(502, 4) = 0.7 'beta

ActiveCell.Offset(503, 4) = 0.7 'beta

ActiveCell.Offset(503, 3) = 0.687 'beta-B

ActiveCell.Offset(504, 3) = 0.653 'gamma-B

ActiveCell.Offset(504, 4) = 0.55 'gamma-B

ActiveCell.Offset(505, 4) = 0.55 'gamma-B

ActiveCell.Offset(506, 4) = 0.55 'gamma-B

ActiveCell.Offset(507, 4) = 0.55 'gamma-B

ActiveCell.Offset(508, 4) = 0.55 'gamma-B

ActiveCell.Offset(509, 4) = 0.55 'gamma-B

ActiveCell.Offset(509, 3) = 0.482 'beta-B

ActiveCell.Offset(510, 3) = 0.362 'gamma-B



For i = 1 To length - 11

ActiveCell.Offset(509 + i, 4) = 0.008

Next



End Sub
```

APPENDIX E

BEFORE ALUMINIZATION SAMPLE PICTURES

Sample 1: 600 micrometer thick sample

Sample 2: 400 micrometer thick sample

Sample 3: 250 micrometer thick sample

Sample 4: 100 micrometer thick sample (Interrupted)

Sample 5: 100 micrometer thick sample

REFERENCES

[1] - Perez-Bergquist, S.J., "Vapor Phase Strengthening of Nickel-Based Alloys for Actively-Cooled Thermostructural Panels", 2010

[2] – Reed, R., The Superalloys Fundamentals and Applications, Cambridge University Press, 2006

[3] – Caves, R., Levine, S., "Thermodynamics and Kinetics of Pack Aluminide Coating Formation on IN -100", Journal of The Electrochemical Society, 1974

[4] – Ardell, A., "Precipitation Hardening," Metallurgical Transactions A, v 16A, Dec 1985, p. 2131-2165

[5] - Goward, G., Boone, D., and Giggins, C., "Formation and Degradation Mechanisms of Aluminide Coatings on Nickel-Base Superalloys," Transactions of the ASM, 228-240

[6] – Janssen, M., and Reick G., "Reaction Diffusion and Kirkendall-Effect in the Nickel-Aluminum System," Transactions of the Metallurgical Society of AIME, Vol 239, n 9, p. 1372-1385, 1967

[7] – Goward, G., and Boone, D., "Mechanisms of Formation of Diffusion Aluminide Coatings on Nickel-Base Superalloys," Oxidations of Metals, vol 3 n 5, p. 475-495

[8] – Kozar, R., Suzuki, A., Milligan, W., Schirra, J., Savage, M., and Pollock, T., "Strengthening Mechanisms in Polycrystalline Multimodal Nickel-Base Superalloys," Metallurgical and Materials Transactions A, v 40A, July 2009, 1588-1603

[9] – Pollock, T., Tin, S., "Nickel-Based Superalloys for Advanced Turbine Engines: Chemistry, Microstructure, and Properties," Journal of Propulsion and Power, vol 22, n 2, March-April 2006, p. 361-374

[10] – Gabb, T., Draper, S., Hull, D., Mackay, A., Nathal, M., "The Role of Interfacial Dislocation Networks in High Temperature Creep of Superalloys," Materials Science and Engineering. A 118(1989), 59-69

[11] – Watanbe, M., Horita, Z., Sano, T., Nemoto, M., "Electron Microscopy Study of Ni/Ni3Al Diffusion-Couple Interface – II. Diffusivity Measurement" Acta metallurgica v 42 n 10 (1994), p. 3389-3396

[12] – Das, D., Vakil, S., Joshi, S., "Evolution of Aluminide Coating Microstructure on Nickel-Base Cast Superalloy CM-247 in a Single-Step High Activity Aluminizing Process," Metallurgical and Materials Transactions A, v 29A Aug 1998, 2173-2188

[13] – Nicholls, J., Stephenson, D., "High Temperature Coatings for Gas Turbines", Intermetallic Compounds: Vol 2 ed J.H. Westbrook, R.L. Fleischer (John Wiley & Sons) (1995)

[14] – Seigle, L., Sivakumar, R., "On the Kinetics of Pack-Aluminization Process", Metallurgical Transactions A, V 7A, Aug 1976, 1073-1079

[15] – Nicholls, J., "Design Oxidation – Resistant Coatings", J. Materials v 52, Jan. 2000, 28-35

[16] - Streiff, R., Boone, D. H. , Streiff, R. and N'Gandu Muamba, J. M., "Surface Morphology of Diffusion Aluminide Coatings", Thin Solid Films, 119 (1984) 291-300

[17] – Goward, G.W., Boone, D.H., "The Use of Nickel-Aluminum Intermetallic Systems as Coatings for High-Temperature Nickel-Base Alloys" Pratt & Whitney, Middletown - Adv. Materials Research & Development Lab, 545-564

[18] – Gupta, B.K., Seigle, L.L., "The Effect on Kinetics of Pack Aluminization of Varying Activator", Thin Solid Films v 73 (1980) 365-371

[19] – Bianco, R., Harper, M., Rapp, R., "Codeposition of Elements in Diffusion Coatings by the Halide Activated Pack Method", Department of Navy ONR RF Project 768203/723314, Sept. 1991

[20] – Voudouris, N., Christoglou, C., Angelopoulos, G., "Formation of Aluminide Coatings on Nickel by a Fluidised Bed CVD Process", Surface and Coatings Technology v 141 (2000), 275-282

[21] – Hickl, A., Heckel, R., "Kinetics of Phase Layer Growth during Aluminide Coating of Nickel", Metallurgical Transactions A, 6A (1975) 431-440

[22] – Glicksman, M.E., Diffusion in Solids: Field Theory, Solid-State Principles & Applications, John Wiley & Sons, New York (2000)

[23] – Balluffi, R., Allen, S., Carter, W. C., Kinetics of Materials, John Wiley & Sons, New Jersey (2005)

[24] – Watanbe, M., Horita, Z., Sano, T., Nemoto, M., "Electron Microscopy of Ni/Ni3Al Diffusion Couple Interface – II Diffusivity Measurement" Acta Metall. Mater. V42 n10 (1994) 3389-3396

[25] – Jost, W., Diffusion in Solids, Liquids, and Gases, Academic Press, New York (1960)

[26] – Pichoir, R., "Influence of the Mode of Formation on Oxidation and Corrosion Behavior of NiAl Type Protective Coatings" Holmes, D.R., Rahmel, A., Materials and Coatings To Resist High Temperature, Applied Science Publishers, London UK

[27] – Crank, J. The mathematics of Diffusion, Oxford University Press (1956)

[28] – Heckel, R.W., Hickl, A.J., Zaehring, R.J., Tanzilli, R.A., "Transient Growth of Second Phases During Solution Treatment", Metallurgical Transactions, V3, Oct 1972, 2565-2569

[29] – Heckel, R.W., Yamada, M., Ouchi, C., Hickl, A.J., "Aluminide Coating of Iron", Thin Solid Films, 45, (1977) 367-373

[30] – Ardell, A.J., Nicholson, R.B., "The Coarsening of γ' in Ni-Al Alloys", J. Phys Chem. Solids v27 (1966), 1793-1804

[31] – Lifshitz, I.M., Slyozov, V.V., "The Kinetics of Precipitation from Supersaturated Solid Solutions" J. Phys. Chem. Solids, Pregamon Press 1961, v 19, n 1/2 p35-50

[32] – Laurencot, P. "The Lifshitz-Slyozov-Wagner Equation with Conserved Total Volume" Siam J. Math Anal. V34 n2 (2002) 257-272

[33] – Chellman, D.J., Ardell, A.J., "The Coarsening of γ' Precipitates at Large Volume Fractions" Acta Metallurgica, v22, n5, 1974, 577-588

[34] – Taylor, A., Doyle, N.J., "Further Studies on Nickel Aluminum System I., The β-NiAl, and δ Ni2Al3 Phase Fields", J. Appl. Cryst. 5 (1972) 201-209

[35] – Taylor, A., X Ray Metallography, John Wiley & Sons, New York (1961)

[36] – Bradley, A.J., Taylor, A., "An X-Ray Analysis of the Nickel-Aluminum System", Proceedings of the Royal Society of London Series A, Mathematical and Physical Sciences, v 159 n 896, March 1937, 56-72

[37] – Gusseva, L.N., "Nature of the Beta Phase of Nickel-Aluminum System" Dokl. Akad. Nauk SSSR 77, 415 (1951)

[38] – Cooper, M.J., "An Investation of the Ordering of the Phases CoAl and NiAl", Phil. Mag 8, 805

[39] – Singh, A.R.P., "Mechanisms of Ordered Gamma Prime Precipitation in Nickel Base Superalloys", (2011)

[40] – Prengamon, M.E., "VAR and ESR: Do They Measure Up", Benet Weapons Laboratory – Watervliet Arsenal Technical Report, Aug 1 1975

[41] – Auburtin, P., Wang, T., Cookcroft, S.L., Mitchell, A., "Freckle Formation and Freckle Criterion in Superalloy Castings", Metallurgical and Materials Transactions B, v 31B, Aug 2000, 801-811

[42] – Matthews, J.C., "A Small Vacuum Induction Furnace", Journal of Scientific Instruments, v34, February 1957

[43] – John, J.T., Kale, G., Bharadwaj, S.R., Srinivasa, R.S., De, P.K., "A Kinetic Model for Iron Aluminide Coating by Low Pressure Chemical Vapor Deposition: Part II Model Formulation", Thin Solid Films, 466 (2004) 331-338

[44] – Crank, J., Free and Moving Boundary Problems, Oxford University Press (1984)

[45] – Murray, W., Landis, F., "Numerical and Machine Solutions of Transient Heat-Conduction Problems Involving Melting or Freezing", Transactions of the ASME, May 1959, 106-112

[46] – Courtney, T., Mechanical Behavior of Materials, Waverland Press Inc. 2nd ed. (2005)

[47] – Lee, B.J., Oh, K.H., "Numerical Treatment of the Moving Interface in Diffusional Reactions", Z. Metallkd., 87 (1996) 3, 195-204

[48] – Zhou, Y., North, T., "Kinetic Modeling of Diffusion Controlled, Two-Phase Moving Interface Problems", Modeling Simul. Mater. Sci. Eng. I (1993) 505-516

[49] – Mourisco, A., Baluc, N., Bonneville, J., Schaller, R., "Mechanical Loss Spectrum of Ni3(Al,Ta) Single Crystals", Materials Science and Engineering A 239-240 (1997) 281-286

[50] – Numakura, H., Kurita, N., Koiwa, M., "On the Origin of Anelastic Relaxation Effect in Ni3Al", Philosophical Magazine A, 1999, Vol 79, n4, 943-953

[51] – Shewmon, P., Diffusion in Solids, Publication of the Minerals, Metals, and Materials Society, 1989

[52] – Ezz, S., Pope, D., "Mechanical Properties of Ni$_3$Al and Nickel-Base Alloys with High Volume Fraction of γ'", International Metals Reviews (1984), v29, 136-167

[53] – Divinski, S., Frank, S., Sodervall, U., Herzig, C., "Solute Diffusion of Al-Substituting Elements in Ni3Al and the Diffusion Mechanism of the Minority Component", Acta Mater., (1998), Vol 46, n 12, 4369-4380

[54] – Pan, Y., Adams, B.L., Olson, T., Panagotou, N., "Grain Boundary Structure Effects on Intergranular Stress Corrosion Cracking of Alloy X-750" Acta Metallurgica, (1996), v44, n12, 4685-4695

[55] – Baldan, A., "Review Progress in Ostwald Ripening Theories and Their Applications to Nickel-Base Superalloys Part I: Ostwald Ripening Theories", Journal of Material Science, (2002), 37, 2171-2202

[56] – Mao, J., "Gamma Prime Precipitation Modeling and Strength Responses in Powder Metallurgy Superalloys", (2002)

[57] – Miller, M.K., Burke, M.G., "An AFPIM/AEM Characterization of Alloy X-750", Applied Surface Science, (1993), 67, 292-298

[58] – Wagner, C., "Theorie der Alterung von Niederschlagen durch Umlosen", Z. Elektrochemie, (1961), 65:581-594

[59] – Ratke, L., Vorhees, P.W., Growth and Coarsening: Ostwald Ripening in Material Processing, Springer, 2002

[60] – Aoki, K., Izumi, O., "Defect Structures and Long Range Parameters in Off-Stoichiometric Ni_3Al", Physica Status Solidi, 32A (1975), 657-664

[61] – Epstein, A., "Millimeter-Scale, MEMS Gas Turbine Engines", Proceedings of ASME Turbo Expo 2003, June 16-19, 2003, Atlanta, GA, USA

[62] – Haasen, P., Physical Metallurgy, Cambridge University Press, 1996

[63] – Garat, V., Cloue, J.M., Viguier, B., Andrieu, E., "Influence of Portevin-Le Chatelier Effect on Rupture Mode of Alloy 718 Specimens", Journal of Nuclear Materials, Vol 375, Issue 1, March 30, 2008, 95-101

[64] – Shankar, S., Seigle, L.L., "Interdiffusion and Intrinsic Diffusion in the NiAl (δ) phase of the Al-Ni System", Metallurgical Transactions A, volume 9A, October 1978, 1467-1476

[65] – Kahlweit, M., "Uber die Alterung von Niederschlagen durch Umlosung", Zeitschrift fur Physikalische Chemie Neue Folge, Bd. 36. S. 292-298 (1963)

[66] – Nesbitt, J.A., Heckel, R.W., "Interdiffusion in Ni-Rich, Ni-Cr-Al alloys at 1100 and 1200 deg C: Part I: Diffusion Paths and Microstructures", Metallurgical Transactions A, vol 18, number 12, December 1987, 2061-2073, 2076-2086

[67] – Schuh, C., "Modeling Gas Diffusion into Metals with a Moving Boundary Phase Transformation", Metallurgical and Materials Transactions A, v 31A, October 2000, 2411-2421

[68] - Sudbrack, C., "Decomposition Behavior in Model Ni-Al-Cr-X Superalloys: Temporal Evolution and Compositional Pathways on a Nanoscale", 2004

[69] – Pollock, T., Johnson, S.J., Adharapurapu, R.R., "Post-Fabrication Vapor Phase Strengthening of Nickel-Based Sheet Alloy for Thermostructural Panels", Superalloys 2008, TMS, Warrendale , PA, 271 (2008)

[70] – Steiner, A., Komarek, K.L., "Thermodynamic Activities of Solid Nickel-Aluminum Alloys", Transactions of Metallurgical Society of AIME, 1964, v230, 786-790

[71] – Chase, M., "NIST-JANAF Thermochemical Tables 4th ed.", J. Phys. Chem. Ref. Data, 1998

[72] – Seigle, L.L., Gupta, B.K., Shankar, R., Sarkhel, A.K., "Kinetics of Pack Aluminization in Nickel", NASA Lewis Research Center, 1978

[73] – Pavi, V.A., Choquet, P., Rapp, R.A., "Thermodynamics of Simultaneous Chromizing-Aluminizing in Halide Activated Cementation Packs", Department of Navy Office of Naval Research, June 1988

[74] – Divinski, S., Herzig, C., "On the Six-Jump Cycle Mechanism of Self-Diffusion in NiAl", Intermetallics 8 (2000), 1357-1368

[75] – Wolff, J., Franz, M., Kluin, J.E., Schmid, D., "Vacancy Formation in Nickel and alpha-Nickel Carbon Alloy", Acta mater. V 45, n 11, (1997), 4759-4764

[76] – Gupta, D., Diffusion Processes in Advanced Technological Materials, William Andrew Publishing, Norwich NY, 2005

[77] – Ortega, M.G., Ramos de Debiaggi, S.B, Monti, A.M., "Self-Diffusion in FCC Metals: Static and Dynamic Simulations in Aluminum and Nickel", Phys. Stat. Sol. (b), 234, no. 1, 506-521 (2002)

[78] – Duan, J., "Atomistic Simulations of Diffusion Mechanisms in Off-Stoichiometric Al-Rich Ni3Al", J. Phys. Condens. Mater. 19 (2007)

[79] – Danckwerts, P.V., "Unsteady-State Diffusion or Heat-Conduction with Moving Boundary", Trans. Faraday. Soc. 46, 701-712

[80] – Jones, R., Jackman, L., "The Structural Evolution of Superalloy Ingots during Hot Working", JOM, 51 (1) (1999), 27-31

[81] – ASTM E-407-07, "Standard Practice for Microetching Metals and Alloys", May 2007

[82] - Remartinez, B., Pastor, J.I., Santamaria, J., "Integrainular Stress Corrosion Cracking Susceptibility of Inconel X-750: State of the Art", European Conference on Fracture 13, San Sebastian 2000, February 8, 2013

[83] – Goldstein, J., Newbury, D., Joy, D., Lyman, C., Echlin, P., Lifshin, E., Sawyer, L., Michael, J., Scanning Electron Microscopy and X-Ray Microanalysis (3rd Ed.), Springer, 2003.

[84] – Thompson, A., Attwood, D., Gullikson, E., Howells, M., Kortright, J., Robinson A., Underwood, J., Kim K., Kirz, J., Lindau, I., Pianetta, P., Winick, H., Williams, G., Scofield J., X-Ray Data Booklet, (2nd ed.), Lawrence Berkeley National Lab, January 2001

[85] – Hafner, B., "Energy Dispersive Spectroscopy on the SEM: A Primer", Characterization Facility, University of Minnesota – Twin Cities, 2007